Cell

S. aureus drives itch and scratch-induced skin damage through a V8 protease-PAR1 axis

Graphical abstract

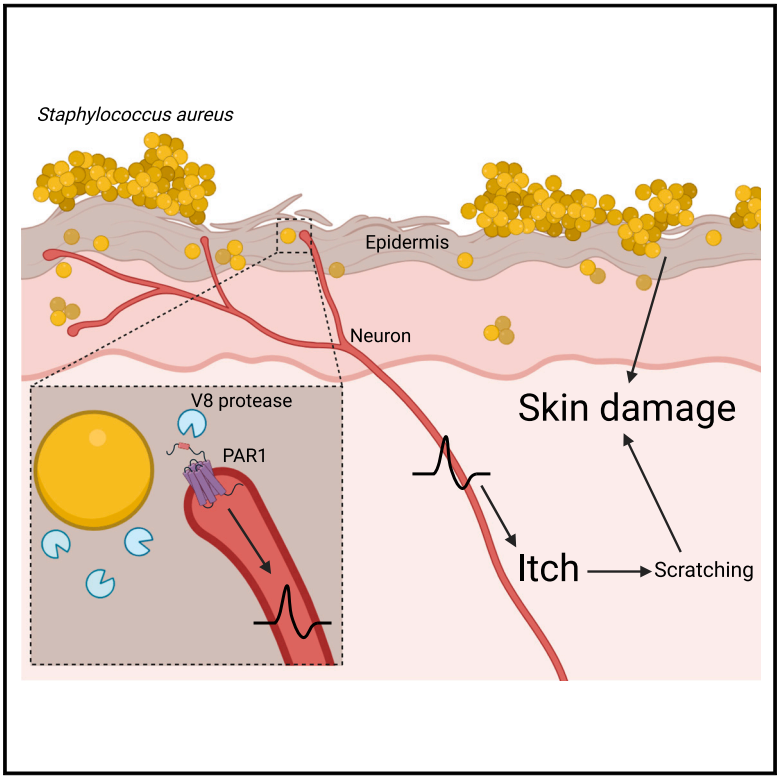

Authors

Liwen Deng, Flavia Costa, Kimbria J. Blake, ..., Rithwik Ramachandran, Alexander R. Horswill, Isaac M. Chiu

Correspondence

isaac_chiu@hms.harvard.edu

In brief

Itch evokes a desire to scratch, but the link between microbes and itch was unclear. *Staphylococcus aureus*, a bacterial pathogen, secretes a protease V8 that activates PAR1 expressed on neurons to drive itch and skin damage.

Highlights

- *S. aureus* induces itch and scratch damage with epicutaneous skin exposure
- V8 protease (SspA) is necessary and sufficient for itch during *S. aureus* exposure
- *S. aureus* V8 activates mouse and human sensory neurons through PAR1
- PAR1 deficiency or blockade abrogates *S. aureus*-induced itch and skin damage

Deng et al., 2023, Cell *186*, 5375–5393
November 22, 2023 © 2023 Elsevier Inc.
https://doi.org/10.1016/j.cell.2023.10.019

CellPress

Cell

CellPress

Article

S. aureus drives itch and scratch-induced skin damage through a V8 protease-PAR1 axis

Liwen Deng,[1] Flavia Costa,[2,10] Kimbria J. Blake,[1,10] Samantha Choi,[1] Arundhasa Chandrabalan,[3] Muhammad Saad Yousuf,[4] Stephanie Shiers,[4] Daniel Dubreuil,[5] Daniela Vega-Mendoza,[6] Corinne Rolland,[7] Celine Deraison,[7] Tiphaine Voisin,[1] Michelle D. Bagood,[8] Lucia Wesemann,[1] Abigail M Frey,[1] Joseph S. Palumbo,[9] Brian J. Wainger,[5] Richard L. Gallo,[8] Juan-Manuel Leyva-Castillo,[6] Nathalie Vergnolle,[7] Theodore J. Price,[4] Rithwik Ramachandran,[3] Alexander R. Horswill,[2] and Isaac M. Chiu[1,11,*]

[1]Department of Immunology, Harvard Medical School, Boston, MA 02215, USA
[2]Department of Immunology and Microbiology, University of Colorado Anschutz Medical Campus, Aurora, CO 80045, USA
[3]Department of Physiology and Pharmacology, University of Western Ontario, London, Ontario N6A 5C1, Canada
[4]Department of Neuroscience and Center for Advanced Pain Studies, University of Texas at Dallas, Richardson, TX 75080, USA
[5]Departments of Neurology and Anesthesia, Critical Care and Pain Medicine, Massachusetts General Hospital, Boston, MA 02114, USA
[6]Division of Immunology, Boston Children's Hospital and Harvard Medical School, Boston, MA 02115, USA
[7]IRSD, Université de Toulouse, INSERM, INRAe, ENVT, Université Toulouse III-Paul Sabatier (UPS), Toulouse, France
[8]Department of Dermatology, University of California, San Diego, La Jolla, CA 92093, USA
[9]Cancer and Blood Diseases Institute, Cincinnati Children's Hospital Medical Center and the University of Cincinnati College of Medicine, Cincinnati, OH, USA
[10]These authors contributed equally
[11]Lead contact
*Correspondence: isaac_chiu@hms.harvard.edu
https://doi.org/10.1016/j.cell.2023.10.019

SUMMARY

Itch is an unpleasant sensation that evokes a desire to scratch. The skin barrier is constantly exposed to microbes and their products. However, the role of microbes in itch generation is unknown. Here, we show that *Staphylococcus aureus*, a bacterial pathogen associated with itchy skin diseases, directly activates pruriceptor sensory neurons to drive itch. Epicutaneous *S. aureus* exposure causes robust itch and scratch-induced damage. By testing multiple isogenic bacterial mutants for virulence factors, we identify the *S. aureus* serine protease V8 as a critical mediator in evoking spontaneous itch and alloknesis. V8 cleaves proteinase-activated receptor 1 (PAR1) on mouse and human sensory neurons. Targeting PAR1 through genetic deficiency, small interfering RNA (siRNA) knockdown, or pharmacological blockade decreases itch and skin damage caused by V8 and *S. aureus* exposure. Thus, we identify a mechanism of action for a pruritogenic bacterial factor and demonstrate the potential of inhibiting V8-PAR1 signaling to treat itch.

INTRODUCTION

The skin is one of the most exposed barrier sites of the body, susceptible to both injury and pathogen invasion. It is innervated by dorsal root ganglia (DRG) sensory neurons that detect mechanical, thermal, and chemical stimuli, including noxious signals that cause itch or pain. Pruriceptors are the sensory neurons that mediate itch and a desire to scratch.[1–3] Microbes that colonize the skin play key roles in tissue homeostasis and physiology. However, a causative role for microbes in driving itch was previously unknown. We hypothesized that pruriceptors may be activated following exposure to specific microbes, resulting in itch that drives skin damage.

Staphylococcus aureus is an opportunistic bacterial pathogen and a leading cause of human bacterial infections. Atopic dermatitis (AD) is a skin disease characterized by itchy, eczematous lesions. 90% of AD lesions are colonized with *S. aureus*, which is thought to be a trigger of inflammation.[4–7] *S. aureus* is also a leading cause of impetigo, a contagious skin infection characterized by itchy lesions[8]. Despite its association with pruritic conditions, the contribution *of S. aureus* to itch is unclear. *S. aureus* encodes several virulence factors that promote colonization and tissue invasion, including α-hemolysin (Hla), phenol soluble modulins (PSMs), and proteases.[9,10] Methicillin-resistant *S. aureus* (MRSA) continues to spread, necessitating an improved understanding of bacterial pathogenesis and host responses to this pathogen.[4,11] We previously found that nociceptors detect *S. aureus* and its toxins to produce pain during subcutaneous infections.[12–14] Pruriceptor nerve endings are mainly found in the epidermis, unlike nociceptors, which innervate both skin and deeper tissues.[1]

Itch provokes a desire to scratch, a behavioral reflex that could exacerbate skin damage. The importance of the itch-scratch cycle in skin pathology and the negative impact on patient quality of life are well known for conditions including AD,[15] prurigo nodularis,[16] and psoriasis.[17] Scratching produces pain, which can temporarily suppress itch through spinal circuitry.[18,19] Mechanical damage caused by scratching disrupts the skin barrier and can amplify inflammation. Therefore, understanding the triggers that cause itch is critical for treatment of skin diseases.

Here, we find that *S. aureus* epicutaneous exposure induces robust itch and scratch-induced damage, which is mediated by V8 protease. Pruriceptors are activated by V8 protease through proteinase-activated receptor 1 (PAR1). Targeting V8 or PAR1 abrogates itch and barrier damage, leading to improved skin pathology. Our findings uncover a role for bacterial proteases in itch and PAR1 as a candidate for therapeutic development.

RESULTS

Epicutaneous *S. aureus* exposure induces itch and alloknesis

To investigate how *S. aureus* impacts itch, we adapted a murine model of epicutaneous exposure relevant to AD.[20–23] In this model, *S. aureus* is applied topically to depilated back skin under gauze, and mice are wrapped with occlusive Tegaderm tape during bacterial exposure, resulting in epidermal breakdown and inflammation at the inoculation site. At the experimental endpoint, tape and gauze were removed for inflammation and itch analysis (Figures 1A and S1A).

We utilized a USA300/LAC MRSA strain, which represents the leading cause of community-associated MRSA.[24] Female and male mice were treated with MRSA, and inflammation was scored post-exposure. MRSA induced significant exposure-site dermatitis, quantified as a sum of edema, skin scale, erythema, and thickness in both sexes by day 5 post-exposure (Figure 1B). Histology showed hyperkeratosis, spongiosis, and inflammatory infiltrates (Figure S1B). *S. aureus*-exposed mice showed higher transepidermal water loss (TEWL) than controls, indicating disruption of skin barrier function (Figure S1C).

We next investigated the role of *S. aureus* in itch. Spontaneous itch behaviors were assessed by placing mice in an infrared behavior observation box (iBOB) to record animals' activity over 90 min (Figure 1C). Videos were watched by blinded observers to quantify scratching bouts (Video S1). Control mice produced minimal scratching, whereas male and female animals treated with *S. aureus* exhibited significantly increased scratching behaviors (Figure 1D). Time course analysis showed that while dermatitis was observed by day 3 post-bacterial exposure, significantly increased scratching behaviors occurred by day 5 after *S. aureus* application (Figures S1D and S1E).

Alloknesis is itch evoked by innocuous mechanical stimuli or touch.[1,25] It is a form of dysesthesia driven by pruriceptor sensitization or spinal cord changes[25,26] and is regulated by Merkel cells.[27] Alloknesis can potentiate the itch-scratch cycle in AD patients. In mice, we measured alloknesis by stimulation with a 0.07 g filament that normally does not elicit responses but induces itch following sensitization.[28] We stimulated mice with this filament nine times and quantified scratching (Video S2). MRSA application induced significant alloknesis compared with PBS-treated controls (Figure 1E). While prior reports showed sex-dependent differences in itch,[29,30] we found no differences in MRSA-induced itch and alloknesis between female and male mice (Figures 1D and 1E).

Itch-induced scratching exacerbates skin damage

Itch-evoked scratching exacerbates skin damage in AD patients. To quantify damage caused by scratching, *S. aureus*-exposed mice were allowed to freely scratch their backs for 7 h after Tegaderm/gauze removal. Total area of damaged skin was quantified using image analysis. Compared with controls, mice inoculated with MRSA had dramatically increased total damaged skin following scratching, resulting in areas of skin damage beyond the bacterial exposure site (Figure 1F). We confirmed that scratching drives damage by wrapping a cohort of bacterial-exposed mice with bandages after Tegaderm/gauze removal. Wrapped mice prevented from scratching showed significantly less skin damage than mice allowed to scratch (Figure 1G). As a second way to prevent scratching, we trimmed the nails of mice after Tegaderm/gauze removal (Figure S1F). Nail trimming reduces itch/scratch-induced damage in mice.[31] Female and male mice that received nail trims had less skin damage than control mice after 7 h of recording (Figure S1G). Thus itch-induced scratching significantly exacerbates skin damage.

Subcutaneous *S. aureus* infection does not induce itch

S. aureus is also a leading cause of human abscesses due to subcutaneous infections.[11,24] However, dermonecrotic skin infections are painful but not itchy. We next determined whether deeper infections by *S. aureus* caused itch. We infected mice by injecting MRSA subcutaneously into their backs, inducing skin lesions by day 5 (Figure 1H). Epicutaneous MRSA applications were performed in parallel, and itch behaviors were measured. While spontaneous itch and alloknesis occurred after epicutaneous MRSA exposure, mice infected subcutaneously did not show spontaneous itch or alloknesis (Figures 1I and 1J). Therefore, while epicutaneous application causes itch, subcutaneous infection does not, indicating that bacterial localization affects behavioral phenotypes.

MYD88, mast cells, and basophils do not mediate *S. aureus* itch

Given that *S. aureus* exposure mediates itch, determining mechanisms by which this occurs could lead to therapies to limit itch-induced skin damage. Previous studies showed that *S. aureus* exposure induces interleukin (IL)-36 release, which activates IL-36 receptor (IL-36R) signaling through MYD88 to drive skin inflammation.[20] Using *Myd88*$^{-/-}$ mice, we observed significant reductions in dermatitis and TEWL after *S. aureus* exposure, compared with wild-type (WT) mice (Figures S2A and S2B). Bacterial load did not differ (Figure S2C). However, we did not detect differences in spontaneous itch behaviors or alloknesis in *Myd88*$^{-/-}$ mice compared with controls following *S. aureus* exposure (Figures S2D and S2E).

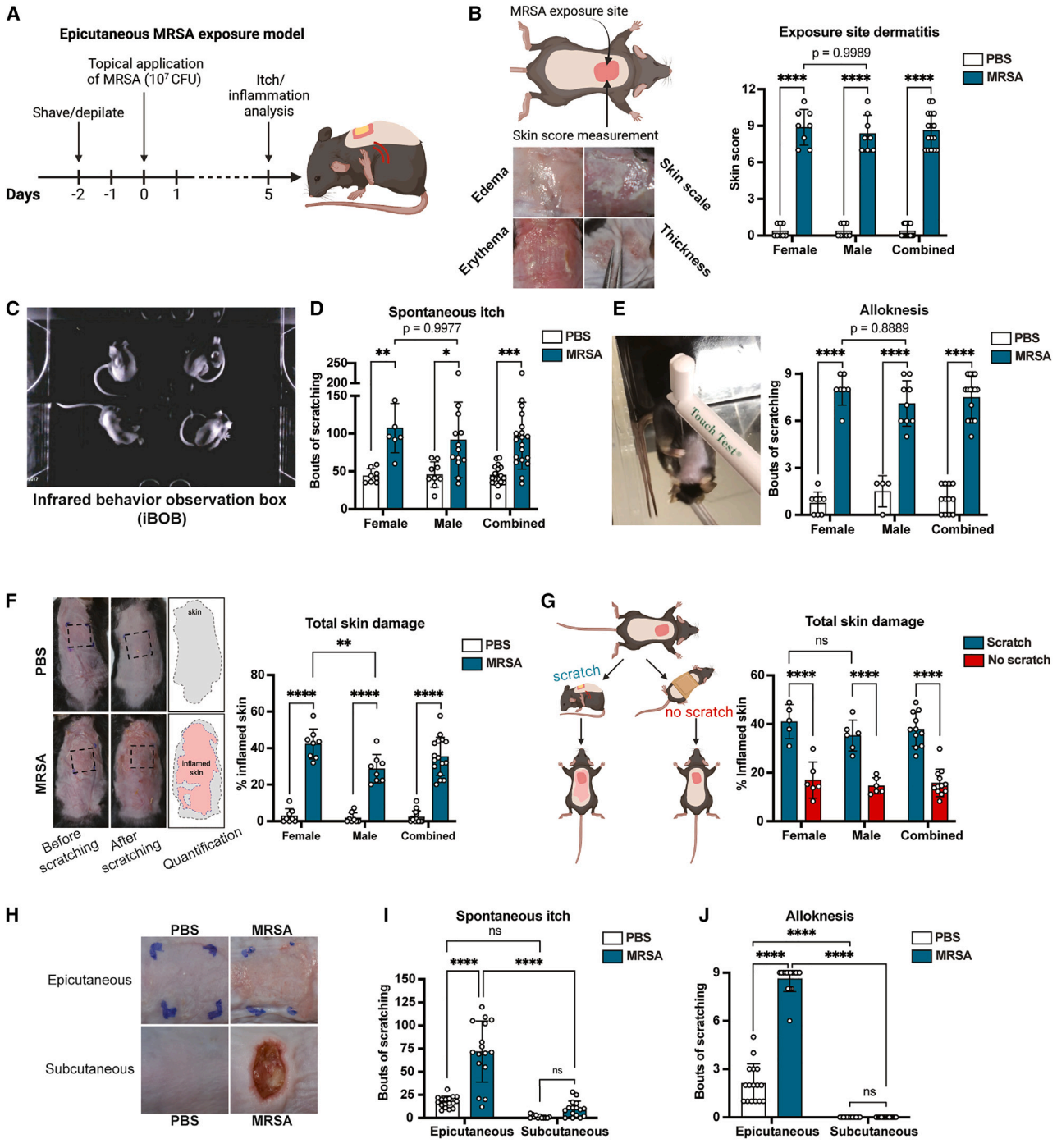

Figure 1. Epicutaneous *S. aureus* induces itch and scratch-induced skin pathology

(A) Murine model of *S. aureus* exposure and itch analysis.

(B–E) 5 days after epicutaneous exposure, dermatitis (B), spontaneous itch (C and D), and (E) alloknesis were measured (n = 8–13 males, 6–8 females per group).

(F) Analysis of total skin damage after scratching (n = 8 males, 8 females per group).

(G) Total skin damage in mice allowed to scratch or prevented from scratching (n = 6 males, 5–6 females per group).

(H–J) Mice inoculated with *S. aureus* epicutaneously or infected subcutaneously; representative images (H), spontaneous itch (I), and alloknesis (J) on day 5 (n = 16 per group).

For each panel, data combined from 2 independent experiments are shown. Data are represented as mean ± SD.

Statistical analysis: in (B), (D)–(G), (I), and (J), two-way ANOVA with Sidak's multiple comparisons. *p < 0.05; **p < 0.01; ***p < 0.001; ****p < 0.0001; ns, not significant. See also Figures S1–S3.

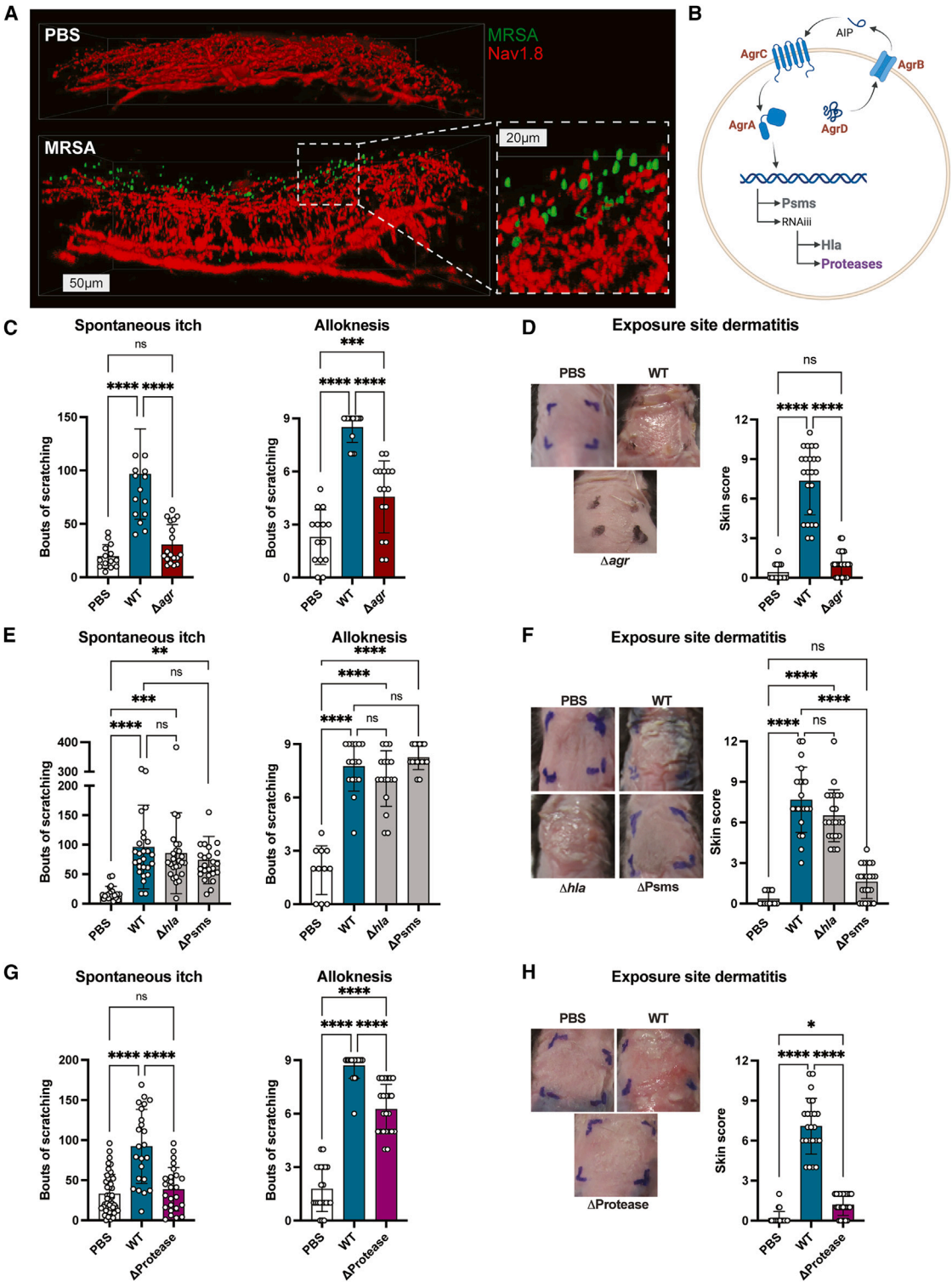

Figure 2. Bacterial factors including Agr quorum sensing and proteases mediate itch

(A) Whole-mount images of skin from *Nav1.8*-tdTomato mice treated with PBS or GFP-MRSA (scale bars, 50 or 20 μm).

(B) Agr quorum sensing regulates expression of phenol soluble modulins (PSMs), alpha-toxin (Hla), and proteases.

(C and D) Spontaneous itch, alloknesis (C), and dermatitis scores (D) recorded for control mice (PBS) or mice inoculated with WT or Δ*agr* MRSA (n = 10 males, 10 females per group).

(legend continued on next page)

Mast cells are key drivers of itch by releasing pruritogens including histamine, serotonin, and tryptase.[32] We utilized *Kit*$^{W\text{-}sh}$ mice, which lack mast cells, to determine their role in *S. aureus* itch. We found no difference in dermatitis or TEWL between *Kit*$^{W\text{-}sh}$ and WT animals following *S. aureus* application (Figures S2F and S2G), but there was an increase in bacterial load in *Kit*$^{W\text{-}sh}$ mice (Figure S2H). We did not detect differences between WT and *Kit*$^{W\text{-}sh}$ mice in spontaneous itch and alloknesis following MRSA exposure (Figures S2I and S2J). Basophils also drive itch in AD by release of leukotrienes, histamine, and serotonin.[33,34] To determine whether basophils mediated itch during *S. aureus* exposure, we treated mice with Ba103 antibody to deplete basophils[35] or with control IgG (Figure S2K). Flow cytometry revealed basophil recruitment in mouse skin following *S. aureus* exposure and that Ba103 antibody successfully eliminated basophils (Figure S2L). After *S. aureus* exposure, we observed no differences in dermatitis, TEWL, bacterial load, spontaneous itch, and alloknesis between mice treated with Ba103 and mice treated with control IgG (Figures S2M–S2Q). Taken together, MYD88, mast cells, and basophils are not required for *S. aureus*-induced itch or dermatitis.

IL31RA, IL4RA, and lymphocytes do not mediate *S. aureus* itch

Itch is associated with type 2 inflammation and can be driven by cytokines including IL-4, IL-13, and IL-31.[36] We first investigated the role of IL-31 in *S. aureus*-mediated itch. IL-31 was elevated in skin on day 5 after *S. aureus* exposure (Figure S3A). We administered small interfering RNA (siRNA) via intrathecal injection[37] to knock down expression of the IL31 receptor, *Il31ra*, in DRG neurons. RT-qPCR analysis of thoracic DRGs confirmed that *Il31ra* siRNA reduced *Il31ra* expression compared with control siRNA treatment (Figure S3B). Mice treated with *Il31ra* siRNA showed no differences in *S. aureus*-induced dermatitis, TEWL, bacterial load, spontaneous itch, and alloknesis, compared with control siRNA-treated mice (Figures S3C–S3G). Pruriceptors also express *Il4ra*, which mediates IL-4 and IL-13 signaling to drive itch.[33] We next exposed *Il4ra*$^{-/-}$ and WT control mice to *S. aureus*. We observed no differences in dermatitis, TEWL, bacterial load, spontaneous itch, and alloknesis between *Il4ra*$^{-/-}$ and control mice (Figures S3H–S3L). Therefore, type 2 cytokines likely do not mediate *S. aureus*-induced itch.

We next ascertained roles for lymphocytes in itch. *Rag2*$^{-/-}$*Il2rg*$^{-/-}$ mice are deficient in T cells, B cells, natural killer (NK) cells, and innate lymphoid cells (ILCs).[38,39] Following MRSA exposure, we did not observe differences in dermatitis, TEWL, spontaneous itch, and alloknesis in *Rag2*$^{-/-}$*Il2rg*$^{-/-}$ mice, compared with WT control mice (Figures S3M, S3N, S3P, and S3Q). We did recover more tissue bacteria load from *Rag2*$^{-/-}$*Il2rg*$^{-/-}$ mice, indicating that lymphocytes affect bacterial clearance (Figure S3O). Overall, we ruled out a role for MYD88, mast cells, basophils, IL31RA, IL4RA, and lymphocytes in itch (Table S1).

S. aureus localizes near epidermal sensory nerves

Pruriceptive nerve endings are mainly located in epidermis.[40] We hypothesized that bacteria may localize to areas close to nerves during epicutaneous exposure to drive itch. NAV1.8 is a voltage-gated sodium channel expressed in C-fibers including pruriceptors.[41,42] *Nav1.8-Cre* mice were bred with tdTomato reporter mice to label these sensory neurons. Mice were topically treated with GFP-expressing MRSA or PBS. Whole-mount imaging showed *Nav1.8*-TdTomato^{+} nerves in dermis and epidermis. Sensory innervation was maintained throughout the thickened dermis and epidermis below the *S. aureus* exposure site. In MRSA-exposed mice, we observed GFP^{+} bacteria localized close to *Nav1.8*-TdTomato+ sensory nerves in the epidermis (Figure 2A).

S. aureus Agr is required for itch

Because bacteria were localized close to nerve endings, we hypothesized that secreted factors from *S. aureus* could activate neurons to drive itch. *S. aureus* virulence factors are regulated by its Agr quorum sensing system, including expression of multiple cytolytic toxins and proteases (Figure 2B).[43] Mice were exposed to WT MRSA or an Δ*agr* isogenic mutant strain. We observed significant reductions in spontaneous itch and alloknesis in mice exposed to Δ*agr* MRSA compared with WT MRSA (Figure 2C). Δ*agr* strain also induced less dermatitis (Figure 2D). Fewer bacteria were recovered from skin of Δ*agr* MRSA compared with WT MRSA-exposed mice (Figure S4A). Thus, Agr mediates both itch and inflammation.

Bacterial toxins (Hla, PSMs) do not mediate *S. aureus* itch

Agr controls expression of PSMs and Hla (Figure 2B). We next tested requirement of these toxins in itch by inoculating mice with WT MRSA or isogenic strains lacking Hla (Δ*hla*) or PSMs (Δ*psmα* Δ*psmβ* Δ*hld*; ΔPsms). Epicutaneous exposure to Δ*hla* or ΔPsms MRSA resulted in similar spontaneous itch and alloknesis as WT MRSA (Figure 2E). MRSA ΔPsms caused less exposure-site dermatitis than WT MRSA, whereas MRSA Δ*hla* induced similar inflammation as WT MRSA (Figure 2F). These results are in line with previous reports demonstrating PSMs driving inflammation.[20,23] We observed no differences in bacterial load for WT and Δ*hla* MRSA, and a decrease in bacterial load for ΔPsms MRSA (Figure S4A). Thus, *S. aureus* Hla and PSMs are not required for exposure-induced itch. Furthermore, itch and inflammation can be decoupled, given that MRSA ΔPsms induced significant itch despite an absence of exposure-site dermatitis (Figures 2E and 2F).

(E and F) Spontaneous itch, alloknesis (E), and dermatitis scores (F) for control mice (PBS) or mice inoculated with WT, Δ*hla*, or ΔPSMs MRSA (n = 8–15 males, 8–16 females per group).

(G and H) Spontaneous itch, alloknesis (G), and dermatitis scores (H) for control mice (PBS) or mice inoculated with WT or ΔProtease MRSA (n = 12 males, 12 females per group).

For each panel, data combined from 4 to 6 independent experiments are shown. Data are represented as mean ± SD.

Statistical analysis: in (C)–(H), one-way ANOVA. *p < 0.05; **p < 0.01; ***p < 0.001; ****p < 0.0001; ns, not significant. See also Figure S4 and Table S1.

Proteases are necessary for *S. aureus* itch

Proteases from plants, allergens, and mammals have been shown to cause itch.[44,45] *S. aureus* produces 10 proteases including cysteine, serine, and metalloproteases,[46] and these proteases are under the control of Agr (Figure 2B). We next tested the requirement for *S. aureus* proteases in itch by inoculating mice with WT MRSA or an isogenic mutant lacking genes for all 10 proteases (Δ*aur* Δ*sspAB* Δ*scpA spl*::erm; ΔProtease).[47] Spontaneous itch behaviors and alloknesis were significantly reduced in mice exposed to MRSA ΔProtease compared with WT MRSA (Figure 2G). MRSA ΔProtease strain was shown previously to induce less inflammation.[48] We found a similar reduction in dermatitis in animals inoculated with MRSA ΔProtease compared with WT MRSA (Figure 2H), and decreased bacterial load (Figure S4A). Therefore, *S. aureus* proteases are necessary for itch and inflammation.

We next aimed to identify the role of specific *S. aureus* protease(s) in itch. Compared with WT MRSA, treatment with MRSA lacking aureolysin (Δ*aur*) resulted in no difference in dermatitis, whereas a strain deficient in both staphopain A and staphopain B (Δ*scpA* Δ*sspB*) caused a slight decrease in dermatitis (Figure S4B). Mice inoculated with Δ*aur* or Δ*scpA* Δ*sspB* had no differences in spontaneous itch, alloknesis, or bacterial load, compared with mice treated with WT MRSA (Figures S4A, S4C, and S4D). MRSA secretes 6 serine protease-like proteins (Spls). MRSA lacking all serine protease-like proteins SplA-F (*spl*::erm) caused a similar degree of dermatitis, spontaneous itch, and alloknesis as WT MRSA (Figures S4B–S4D). These data rule out 9/10 known proteases in MRSA-induced itch, narrowing the search to serine protease V8, which is encoded by *sspA* gene.[49]

S. aureus V8 protease contributes to itch and skin inflammation

To test the requirement of V8 protease in itch, we generated a *sspA* deletion mutant (Δ*sspA*) that does not disrupt the downstream *sspB* gene encoding staphopain B (Figure S5A). We also engineered a chromosomally complemented strain Δ*sspA* + *sspA* and confirmed the loss of V8 protease activity in Δ*sspA* and restoration of its protease activity in the Δ*sspA* + *sspA* complemented strain (Figure S5A). Epicutaneous application of Δ*sspA* MRSA resulted in significantly less itch behaviors measured by spontaneous itch and alloknesis, compared with WT bacteria (Figures 3A and 3B). Itch behaviors were significantly restored in mice exposed to the MRSA Δ*sspA* + *sspA* strain (Figures 3A and 3B). Reduction in scratching resulted in decreased total skin damage in animals exposed to MRSA Δ*sspA* (Figure 3C). Epicutaneous application of Δ*sspA* MRSA resulted in a reduction in dermatitis and lower TEWL measurements, indicating reduced skin barrier damage, compared with mice inoculated with WT MRSA or the complemented MRSA strain (Figures 3D and S5B). We observed no differences between WT MRSA and MRSA Δ*sspA* in adherence to KERTr keratinocyte cells *in vitro*, suggesting that reduction in itch and inflammation is independent of adherence defects (Figure S5C). We did observe a decrease in tissue bacterial load in mice infected with Δ*sspA* mutant (Figure S5D). Therefore, V8 protease is a critical bacterial factor necessary for bacterial-induced itch. All mutant bacterial strains used in this study and the roles of bacterial factors on itch and inflammatory parameters are summarized in Table S1.

V8 is upregulated in mouse skin and human AD skin lesions

Having identified V8 protease as a mediator of itch, we next quantified *sspA* transcript at different time points in the *S. aureus* exposure model (Figure 3E). *sspA* transcript increased over time, becoming significantly higher on day 5, compared with day 1 post-exposure (Figure 3F). By contrast, *psmA1* transcript did not change, and we did not detect *hla* transcript from mouse skin samples during MRSA exposure (Figures 3G and 3H). The timing of increased *sspA* transcript coincides with when we observed robust induction of itch (Figure S1E). We next determined whether *S. aureus* V8 (*sspA*) is expressed in human skin samples relevant to disease. We obtained skin swabs from healthy individuals and non-lesional and lesional skin from AD patients. We observed significantly higher amounts of *sspA* transcript in lesional AD skin samples, compared with skin samples from healthy controls (Figure 3I).

V8 injection induces itch and skin damage

We next tested whether purified V8 protease causes spontaneous itch or pain behaviors. Following intradermal cheek injections, pruritogens induce mice to scratch with the hind paw, whereas pain-inducing algogens cause mice to wipe with the forelimb (Figure 3J).[50,51] We found that injecting 40 units of activity (U) V8 protease induced robust itch and not pain behaviors (Figures 3K and 3L). As a positive control , we injected mice with histamine, a pruritogen that produced itch (Figures 3K and 3L). By contrast, the TRPV1 ligand capsaicin caused pain behaviors but not itch (Figures 3K and 3L). V8 protease injection induced itch in a dose-dependent manner (Figure S5E). Itch likely depends on protease activity, as mice injected with heat-inactivated V8 did not exhibit increased scratching, compared with untreated V8 (Figure S5F). While 40 U of V8 protease induced itch specifically, 200 U of V8 caused both itch and pain behaviors (Figures S4G and S4H).

V8 protease injection was also sufficient to cause alloknesis. Mice were injected with vehicle, histamine, or V8, followed by alloknesis measurements (Figure 3M). V8 protease resulted in significantly higher alloknesis at every time point measured up to 1 h, compared with histamine and buffer alone (Figure 3N), and remained elevated in V8-treated mice at 3 h post-injection (Figure S5I).

We next tested whether V8-induced scratching drives skin damage. Mice were injected intradermally into back skin with PBS or V8. One set of V8-injected mice were allowed to scratch while another group was prevented from scratching by wrapping with bandages (Figure S5J). At 3 and 6 h post-injection, V8 protease-injected mice that could scratch exhibited higher TEWL than PBS-injected controls, indicating skin barrier damage (Figures S5K and S5L). In contrast, V8 protease did not induce higher TEWL in animals prevented from scratching, compared with PBS-injected controls (Figures S5K and S5L).

V8 protease cleaves PAR1

We hypothesized that specific host receptors may mediate neuronal recognition of V8 protease to drive itch. PARs are G protein-coupled receptors activated by proteolytic cleavage of an extracellular N-terminal domain, leading to exposure of a tethered

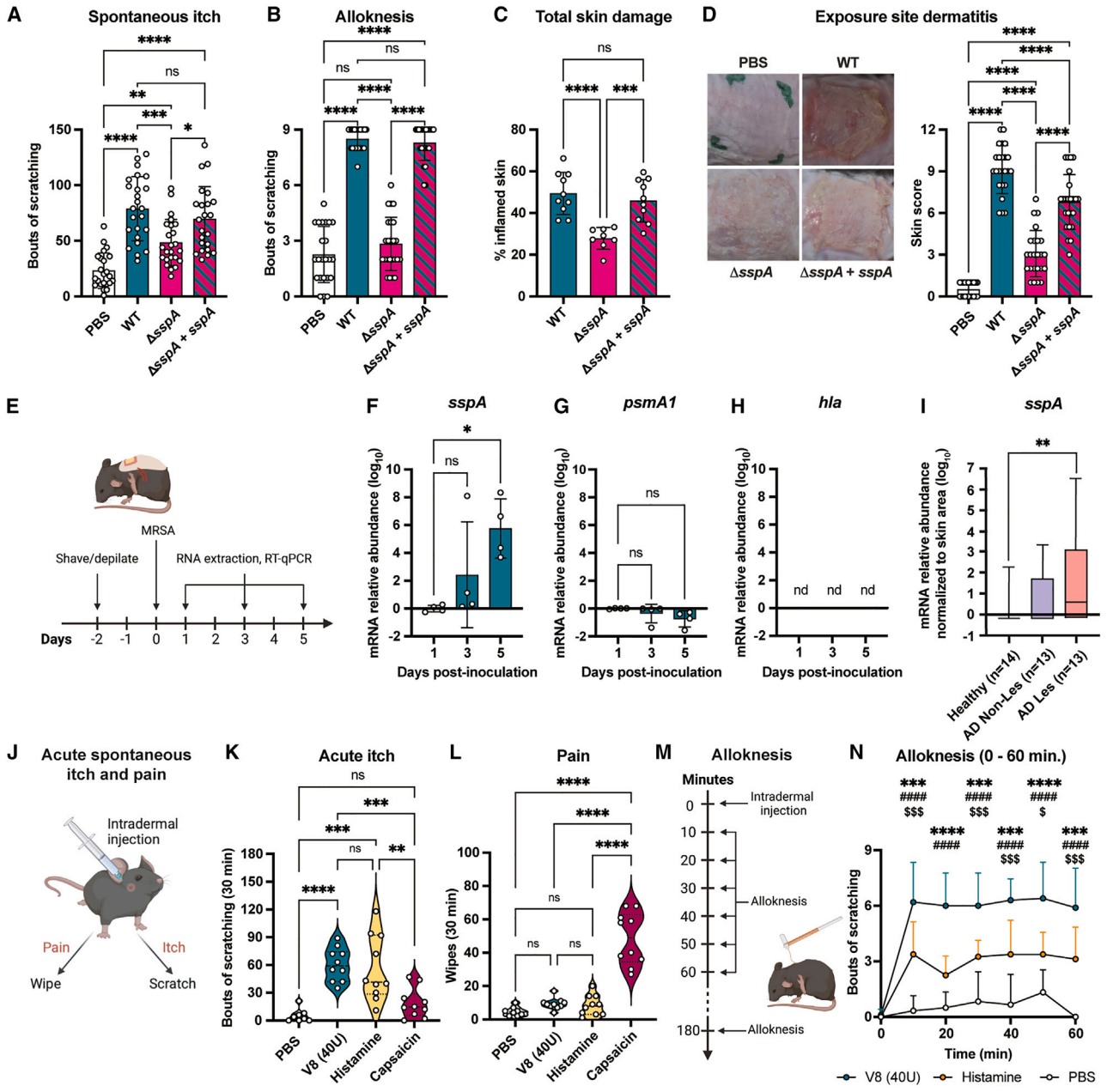

Figure 3. *S. aureus* V8 protease contributes to itch and inflammation

(A and B) Spontaneous itch (A) and alloknesis (B) for control mice (PBS) or mice inoculated with WT, Δ*sspA*, or Δ*sspA* + *sspA* MRSA (n = 11–12 males, 12 females per group).

(C) Total skin damage for control (PBS) or mice inoculated with WT, Δ*sspA*, or Δ*sspA* + *sspA* MRSA (n = 4–5 males, 4–5 females per group).

(D) Representative skin images and dermatitis scores from control mice (PBS) or mice inoculated with WT, Δ*sspA*, or Δ*sspA* + *sspA* MRSA (n = 11–12 males, 12 females per group).

(E–H) Skin collected from mice at 1, 3, and 5 days post-inoculation with MRSA quantified for *sspA* (F), *psmA1* (G), and *hla* (H) transcripts (normalized to 1 day post-inoculation) (n = 2 males, 2 females per group).

(I) Quantification of *sspA* mRNA from skin swabs from healthy human subjects or non-lesional and lesional skin from AD patients (n = 13–14 per group).

(J) Mouse acute itch and pain behavior.

(K and L) Acute itch (K) and pain (L) following intradermal injection with PBS, V8, histamine, or capsaicin (n = 4–5 males, 4–5 females per group).

(M) Mouse intradermal injection and alloknesis model.

(N) Alloknesis after injection with PBS, V8, or histamine (n = 3–5 males, 3–5 females per group).

For each panel, data combined from 2 independent experiments are shown. Data are represented as mean ± SD.

Statistical analysis: in (A)–(D), (F)–(I), (K), and (L), one-way ANOVA. In (N), two-way ANOVA, Tukey's multiple comparisons. *V8 vs. histamine; #histamine vs. PBS; $V8 vs. PBS; *p < 0.05; **p < 0.01; ***p < 0.001; ****p < 0.0001; ns, not significant. See also Figure S5.

ligand that induces activation.[52,53] Humans and mice express four PAR family members, with PAR1, PAR2, and PAR4 having intracellular signaling capabilities.[54,55] PARs are expressed in pruriceptive neurons and their activities are linked to itch.[45]

We employed a luminescence-based PAR cleavage assay[56] to determine whether V8 can proteolytically cleave PARs (Figure 4A). V8 protease potently cleaved human PAR1 (hPAR1) (EC_{50} = 4 U/mL) but did not cleave PAR2 and had modest activity in cleaving PAR4 (EC_{50} = 219 U/mL) (Figure 4B). As positive controls, we performed PAR cleavage assays with canonical PAR-ligand proteases thrombin (PAR1, PAR4) or trypsin (PAR2) (Figure 4C). As a second assay, human embryonic kidney 293 (HEK293) cells expressing PAR1, tagged N-terminally with mRFP and C-terminally with eYFP, were exposed to V8. Microscopy showed V8 treatment resulting in cleavage and removal of N-terminal mRFP tag. Only cleaved receptor (solely eYFP-positive) was detected at cell membrane after V8 exposure (Figure S6A).

To map potential V8 cleavage sites in N terminus of PAR1, we incubated a limiting concentration of V8 protease with C-terminally His_6-tagged ligand of hPAR1 ($hPAR1^{22–102}$) attached to Ni-NTA beads. Mass spectrometry analysis of supernatant identified 10 cleavage sites (Figures 4D and S6B; Table S2), including sites upstream and downstream of canonical thrombin cleavage site (R^{41}/S^{42}), and several peptide fragments. V8 protease did not cleave at E/D|P, possibly due to steric hindrance documented with other proteases.[57] We tested whether V8 protease cleaves the tethered ligand and disarms PAR1 by monitoring thrombin-evoked calcium signaling in HEK cells expressing hPAR1 after exposure to V8. We observed no change in intracellular calcium between cells treated with thrombin alone or pre-treated with 2 U/mL V8 protease and thrombin, indicating that at a lower concentration, V8 cleaves upstream of the thrombin cleavage site (Figure S6C). At 20 U/mL, V8 abrogated responses to thrombin, suggesting that V8 can cleave downstream of thrombin site at higher concentrations (Figure S6D). We further tested whether V8 affected PAR1 activation by the synthetic peptide TFLLR-NH_2, observing no inhibition of TFLLR-NH_2 response with 2 and 20 U/mL V8 protease (Figures S6E and S6F). Intact TFLLR-NH_2 responses suggest that V8 does not cleave at receptor sites involved in tethered ligand binding such as extracellular loops and the ligand binding pocket.

PAR1 is expressed by DRG neurons

PAR1 expression and activation has been demonstrated in human and mouse DRG neurons.[58,59] We determined whether PAR1 is expressed in DRG neurons linked to itch. PAR1 is encoded by the *F2r* gene.[53,60] We performed RNAscope *in situ* hybridization (ISH) analysis in mouse DRG to visualize *F2r* transcripts along with pan-neuronal marker *Tubb3* (Figure 4E), finding *F2r* expression in 40% of mouse DRG neurons (Figure 4F). Analysis of a single-cell RNA sequencing (scRNA-seq) dataset of mouse neurons[61] showed *F2r* expression in several DRG subsets, including neurons previously linked to itch: NP2 neurons that express *Mrgpra3* and *Hrh1*[2,32] and peptidergic neurons that express *S1pr3*[62] (Figure S7A). We also performed RNAscope analysis of *F2R* expression in human DRG samples, observing *F2R* in 35% neurons, in accordance with previous studies.[59] $F2R^+$ neurons were small in diameter (average 53.1 μm) and positive for *TRPV1* and *NPPB*, a marker of pruriceptive neurons[63,64] (Figures 4G and 4H). Mining scRNA-seq data of human DRG neurons, we detected enrichment of *F2R* in a subset of putative pruriceptors expressing *NPPB*, *IL31RA*, and *GFRA2* (Figure S7B).[65]

V8 activates mouse and human DRG neurons

Having confirmed that purified V8 protease induces itch and cleaves PAR1, we next tested whether V8 could directly activate sensory neurons. Mouse DRG neurons were loaded with the calcium indicator Fura-2, followed by application of vehicle or V8 protease. V8 protease induced DRG neuron calcium influx, including a concentration-dependent increase in the number of responsive neurons and the amplitude of calcium responses to V8 (Figures S7C and S7D). We subsequently analyzed neuronal responses to 40 U/mL V8, an amount that induced itch *in vivo* (Figure 3) and at mid-dose range (Figure S7C). At 40 U/mL, V8 protease induced intracellular calcium responses in ~10% of mouse DRG neurons (Figure 5B). Neurons were subsequently exposed to pruritogens histamine, chloroquine, or sphingosine-1-phosphate (S1P), followed by capsaicin and KCl to mark ligand-responsive subsets (Figure 5A). Many V8-responsive cells also responded to pruritogens: V8 activated 25% histamine-responsive, 38% chloroquine-responsive, and 25% S1P-responsive neurons; V8 activated 22% capsaicin-responsive neurons (Figures 5B and S7E).

We previously showed that *S. aureus* Hla and N-formylated peptides can activate DRG neurons to mediate pain.[12] Using calcium imaging, we determined whether V8-responsive neurons also responded to Hla or the N-formylated peptide fMLF. Hla induced the highest proportion of DRG neuron responses, followed by V8, then fMLF (Figure S7F). Approximately 74% V8-responsive neurons responded to Hla, and ~26% V8-responsive neurons responded to fMLF (Figure S7F). We next performed intradermal cheek injections with Hla or fMLF. While fMLF did not induce itch or pain, Hla injection induced both itch and pain (Figure S7G). These data suggest that while Hla is capable of inducing itch, it is not necessary for bacterial itch given that Δ*hla* MRSA did not show abrogated itch following *S. aureus* exposure (Figure 2).

We also tested whether human DRG neurons could respond to V8 with freshly dissociated DRG neurons dissected from organ donors. Human neurons were loaded with the calcium indicator Fluo-4, and intracellular calcium changes measured after treatment with V8 protease and capsaicin (Figure 5C). Here, 26.5% of human DRG neurons were activated by V8, and 95.5% of V8-responsive cells responded to capsaicin (Figure 5D). These data show that V8 can induce calcium influx in both mouse and human DRG neurons.

PAR1 mediates V8-induced neuronal activation and itch

To test whether V8 activation of neurons is dependent on PAR1, we performed calcium imaging of DRG neurons from WT ($F2r^{+/+}$) or $F2r^{-/-}$ mice. Compared with neurons from WT animals, $F2r^{-/-}$ neurons were not responsive to treatment with V8 protease (Figure 5E). We asked if blocking protease activity or PAR1 signaling reduces neuron responses to V8. Mouse DRG neurons were pre-treated with serine protease inhibitor TLCK[66,67] or PAR1 antagonist vorapaxar[68] (Figure 5F). Pre-treatment with TLCK or vorapaxar eliminated V8-induced calcium influx in neurons (Figures 5F and 5G). In contrast, neither vorapaxar nor

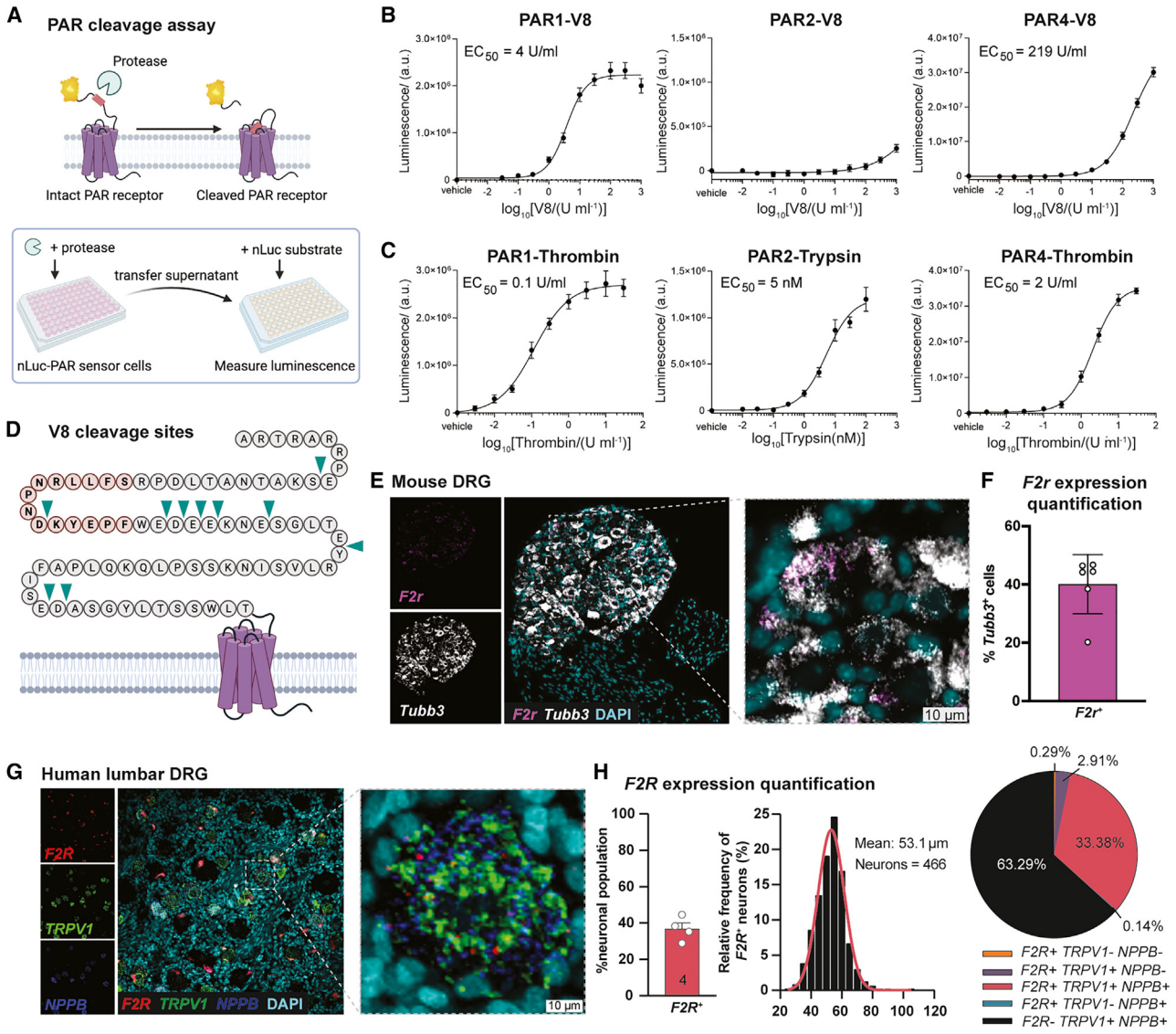

Figure 4. V8 protease cleaves PAR1, which is expressed by pruriceptors

(A) PAR cleavage assays using nLuc-PAR-eYFP-CHO cells.

(B and C) Cleavage data of human PAR1, 2, and 4 by V8 protease or thrombin (for PAR1 and PAR4) or trypsin (for PAR2).

(D) V8 cleavage sites (arrows) on N terminus of human PAR1 identified by mass spectrometry.

(E) Representative images of RNAscope hybridization of mouse DRG sections for *F2r* and *Tubb3*.

(F) Quantification of *F2r* expression in *Tubb3*-positive mouse neurons averaged per mouse (n = 3 males, 3 females). Data are represented as mean ± SD.

(G) Representative images of RNAscope hybridization of human DRG sections for *F2R*, *TRPV1*, and *NPPB*. Total of 1,328 neurons analyzed across 4 donors.

(H) Quantification of *F2R* expression in human neurons, proportions and frequency by size, and marker expression. See also Figure S6 and Table S2.

TLCK affected responses to capsaicin (Figures 5F and 5H). These results demonstrate that PAR1 is required for V8 activation of sensory neurons.

We next tested the requirement of PAR1 for V8-induced itch *in vivo*. We performed intradermal cheek injections with PBS or V8 protease into WT and $F2r^{-/-}$ mice. V8 elicited significantly less scratching in $F2r^{-/-}$ mice than WT mice and there were no significant differences between V8 and PBS-treatment in $F2r^{-/-}$ mice (Figure 6A). To determine whether V8 induces immune cell recruitment dependent on *F2r*, we performed flow cytometry to characterize skin immune cells in WT and $F2r^{-/-}$ mice after treatment with PBS or V8 (Figure S8A). We observed a baseline increase in T cells in $F2r^{-/-}$ mice, compared with WT, and increased T cells in WT mice treated with V8, compared with PBS. Macrophages decreased in $F2r^{-/-}$ mice at baseline and further decreased in mice injected with V8. There were no changes in neutrophils, eosinophils, mast cells, basophils, and dendritic cells (Figure S8B).

We examined the contribution of other protease-activated receptors in V8-induced itch. DRG neurons express members of

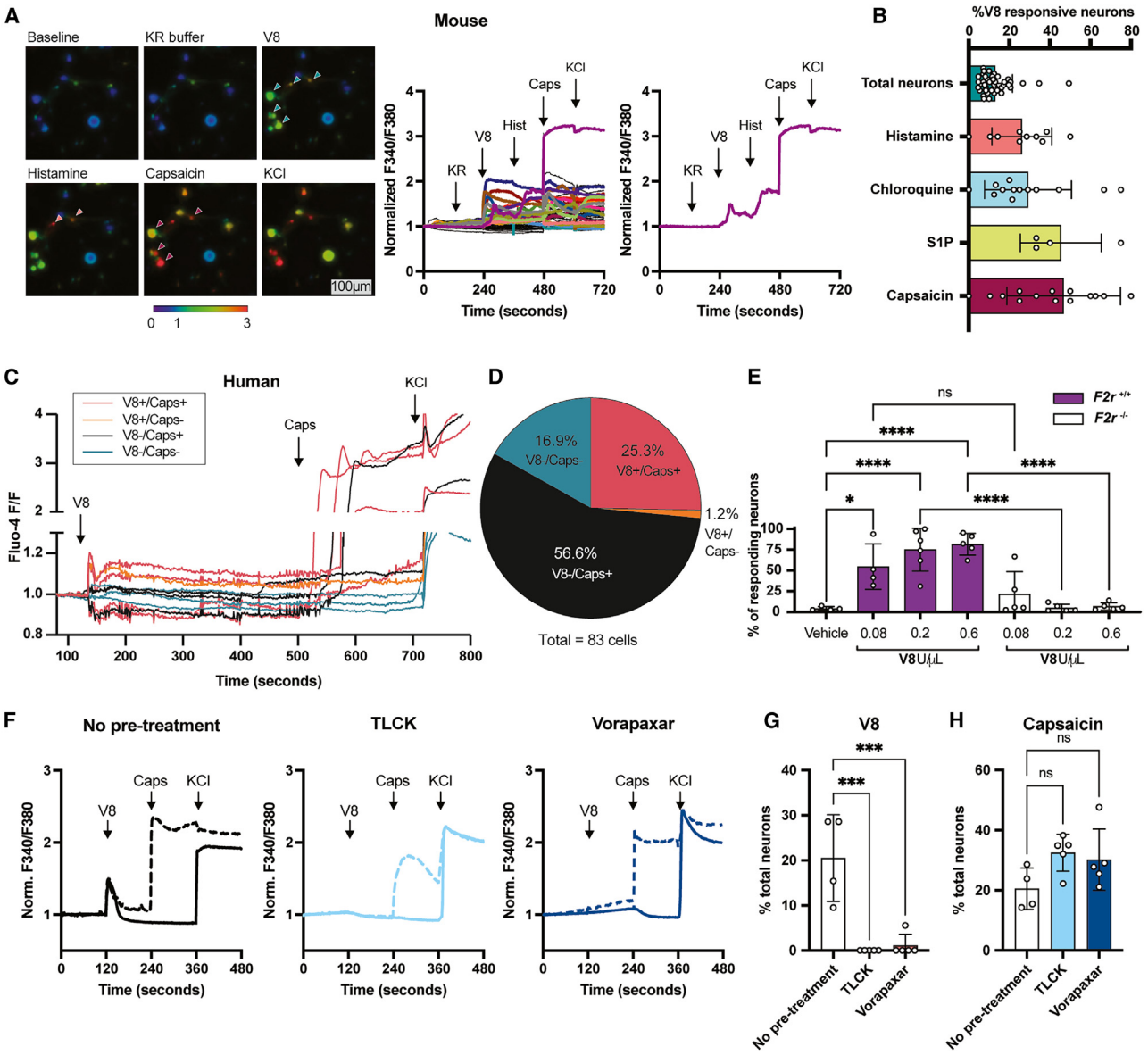

Figure 5. V8 protease directly activates pruriceptor neurons in a PAR1 (*F2r*)-dependent manner

(A) Representative Fura-2 ratiometric fields and calcium traces of mouse DRG neurons. Scale bars, 100 μm.

(B) Percentages of total neurons (responsive to KCl) (n = 41 fields), histamine-responsive (n = 10 fields), chloroquine-responsive (n = 14 fields), S1P-responsive (n = 4 fields), and capsaicin-responsive (n = 16 fields) neurons that also respond to V8.

(C) Calcium traces of human DRG neurons from a representative dish treated with V8, capsaicin, and KCl.

(D) Pie chart showing human neuron populations responding to V8 and capsaicin (V8+/Cap+), V8 alone (V8+/Cap−), capsaicin alone (V8−/Cap+), and unresponsive to either (V8−/Cap−).

(E) Calcium imaging analysis of DRG neurons from $F2r^{+/+}$ and $F2r^{-/-}$ mice treated with increasing doses of V8.

(F) Representative calcium traces of DRG neurons treated with V8, capsaicin, and KCl with no pre-treatment (left) or 5 min post-treatment with TLCK (middle) or vorapaxar (right).

(G and H) Percentage of untreated neurons and neurons pre-treated with TLCK or vorapaxar responding to V8 (G) or capsaicin (H).

For each panel, data combined from 5 independent experiments are shown. Data are represented as mean ± SD.

Statistical analysis: in (B), (E), (G), and (H), one-way ANOVA. *p < 0.05; ***p < 0.001; ****p < 0.0001; ns, not significant. See also Figure S7.

the Mas-related G-coupled receptors (MRGPRs) family, including MRGPRA3, MRGPRX1, and MRGPRD, which have been linked to itch.[69] We found that mice lacking the Mrgpr locus ($Mrgpr^{-/-}$) showed similar acute itch behaviors following V8 intradermal cheek injection as WT mice (Figure S9A). PAR2, encoded by *F2rl1*, mediates protease-induced itch responses.[45,70] However, we did not find PAR2 cleavage by V8 (Figure 4B). $F2rl1^{-/-}$ mice also showed similar itch as WT mice when injected with V8 (Figure S9A).

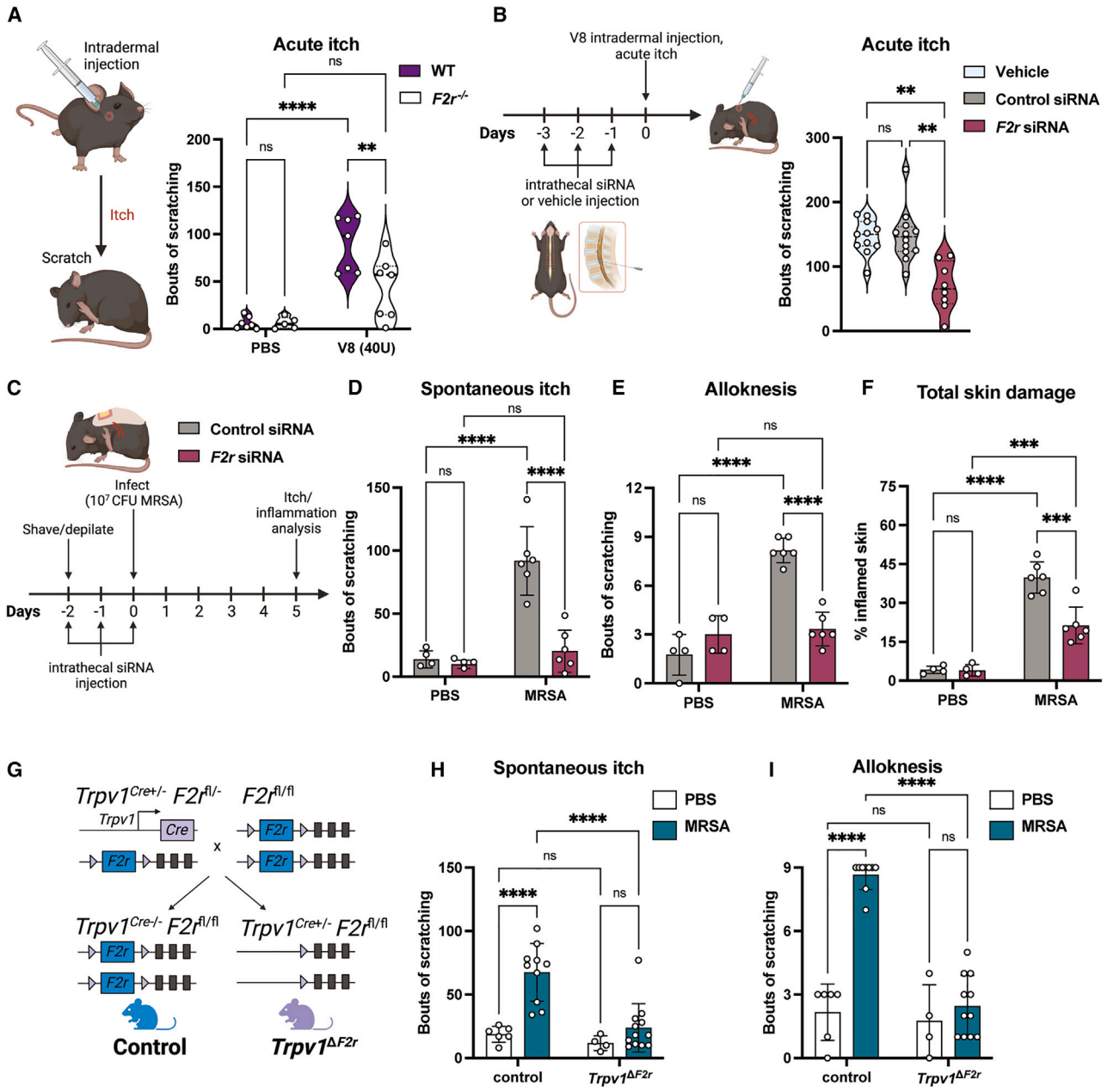

Figure 6. Neuronal PAR1 (*F2r*) is required for V8 and *S. aureus*-induced itch

(A) PBS or V8 protease injected intradermally into cheek of wild-type ($F2r^{+/+}$) and $F2r^{-/-}$ mice, spontaneous scratching over 30 min (n = 3–4 males, 2–4 females per group).

(B) Acute itch behaviors measured for mice treated with vehicle, control siRNA, or *F2r* siRNA (n = 4–6 males, 4–6 females per group).

(C–F) Mice receiving intrathecal siRNA injections were treated with PBS or exposed to MRSA. Spontaneous itch (D), alloknesis (E), and scratch-induced skin damage (F) measured 5 days post-exposure (n = 4–6 males per group).

(G) Generation of $Trpv1^{\Delta F2r}$ and *Trpv1-Cre*$^{-}$ control mice.

(H and I) Spontaneous itch (H) and alloknesis (I) for $Trpv1^{\Delta F2r}$ and control mice treated with PBS or exposed to MRSA (n = 3–8 males, 1–6 females per group).

For each panel, data combined from 2 to 3 independent experiments are shown. Data are represented as mean ± SD.

Statistical analysis: in (A), (D)–(F), (H), and (I), two-way ANOVA, Sidak's multiple comparisons. In (B) and (E), Mann-Whitney test. **p < 0.01; ***p < 0.001; ****p < 0.0001; ns, not significant. See also Figure S8.

F2r targeting in DRG neurons inhibits V8 and *S. aureus* itch

We next determined the role of *F2r* in DRG neurons in V8-induced itch using siRNA and conditional knockout approaches. Using intrathecal injections of siRNA to target sensory neurons,[37] we injected mice with vehicle, control siRNA, or *F2r* siRNA (Figure 6B). RT-qPCR of thoracic DRGs confirmed efficient knockdown of *F2r* in animals treated with *F2r* siRNA but not control siRNA (Figure S9B). We next injected V8 protease intradermally into the upper backs of mice to observe spontaneous scratching behaviors. *F2r* siRNA-treated animals had significantly reduced V8-induced itch, compared with mice injected with vehicle or control siRNA (Figure 6B). We next determined if *F2r* knockdown in DRGs inhibits itch during epicutaneous *S. aureus* exposure. Following *F2r* or control siRNA injection, mice were inoculated with WT MRSA or treated with PBS (Figure 6C). At 5 days post-exposure, we observed no differences in dermatitis, skin barrier damage (TEWL), and tissue bacterial load between control and *F2r* siRNA-treated mice (Figures S9C–S9E). We observed a significant reduction in spontaneous itch behaviors and alloknesis for mice injected with *F2r* siRNA (Figures 6D and 6E). *F2r* knockdown mice also showed less total skin damage caused by scratching (Figure 6F). Therefore, knockdown of *F2r* expression in DRG neurons leads to inhibition of itch caused by V8 protease and *S. aureus*.

To target *F2r* specifically in sensory neurons, we generated $Trpv1^{\Delta F2r}$ conditional knockout mice by crossing *Trpv1-Cre* with $F2r^{fl/fl}$ mice (Figure 6G). *Trpv1-Cre* lineage-based analysis has shown that it targets both peptidergic and non-peptidergic C-fibers.[71] $Trpv1^{\Delta F2r}$ mice or *Cre*-negative control littermates were treated with PBS or exposed to MRSA. We found no differences in dermatitis, TEWL, and skin bacterial load between the two groups (Figures S9F–S9H). Similar to mice injected intrathecally with *F2r* siRNA, $Trpv1^{\Delta F2r}$ mice exhibited significantly less spontaneous itch and alloknesis following MRSA exposure, compared with control mice (Figures 6H and 6I).

PAR1 pharmacological inhibition reduces *S. aureus* itch and skin damage

We next investigated the therapeutic potential of PAR1 blockade in blocking itch and skin pathology. Vorapaxar is a PAR1 antagonist approved by the Food and Drug Administration (FDA) as a drug for reducing the risk of thrombotic cardiovascular events.[72] We found that co-administration of V8 and vorapaxar in mice resulted in significantly reduced scratching for all doses of vorapaxar tested (Figure 7A). We also tested the effect of another PAR1 antagonist, SCH79797, and found that all doses of this drug reduced scratching responses to V8 (Figure S9I). In contrast, PAR4 antagonist BMS986120 minimally affected V8-induced itch, although it did have anti-pruritic effects at the highest dose (Figure S9J). SCH79797 has direct antimicrobial effects, whereas vorapaxar does not affect bacterial growth.[73,74] Therefore, we focused on vorapaxar for further tests in mice.

Vorapaxar significantly reduced V8 protease-induced alloknesis. We found that vorapaxar treatment reduced alloknesis responses up to 3 h after V8 injection (Figures 7B and 7C). Mice injected with V8 protease had higher TEWL measurements in back skin, a measure of skin barrier damage, which could be blocked by vorapaxar treatment or wrapping with bandages to prevent scratching (Figure 7D). Therefore, PAR1 blockade reduced itch and barrier damage after V8 injection.

We next investigated whether vorapaxar could treat itch during *S. aureus* exposure. Mice were gavaged daily with vorapaxar or vehicle control (Figure 7E). Similar to *F2r* siRNA, vorapaxar treatment had no effect on dermatitis, TEWL, and bacterial load (Figures 7F and S9K–S9M). Vorapaxar significantly reduced spontaneous itch behaviors and alloknesis following epicutaneous *S. aureus* application (Figures 7G and 7H). We also recorded less skin damage from scratching for the mice treated with vorapaxar and MRSA (Figures 7I and 7J). In summary, pharmacological inhibition of PAR1 in mice significantly reduces itch behaviors that drives skin damage during bacterial exposure.

DISCUSSION

The underlying mechanisms of itch during microbial exposure were not previously understood. Here, we established that the human pathogen *S. aureus* induces robust itch and scratch-induced damage during epicutaneous exposure. By screening through several bacterial genetic mutants *in vivo* for itch induction (Table S1), we find V8 protease as both necessary and sufficient for exposure-induced itch and alloknesis. *S. aureus* V8 induced mouse and human pruriceptor neuron activation and cleaved PAR1. PAR1 inhibition prevented neuronal activation, itching, and skin damage. Our findings reveal a role for bacteria in causing itch and highlight the importance of the itch-scratch cycle in skin injury.

Given that *S. aureus* produces 10 proteases, it was striking that V8 protease was specifically necessary for bacteria-mediated itch. Staphopains A and B, aureolysin, and SPLs did not contribute to itch. V8 is a serine protease with specificity to cleaving after glutamic acids and in some conditions after aspartates.[75] V8 protease has been shown to be a dominant *S. aureus* virulence factor causing damage to keratinocytes.[76] Topical application of V8 was shown to increase TEWL and serum IgE levels in hairless mice.[77] A recent study profiled skin from healthy adults and AD patients for *S. aureus* virulence factors, and *sspA* transcript was detected in samples from both healthy and AD skin.[78] We found *sspA* transcript increased in AD skin lesions compared with healthy skin samples. Reports have demonstrated that nearly all *S. aureus* isolates contain the *sspA* gene.[79–81] Therefore, V8 could be a conserved itch-inducing mechanism, though it remains to be determined if other strains also drive itch in the same fashion. Antibodies specific to V8 can also be detected from humans who have previously been infected with *S. aureus* and in the general population.[82,83]

In addition to V8, *S. aureus* Hla activated DRG neurons and induced itch and pain when injected. PSMs can also cause itch and pain when injected into the mouse cheek.[84] While Hla and PSMs can induce itch, we found no difference in itch or alloknesis in mice inoculated with *S. aureus* deficient in these toxins (Figure 2). Levels of Hla and PSMs produced by *S. aureus* on the skin may be insufficient to induce itch. Matching this point, while *sspA* transcripts were high at day 5 following

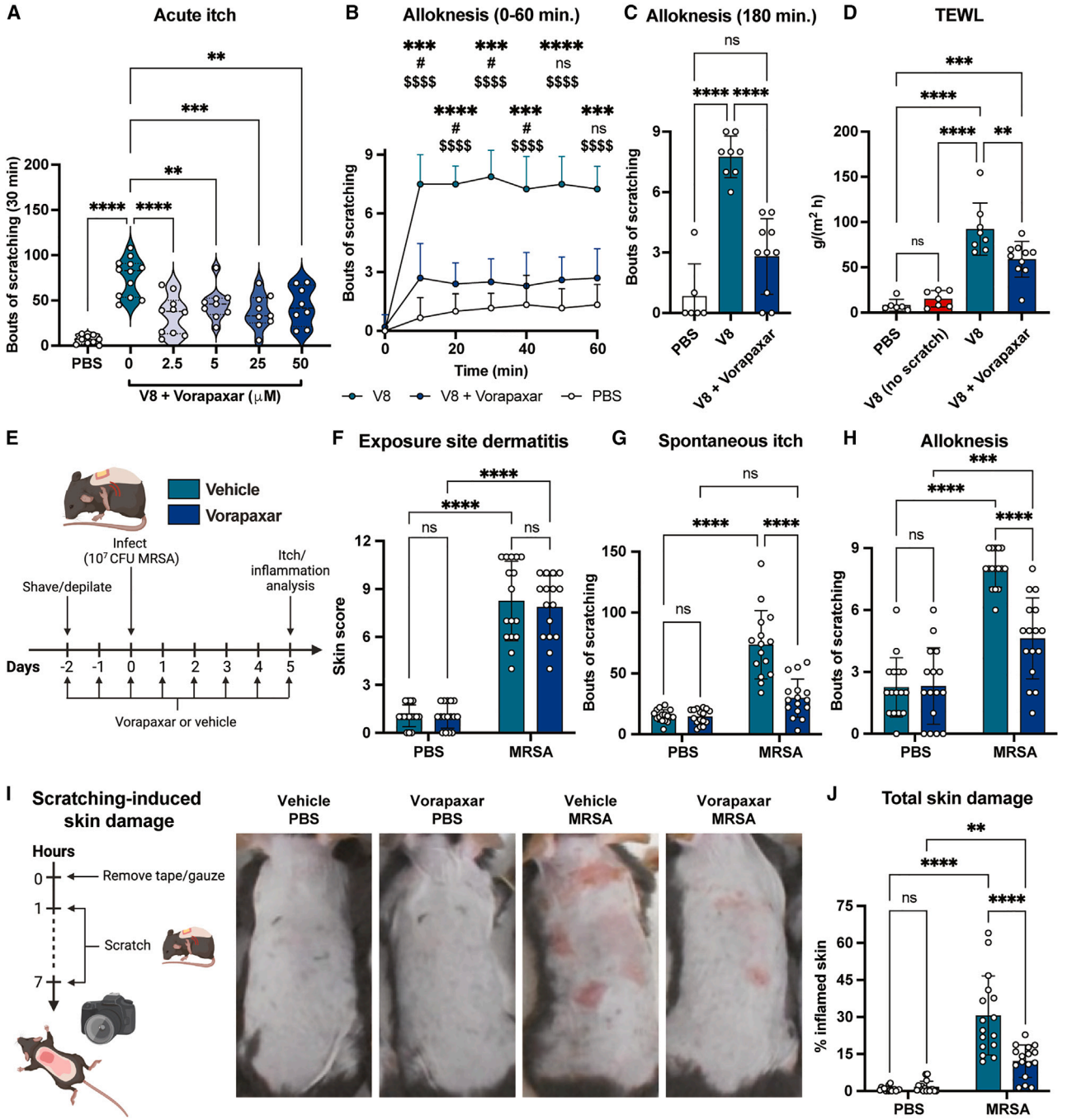

Figure 7. Treatment with PAR1 antagonist reduces itch and skin damage during *S. aureus* exposure

A) Bouts of scratching following cheek injection with PBS or V8, with increasing doses of vorapaxar (n = 4–6 males, 4–6 females per group).

(B and C) Alloknesis measured every 10 min for 1 h (B) and 3 h (C) after cheek injection with PBS, V8, or V8 + vorapaxar (n = 3–5 males, 3–5 females per group).

(D) Mice injected with PBS, V8, or V8 + vorapaxar were allowed to scratch; TEWL measured 3 h post-injection. One group of V8-injected mice were wrapped in bandages to prevent scratching.

(E–J) Mice gavaged daily with vehicle or vorapaxar from 2 days before exposure to PBS or MRSA. Dermatitis scores (F), spontaneous itch (G), alloknesis (H), and scratch-induced skin damage (I and J) measured for control and MRSA-exposed mice treated with vehicle or vorapaxar (n = 7–8 males, 8 females per group). For each panel, data combined from 2 independent experiments are shown. Data are represented as mean ± SD.

Statistical analysis: in (A), (C), and (D), Mann-Whitney test and in (B), two-way ANOVA with Tukey's multiple comparisons: *V8 vs. V8 + vorapaxar; #V8 + vorapaxar vs. PBS; $V8 vs. PBS. In (F) –(H) and (J), two-way ANOVA with Sidak's multiple comparisons. *$p < 0.05$; **$p < 0.01$; ***$p < 0.001$; ****$p < 0.0001$; ns, not significant. See also Figure S9.

MRSA inoculation, we did not observe increased *psma1* or *hla* transcripts (Figure 3). How *S. aureus* regulates expression of these factors on skin surface remains to be determined.

Non-microbial proteases have been linked to itch. Our study adds a bacterial protease as a pruritogen that acts through PAR1. Many previous reports have focused on the action of proteases on PAR2 and PAR4 in itch.[45] Plant proteases, including cowhage mucanain, bromelain, and papain, induce itch by acting via PAR2 and PAR4. Keratinocytes and immune cells express cathepsin S, which can induce itch through PAR2 and PAR4. Mast cell tryptase and chymase can also induce itch. A recent report found that mast cell tryptase activates PAR1 to cause anaphylaxis.[85] Keratinocytes produce kallikrein (KLK) proteases, including KLK5 and KLK14, which can cleave PAR2[86] and drive itch.[87,88] *S. aureus* can also induce keratinocyte expression of KLKs.[89] Our finding that PAR1 mediates itch during *S. aureus* exposure introduces this receptor as a driver of itch. PAR1 was expressed across several sensory neurons in mice, including those expressing *Nppb*, *Mrpgra3*, and *S1pr3*.[2,61] In humans, PAR1 expression was more linked to $NPPB^+$ neurons.[65] How protease activation of $PAR1^+$ neuronal subsets induces signaling at the cellular level remains to be fully determined.

We observed that dermatitis at the site of bacterial exposure can be decoupled from itch and scratching behavior. PSMs and MYD88 were previously shown to drive inflammation.[20,23] We found that bacteria lacking PSMs caused decreased dermatitis but still induced itch; similarly, $Myd88^{-/-}$ mice showed decreased dermatitis but still scratched. Therefore, itch and scratching behavior do not require pre-existing inflammation and skin barrier disruption.

The role of other microbial proteases in itch requires further investigation. Bacteria produce numerous proteases that have various roles in health and disease.[90] *Staphylococcus epidermidis*, an opportunistic pathogen frequently found on healthy and AD skin, makes the protease EcpA that causes skin damage in AD patients.[91] *Streptococcus pyogenes*, another skin pathogen, produces proteases including SpeB that impact skin infection.[92] Beyond bacteria, how fungi, viruses, and parasites or their proteases contribute to itch are unknown.

Neuronal sensing of pathogens can mediate early defense responses to infection through neurogenic inflammation.[93] Nociceptors release neuropeptides including calcitonin gene-related peptide (CGRP) or substance P (SP) to mediate vascular[94,95] and immune changes.[96] PAR1 activation on primary afferents can induce release of CGRP and SP, provoking neurogenic inflammation.[97] Neuronal PAR1 activation could therefore mediate depletion of neuropeptides from primary afferents and downstream immune modulation.

Pathogens may hijack itch and other neural reflexes for their advantage. *Mycobacterium tuberculosis* (Mtb) directly activates vagal nociceptor neurons through a sulfolipid SL-1 to mediate coughing in guinea pigs, which could facilitate pathogen transmission.[98] *S. aureus* induces itch and scratching behaviors that mediate skin damage. This may impact bacterial spread deeper in the skin or result in dissemination to distant body sites. Scratching could also facilitate bacterial spread to other hosts. Further investigation into how bacteria induce maladaptive behaviors including itch to mediate invasion and dissemination is needed.

We found that blocking PAR1 reduced itch in mice, and V8 activates and cleaves hPAR1. Therefore, PAR1 could be an attractive candidate to target for itch therapies. Vorapaxar is currently FDA-approved for prevention of thrombotic cardiovascular events.[72] Future development of topical application of such PAR1 antagonists could avoid adverse events caused by systemic delivery. There is interest in intrathecal injection as a method to deliver therapeutic siRNAs to modulate gene expression in neurons.[99] Itch is a major cause of suffering for the many patients with pruritic diseases accompanied by microbial dysbiosis.[15,19,100,101] Targeting PAR1 or bacterial proteases including V8 may be promising approaches. Therefore, our study reveals a bacterial-driven itch mechanism that contributes to skin pathology and may be targeted for therapeutic treatment of itch.

Limitations of the study

While our study shows that V8 protease mediates *S. aureus*-induced itch and acts through PAR1 on pruriceptors, we cannot fully rule out indirect mechanisms by which V8 could act. V8 could activate endogenous mammalian proteases, which may in turn act on PAR1. V8 protease cleaves human pro-thrombin, although the activity of this cleavage product is unknown,[102] and thrombin is a PAR1 agonist that can be produced by keratinocytes.[103] Another limitation is that though PAR1 knockdown and pharmacological blockade by vorapaxar greatly reduces itch caused by both V8 and *S. aureus* exposure, it does not completely abrogate itch down to baseline levels in animals injected with V8 protease (Figures 6 and 7). Therefore, V8 could partially induce itch via mechanisms independent of PAR1. We observed a reduction in skin bacterial load in mice inoculated with Δ*sspA* MRSA, suggesting a fitness defect. More studies are needed to understand how V8 promotes MRSA virulence. V8 protease may act directly on keratinocytes, immune cells, or other skin cells to drive inflammation and barrier damage. V8 might also synergize with other *S. aureus* factors such as PSMs to drive tissue damage, resulting in deeper infection and pain. Because pain behavior analysis is not optimized for mouse back, it is not currently possible to assess how pain contributes to this model. While the model of epicutaneous *S. aureus* inoculation is widely used for topical exposure, it involves occlusion by Tegaderm tape, and it is self-limiting, which may not reflect *S. aureus* dynamics in human AD lesions. It also mimics aspects of infection such as bacterial epidermal invasion. Additional studies are needed to examine V8 protease and PAR1 in itch in the context of human *S. aureus* colonization and AD. It would be of interest to test if human DRG neurons responding to V8 protease can response to other pruritogens. Due to limitations in availability of human donors, we mainly utilized mouse DRG neurons in this study. Future studies with human neurons are needed to show what subsets of neurons can respond to V8 protease and mediation through PAR1.

STAR★METHODS

Detailed methods are provided in the online version of this paper and include the following:

- KEY RESOURCES TABLE
- RESOURCE AVAILABILITY

SUPPLEMENTAL INFORMATION

Supplemental information can be found online at https://doi.org/10.1016/j.cell.2023.10.019.

ACKNOWLEDGMENTS

We thank Gabriel Nunez (U. Michigan) and Matsumoto Masanori for teaching us the epicutaneous MRSA model. We thank Michael Otto (NIH) for providing ΔPsms strain of MRSA. We thank Larissa Staurengo-Ferrari, Daping Yang, Himanish Basu, Felipe Pinho-Ribeiro, Antonia Wallrapp, Glendon Wu, Jon Sautter, Brian Kim, Dan Kaplan, and Heidi Kong for helpful discussions. We thank Lora Bankova for calcium imaging support. We thank Jorge C. Escalante-Semerena for the pTEV20 vector for expression of PAR1 recombinant N terminus and Greg Sabat (U. Wisconsin-Madison Mass Spectrometry Core) for mass spectrometry and analysis. We thank Dana-Farber/Harvard Cancer Center (supported by NIH/NCI 5P30CA06516) Rodent Histopathology Core. We thank INSERM U1291 Image Core Facility. We are grateful to organ donors and their families for the gift of life and research provided by their organ donation. We thank Dr. Geoffrey Funk and Anna Cervantes at Southwest Transplant Alliance for surgical extraction of human DRGs. Graphical abstract and figure schematics were created with Biorender.com. This study was supported by funding from the NIH R01AI168005 (NIAID) to A.R.H and I.M.C; Food Allergy Science Initiative to I.M.C.; Burroughs Wellcome Fund to I.M.C.; Drako Family Fund to I.M.C.; Jackson-Wijaya Research Fund to I.M.C.; R01AI153185 (NIAID) to A.R.H; Canadian Institutes of Health Research (CIHR) grant 376560 and 469411 to R.R.; NIH R01NS065926, R01NS102161, and R01NS111929 (NINDS) to T.J.P.; NIH R37AI052453, R01AR076082, U01AI152038, and UM1AI151958 to R.L.G.; NIH R01AI153185 to R.L.G. and A.R.H., NIH R01JL160582 to J.S.P.; NIH F32AI172080 to F.C.; NIH T32AI049928 to A.M.F.; ANR-PARCURE PRCE-CE18, 2020 to N.V.; and NIH 1R21AG075419 to B.J.W.

AUTHOR CONTRIBUTIONS

Conceptualization, L.D, F.C., K.J.B., A.R.H., and I.M.C.; methodology, L.D., F.C., K.J.B., S.C., T.V., A.R.H., and I.M.C.; validation, L.D., F.C., K.J.B., and S.C.; formal analysis, L.D., F.C., K.J.B., S.C., N.V, and J.-M.L.-C.; investigation, L.D., F.C., K.J.B., S.C., M.S.Y., S.S., A.C., D.D., D.V.-M, T.V., L.W., M.D.B., C.R., C.D., A.M.F., and J.-M.L.-C.; resources, J.S.P., B.J.W., T.J.P., R.R., A.R.H., and I.M.C.; project administration, I.M.C.; funding acquisition, I.M.C. and A.R.H; visualization, L.D. and I.M.C.; supervision, B.W., T.J.P., R.R., A.R.H., R.L.G., and I.M.C.; writing – original draft, L.D. and I.M.C.; writing – review & editing, L.D., I.M.C., and all authors.

DECLARATION OF INTERESTS

I.M.C. serves on the SAB of GSK Pharmaceuticals. Provisional patent application serial no. 63/438,668, of which some co-authors are inventors, was filed based on these findings.

INCLUSION AND DIVERSITY

We worked to ensure gender balance in the recruitment of human subjects. We worked to ensure ethnic or other types of diversity in the recruitment of human subjects. We worked to ensure sex balance in the selection of non-human subjects.

Received: December 22, 2022
Revised: August 20, 2023
Accepted: October 18, 2023
Published: November 22, 2023

REFERENCES

1. LaMotte, R.H., Dong, X., and Ringkamp, M. (2014). Sensory neurons and circuits mediating itch. Nat. Rev. Neurosci. *15*, 19–31. https://doi.org/10.1038/nrn3641.
2. Bautista, D.M., Wilson, S.R., and Hoon, M.A. (2014). Why we scratch an itch: the molecules, cells and circuits of itch. Nat. Neurosci. *17*, 175–182. https://doi.org/10.1038/nn.3619.
3. Wang, F., and Kim, B.S. (2020). Itch: a paradigm of neuroimmune crosstalk. Immunity *52*, 753–766. https://doi.org/10.1016/j.immuni.2020.04.008.
4. Hwang, J., Jaros, J., and Shi, V.Y. (2020). Staphylococcus aureus in atopic dermatitis: past, present, and future. Dermatitis *31*, 247–258. https://doi.org/10.1097/DER.0000000000000589.
5. Campione, E., Lanna, C., Diluvio, L., Cannizzaro, M.V., Grelli, S., Galluzzo, M., Talamonti, M., Annicchiarico-Petruzzelli, M., Mancini, M.,

Melino, G., et al. (2020). Skin immunity and its dysregulation in atopic dermatitis, hidradenitis suppurativa and vitiligo. Cell Cycle *19*, 257–267. https://doi.org/10.1080/15384101.2019.1707455.

6. Geoghegan, J.A., Irvine, A.D., and Foster, T.J. (2018). Staphylococcus aureus and atopic dermatitis: a complex and evolving relationship. Trends Microbiol. *26*, 484–497. https://doi.org/10.1016/j.tim.2017.11.008.
7. Blicharz, L., Usarek, P., Młynarczyk, G., Skowroński, K., Rudnicka, L., and Samochocki, Z. (2020). Is itch intensity in atopic dermatitis associated with skin colonization by Staphylococcus aureus? Indian J. Dermatol. *65*, 17–21. https://doi.org/10.4103/ijd.IJD_136_19.
8. Johnson, M.K. (2020). Impetigo. Adv Emerg Nurs J. *42*, 262–269.
9. Seilie, E.S., and Bubeck Wardenburg, J. (2017). Staphylococcus aureus pore-forming toxins: the interface of pathogen and host complexity. Semin. Cell Dev. Biol. *72*, 101–116. https://doi.org/10.1016/j.semcdb.2017.04.003.
10. Pietrocola, G., Nobile, G., Rindi, S., and Speziale, P. (2017). Staphylococcus aureus manipulates innate immunity through own and host-expressed proteases. Front. Cell. Infect. Microbiol. *7*, 166. https://doi.org/10.3389/fcimb.2017.00166.
11. Hatlen, T.J., and Miller, L.G. (2021). Staphylococcal skin and soft tissue infections. Infect. Dis. Clin. North Am. *35*, 81–105. https://doi.org/10.1016/j.idc.2020.10.003.
12. Chiu, I.M., Heesters, B.A., Ghasemlou, N., Von Hehn, C.A., Zhao, F., Tran, J., Wainger, B., Strominger, A., Muralidharan, S., Horswill, A.R., et al. (2013). Bacteria activate sensory neurons that modulate pain and inflammation. Nature *501*, 52–57. https://doi.org/10.1038/nature12479.
13. Blake, K.J., Baral, P., Voisin, T., Lubkin, A., Pinho-Ribeiro, F.A., Adams, K.L., Roberson, D.P., Ma, Y.C., Otto, M., Woolf, C.J., et al. (2018). Staphylococcus aureus produces pain through pore-forming toxins and neuronal TRPV1 that is silenced by QX-314. Nat. Commun. *9*, 37. https://doi.org/10.1038/s41467-017-02448-6.
14. Pinho-Ribeiro, F.A., Baddal, B., Haarsma, R., O'Seaghdha, M., Yang, N.J., Blake, K.J., Portley, M., Verri, W.A., Dale, J.B., Wessels, M.R., et al. (2018). Blocking neuronal signaling to immune cells treats streptococcal invasive infection. Cell *173*, 1083–1097.e22. https://doi.org/10.1016/j.cell.2018.04.006.
15. Harrison, I.P., and Spada, F. (2019). Breaking the itch-scratch cycle: topical options for the management of chronic cutaneous itch in atopic dermatitis. Medicines (Basel) *6*. https://doi.org/10.3390/medicines6030076.
16. Kwatra, S.G. (2020). Breaking the itch-scratch cycle in prurigo nodularis. N. Engl. J. Med. *382*, 757–758. https://doi.org/10.1056/NEJMe1916733.
17. Elewski, B., Alexis, A.F., Lebwohl, M., Stein Gold, L., Pariser, D., Del Rosso, J., and Yosipovitch, G. (2019). Itch: an under-recognized problem in psoriasis. J. Eur. Acad. Dermatol. Venereol. *33*, 1465–1476. https://doi.org/10.1111/jdv.15450.
18. Ross, S.E. (2011). Pain and itch: insights into the neural circuits of aversive somatosensation in health and disease. Curr. Opin. Neurobiol. *21*, 880–887. https://doi.org/10.1016/j.conb.2011.10.012.
19. Yosipovitch, G., Greaves, M.W., and Schmelz, M. (2003). Itch. Lancet *361*, 690–694. https://doi.org/10.1016/S0140-6736(03)12570-6.
20. Liu, H., Archer, N.K., Dillen, C.A., Wang, Y., Ashbaugh, A.G., Ortines, R.V., Kao, T., Lee, S.K., Cai, S.S., Miller, R.J., et al. (2017). Staphylococcus aureus epicutaneous exposure drives skin inflammation via IL-36-mediated T cell responses. Cell Host Microbe *22*, 653–666.e5. https://doi.org/10.1016/j.chom.2017.10.006.
21. Patrick, G.J., Liu, H., Alphonse, M.P., Dikeman, D.A., Youn, C., Otterson, J.C., Wang, Y., Ravipati, A., Mazhar, M., Denny, G., et al. (2021). Epicutaneous Staphylococcus aureus induces IL-36 to enhance IgE production and ensuing allergic disease. J. Clin. Invest. *131*. https://doi.org/10.1172/JCI143334.
22. Nakatsuji, T., Hata, T.R., Tong, Y., Cheng, J.Y., Shafiq, F., Butcher, A.M., Salem, S.S., Brinton, S.L., Rudman Spergel, A.K., Johnson, K., et al. (2021). Development of a human skin commensal microbe for bacteriotherapy of atopic dermatitis and use in a phase 1 randomized clinical trial. Nat. Med. *27*, 700–709. https://doi.org/10.1038/s41591-021-01256-2.
23. Nakagawa, S., Matsumoto, M., Katayama, Y., Oguma, R., Wakabayashi, S., Nygaard, T., Saijo, S., Inohara, N., Otto, M., Matsue, H., et al. (2017). Staphylococcus aureus virulent PSMα peptides induce keratinocyte alarmin release to orchestrate IL-17-dependent skin inflammation. Cell Host Microbe *22*, 667–677.e5. https://doi.org/10.1016/j.chom.2017.10.008.
24. Moran, G.J., Krishnadasan, A., Gorwitz, R.J., Fosheim, G.E., McDougal, L.K., Carey, R.B., and Talan, D.A.; EMERGEncy ID Net Study Group (2006). Methicillin-resistant S. aureus infections among patients in the emergency department. N. Engl. J. Med. *355*, 666–674. https://doi.org/10.1056/NEJMoa055356.
25. Andersen, H.H., Akiyama, T., Nattkemper, L.A., van Laarhoven, A., Elberling, J., Yosipovitch, G., and Arendt-Nielsen, L. (2018). Alloknesis and hyperknesis-mechanisms, assessment methodology, and clinical implications of itch sensitization. Pain *159*, 1185–1197. https://doi.org/10.1097/j.pain.0000000000001220.
26. Ikoma, A., Fartasch, M., Heyer, G., Miyachi, Y., Handwerker, H., and Schmelz, M. (2004). Painful stimuli evoke itch in patients with chronic pruritus: central sensitization for itch. Neurology *62*, 212–217. https://doi.org/10.1212/wnl.62.2.212.
27. Feng, J., Luo, J., Yang, P., Du, J., Kim, B.S., and Hu, H. (2018). Piezo2 channel-Merkel cell signaling modulates the conversion of touch to itch. Science *360*, 530–533. https://doi.org/10.1126/science.aar5703.
28. Akiyama, T., Carstens, M.I., Ikoma, A., Cevikbas, F., Steinhoff, M., and Carstens, E. (2012). Mouse model of touch-evoked itch (alloknesis). J. Invest. Dermatol. *132*, 1886–1891. https://doi.org/10.1038/jid.2012.52.
29. Takanami, K., Uta, D., Matsuda, K.I., Kawata, M., Carstens, E., Sakamoto, T., and Sakamoto, H. (2021). Estrogens influence female itch sensitivity via the spinal gastrin-releasing peptide receptor neurons. Proc. Natl. Acad. Sci. USA *118*. https://doi.org/10.1073/pnas.2103536118.
30. Rimoin, L.P., Kwatra, S.G., and Yosipovitch, G. (2013). Female-specific pruritus from childhood to postmenopause: clinical features, hormonal factors, and treatment considerations. Dermatol. Ther. *26*, 157–167. https://doi.org/10.1111/dth.12034.
31. Adams, S.C., Garner, J.P., Felt, S.A., Geronimo, J.T., and Chu, D.K. (2016). A "Pedi" cures all: toenail trimming and the treatment of ulcerative dermatitis in mice. PLoS One *11*, e0144871. https://doi.org/10.1371/journal.pone.0144871.
32. Dong, X., and Dong, X. (2018). Peripheral and central mechanisms of itch. Neuron *98*, 482–494. https://doi.org/10.1016/j.neuron.2018.03.023.
33. Oetjen, L.K., Mack, M.R., Feng, J., Whelan, T.M., Niu, H., Guo, C.J., Chen, S., Trier, A.M., Xu, A.Z., Tripathi, S.V., et al. (2017). Sensory neurons co-opt classical immune signaling pathways to mediate chronic itch. Cell *171*, 217–228.e13. https://doi.org/10.1016/j.cell.2017.08.006.
34. Siracusa, M.C., Kim, B.S., Spergel, J.M., and Artis, D. (2013). Basophils and allergic inflammation; quiz 788. J. Allergy Clin. Immunol. *132*, 789–801. https://doi.org/10.1016/j.jaci.2013.07.046.
35. Obata, K., Mukai, K., Tsujimura, Y., Ishiwata, K., Kawano, Y., Minegishi, Y., Watanabe, N., and Karasuyama, H. (2007). Basophils are essential initiators of a novel type of chronic allergic inflammation. Blood *110*, 913–920. https://doi.org/10.1182/blood-2007-01-068718.
36. Garcovich, S., Maurelli, M., Gisondi, P., Peris, K., Yosipovitch, G., and Girolomoni, G. (2021). Pruritus as a distinctive feature of type 2 inflammation. Vaccines (Basel) *9*. https://doi.org/10.3390/vaccines9030303.
37. Silva, C.R., Melo, B.M.S., Silva, J.R., Lopes, A.H., Pereira, J.A., Cecilio, N.T., Berlink, J., Souza, G.G., Lucas, G., Vogl, T., et al. (2020). S100A9 plays a pivotal role in a mouse model of herpetic neuralgia via TLR4/TNF pathway. Brain Behav. Immun. *88*, 353–362. https://doi.org/10.1016/j.bbi.2020.03.033.

38. Shinkai, Y., Rathbun, G., Lam, K.P., Oltz, E.M., Stewart, V., Mendelsohn, M., Charron, J., Datta, M., Young, F., and Stall, A.M. (1992). RAG-2-deficient mice lack mature lymphocytes owing to inability to initiate V(D)J rearrangement. Cell *68*, 855–867. https://doi.org/10.1016/0092-8674(92)90029-c.

39. Cao, X., Shores, E.W., Hu-Li, J., Anver, M.R., Kelsall, B.L., Russell, S.M., Drago, J., Noguchi, M., Grinberg, A., and Bloom, E.T. (1995). Defective lymphoid development in mice lacking expression of the common cytokine receptor gamma chain. Immunity *2*, 223–238. https://doi.org/10.1016/1074-7613(95)90047-0.

40. Garibyan, L., Rheingold, C.G., and Lerner, E.A. (2013). Understanding the pathophysiology of itch. Dermatol. Ther. *26*, 84–91. https://doi.org/10.1111/dth.12025.

41. Akopian, A.N., Sivilotti, L., and Wood, J.N. (1996). A tetrodotoxin-resistant voltage-gated sodium channel expressed by sensory neurons. Nature *379*, 257–262. https://doi.org/10.1038/379257a0.

42. Sangameswaran, L., Delgado, S.G., Fish, L.M., Koch, B.D., Jakeman, L.B., Stewart, G.R., Sze, P., Hunter, J.C., Eglen, R.M., and Herman, R.C. (1996). Structure and function of a novel voltage-gated, tetrodotoxin-resistant sodium channel specific to sensory neurons. J. Biol. Chem. *271*, 5953–5956. https://doi.org/10.1074/jbc.271.11.5953.

43. Jenul, C., and Horswill, A.R. (2019). Regulation of Staphylococcus aureus virulence. Microbiol. Spectr. *7*. https://doi.org/10.1128/microbiolspec.GPP3-0031-2018.

44. Mack, M.R., and Kim, B.S. (2018). The itch-scratch cycle: a neuroimmune perspective. Trends Immunol. *39*, 980–991. https://doi.org/10.1016/j.it.2018.10.001.

45. Akiyama, T., Lerner, E.A., and Carstens, E. (2015). Protease-activated receptors and itch. Handb. Exp. Pharmacol. *226*, 219–235. https://doi.org/10.1007/978-3-662-44605-8_13.

46. Gimza, B.D., Jackson, J.K., Frey, A.M., Budny, B.G., Chaput, D., Rizzo, D.N., and Shaw, L.N. (2021). Unraveling the impact of secreted proteases on hypervirulence in Staphylococcus aureus. mBio *12*. https://doi.org/10.1128/mBio.03288-20.

47. Wörmann, M.E., Reichmann, N.T., Malone, C.L., Horswill, A.R., and Gründling, A. (2011). Proteolytic cleavage inactivates the Staphylococcus aureus lipoteichoic acid synthase. J. Bacteriol. *193*, 5279–5291. https://doi.org/10.1128/JB.00369-11.

48. Williams, M.R., Costa, S.K., Zaramela, L.S., Khalil, S., Todd, D.A., Winter, H.L., Sanford, J.A., O'Neill, A.M., Liggins, M.C., Nakatsuji, T., et al. (2019). Quorum sensing between bacterial species on the skin protects against epidermal injury in atopic dermatitis. Sci. Transl. Med. *11*. https://doi.org/10.1126/scitranslmed.aat8329.

49. Rice, K., Peralta, R., Bast, D., de Azavedo, J., and McGavin, M.J. (2001). Description of staphylococcus serine protease (ssp) operon in Staphylococcus aureus and nonpolar inactivation of sspA-encoded serine protease. Infect. Immun. *69*, 159–169. https://doi.org/10.1128/IAI.69.1.159-169.2001.

50. Shimada, S.G., and LaMotte, R.H. (2008). Behavioral differentiation between itch and pain in mouse. Pain *139*, 681–687. https://doi.org/10.1016/j.pain.2008.08.002.

51. Yamanoi, Y., Kittaka, H., and Tominaga, M. (2019). Cheek injection model for simultaneous measurement of pain and itch-related behaviors. J. Vis. Exp. https://doi.org/10.3791/58943.

52. Chandrabalan, A., and Ramachandran, R. (2021). Molecular mechanisms regulating Proteinase-Activated Receptors (PARs). FEBS Journal *288*, 2697–2726. https://doi.org/10.1111/febs.15829.

53. Coughlin, S.R. (2000). Thrombin signalling and protease-activated receptors. Nature *407*, 258–264. https://doi.org/10.1038/35025229.

54. Coughlin, S.R. (2005). Protease-activated receptors in hemostasis, thrombosis and vascular biology. J. Thromb. Haemost. *3*, 1800–1814. https://doi.org/10.1111/j.1538-7836.2005.01377.x.

55. Nakanishi-Matsui, M., Zheng, Y.W., Sulciner, D.J., Weiss, E.J., Ludeman, M.J., and Coughlin, S.R. (2000). PAR3 is a cofactor for PAR4 activation by thrombin. Nature *404*, 609–613. https://doi.org/10.1038/35007085.

56. Chandrabalan, A., Firth, A., Litchfield, R.B., Appleton, C.T., Getgood, A., and Ramachandran, R. (2020). Identification of Proteinase Activated Receptor (PAR) cleaving enzymes in human osteoarthritis knee joint synovial fluids. Preprint at bioRxiv.. https://doi.org/10.1101/2020.10.21.336693.

57. Markert, Y., Köditz, J., Ulbrich-Hofmann, R., and Arnold, U. (2003). Proline versus charge concept for protein stabilization against proteolytic attack. Protein Eng. *16*, 1041–1046. https://doi.org/10.1093/protein/gzg136.

58. Martin, L., Augé, C., Boué, J., Buresi, M.C., Chapman, K., Asfaha, S., Andrade-Gordon, P., Steinhoff, M., Cenac, N., Dietrich, G., et al. (2009). Thrombin receptor: an endogenous inhibitor of inflammatory pain, activating opioid pathways. Pain *146*, 121–129. https://doi.org/10.1016/j.pain.2009.07.016.

59. Desormeaux, C., Bautzova, T., Garcia-Caraballo, S., Rolland, C., Barbaro, M.R., Brierley, S.M., Barbara, G., Vergnolle, N., and Cenac, N. (2018). Protease-activated receptor 1 is implicated in irritable bowel syndrome mediators-induced signaling to thoracic human sensory neurons. Pain *159*, 1257–1267. https://doi.org/10.1097/j.pain.0000000000001208.

60. Bahou, W.F., Nierman, W.C., Durkin, A.S., Potter, C.L., and Demetrick, D.J. (1993). Chromosomal assignment of the human thrombin receptor gene: localization to region q13 of chromosome 5. Blood *82*, 1532–1537.

61. Zeisel, A., Hochgerner, H., Lönnerberg, P., Johnsson, A., Memic, F., van der Zwan, J., Häring, M., Braun, E., Borm, L.E., La Manno, G., et al. (2018). Molecular architecture of the mouse nervous system. Cell *174*, 999–1014.e22. https://doi.org/10.1016/j.cell.2018.06.021.

62. Hill, R.Z., Morita, T., Brem, R.B., and Bautista, D.M. (2018). S1PR3 mediates itch and pain via distinct TRP channel-dependent pathways. J. Neurosci. *38*, 7833–7843. https://doi.org/10.1523/JNEUROSCI.1266-18.2018.

63. Akiyama, T., and Carstens, E. (2013). Neural processing of itch. Neuroscience *250*, 697–714. https://doi.org/10.1016/j.neuroscience.2013.07.035.

64. Goswami, S.C., Thierry-Mieg, D., Thierry-Mieg, J., Mishra, S., Hoon, M.A., Mannes, A.J., and Iadarola, M.J. (2014). Itch-associated peptides: RNA-Seq and bioinformatic analysis of natriuretic precursor peptide B and gastrin releasing peptide in dorsal root and trigeminal ganglia, and the spinal cord. Mol. Pain *10*, 44. https://doi.org/10.1186/1744-8069-10-44.

65. Tavares-Ferreira, D., Shiers, S., Ray, P.R., Wangzhou, A., Jeevakumar, V., Sankaranarayanan, I., Cervantes, A.M., Reese, J.C., Chamessian, A., Copits, B.A., et al. (2022). Spatial transcriptomics of dorsal root ganglia identifies molecular signatures of human nociceptors. Sci. Transl. Med. *14*, eabj8186. https://doi.org/10.1126/scitranslmed.abj8186.

66. Kunitz, M. (1947). Isolation of a crystalline protein compound of trypsin and of soybean trypsin-inhibitor. J. Gen. Physiol. *30*, 311–320. https://doi.org/10.1085/jgp.30.4.311.

67. Frydrych, I., and Mlejnek, P. (2008). Serine protease inhibitors N-alpha-tosyl-L-lysinyl-chloromethylketone (TLCK) and N-tosyl-L-phenylalaninyl-chloromethylketone (TPCK) are potent inhibitors of activated caspase proteases. J. Cell. Biochem. *103*, 1646–1656. https://doi.org/10.1002/jcb.21550.

68. Chackalamannil, S., Wang, Y., Greenlee, W.J., Hu, Z., Xia, Y., Ahn, H.S., Boykow, G., Hsieh, Y., Palamanda, J., Agans-Fantuzzi, J., et al. (2008). Discovery of a novel, orally active himbacine-based thrombin receptor antagonist (SCH 530348) with potent antiplatelet activity. J. Med. Chem. *51*, 3061–3064. https://doi.org/10.1021/jm800180e.

69. Liu, Q., and Dong, X. (2015). The role of the Mrgpr receptor family in itch. Handb. Exp. Pharmacol. *226*, 71–88. https://doi.org/10.1007/978-3-662-44605-8_5.

70. Zhao, J., Munanairi, A., Liu, X.Y., Zhang, J., Hu, L., Hu, M., Bu, D., Liu, L., Xie, Z., Kim, B.S., et al. (2020). PAR2 mediates itch via TRPV3 signaling in keratinocytes. J. Invest. Dermatol. *140*, 1524–1532. https://doi.org/10.1016/j.jid.2020.01.012.

71. Warwick, C., Cassidy, C., Hachisuka, J., Wright, M.C., Baumbauer, K.M., Adelman, P.C., Lee, K.H., Smith, K.M., Sheahan, T.D., Ross, S.E., et al. (2021). MrgprdCre lineage neurons mediate optogenetic allodynia through an emergent polysynaptic circuit. Pain *162*, 2120–2131. https://doi.org/10.1097/j.pain.0000000000002227.

72. Tantry, U.S., Bliden, K.P., Chaudhary, R., Novakovic, M., Rout, A., and Gurbel, P.A. (2020). Vorapaxar in the treatment of cardiovascular diseases. Future Cardiol. *16*, 373–384. https://doi.org/10.2217/fca-2019-0090.

73. Gupta, N., Liu, R., Shin, S., Sinha, R., Pogliano, J., Pogliano, K., Griffin, J.H., Nizet, V., and Corriden, R. (2018). SCH79797 improves outcomes in experimental bacterial pneumonia by boosting neutrophil killing and direct antibiotic activity. J. Antimicrob. Chemother. *73*, 1586–1594. https://doi.org/10.1093/jac/dky033.

74. Martin, J.K., 2nd, Sheehan, J.P., Bratton, B.P., Moore, G.M., Mateus, A., Li, S.H., Kim, H., Rabinowitz, J.D., Typas, A., Savitski, M.M., et al. (2020). A dual-mechanism antibiotic kills Gram-negative bacteria and avoids drug resistance. Cell *181*, 1518–1532.e14. https://doi.org/10.1016/j.cell.2020.05.005.

75. Prasad, L., Leduc, Y., Hayakawa, K., and Delbaere, L.T. (2004). The structure of a universally employed enzyme: V8 protease from Staphylococcus aureus. Acta Crystallogr. D Biol. Crystallogr. *60*, 256–259. https://doi.org/10.1107/S090744490302599X.

76. Wang, B., McHugh, B.J., Qureshi, A., Campopiano, D.J., Clarke, D.J., Fitzgerald, J.R., Dorin, J.R., Weller, R., and Davidson, D.J. (2017). IL-1β-induced protection of keratinocytes against Staphylococcus aureus-secreted proteases is mediated by human β-defensin 2. J. Invest. Dermatol. *137*, 95–105. https://doi.org/10.1016/j.jid.2016.08.025.

77. Iida, H., Takai, T., Hirasawa, Y., Kamijo, S., Shimura, S., Ochi, H., Nishioka, I., Maruyama, N., Ogawa, H., Okumura, K., et al. (2014). Epicutaneous administration of papain induces IgE and IgG responses in a cysteine protease activity-dependent manner. Allergol. Int. *63*, 219–226. https://doi.org/10.2332/allergolint.13-OA-0621.

78. Poh, S.E., Koh, W.L.C., Lim, S.Y.D., Wang, E.C.E., Yew, Y.W., Common, J.E.A., Oon, H.H., and Li, H. (2022). Expression of Staphylococcus aureus virulence factors in atopic dermatitis. JID Innov. *2*, 100130. https://doi.org/10.1016/j.xjidi.2022.100130.

79. Kot, B., Piechota, M., Jakubczak, A., Gryzińska, M., Witeska, M., Grużewska, A., Baran, K., and Denkiewicz, P. (2022). The prevalence of virulence determinants in methicillin-resistant Staphylococcus aureus isolated from different infections in hospitalized patients in Poland. Sci. Rep. *12*, 5477. https://doi.org/10.1038/s41598-022-09517-x.

80. Khan, S., Marasa, B.S., Sung, K., and Nawaz, M. (2021). Genotypic characterization of clinical isolates of Staphylococcus aureus from Pakistan. Pathogens *10*. https://doi.org/10.3390/pathogens10080918.

81. Ziebandt, A.K., Kusch, H., Degner, M., Jaglitz, S., Sibbald, M.J., Arends, J.P., Chlebowicz, M.A., Albrecht, D., Pantucek, R., Doskar, J., et al. (2010). Proteomics uncovers extreme heterogeneity in the Staphylococcus aureus exoproteome due to genomic plasticity and variant gene regulation. Proteomics *10*, 1634–1644. https://doi.org/10.1002/pmic.200900313.

82. Meyer, T.C., Michalik, S., Holtfreter, S., Weiss, S., Friedrich, N., Völzke, H., Kocher, T., Kohler, C., Schmidt, F., Bröker, B.M., et al. (2021). A comprehensive view on the human antibody repertoire against Staphylococcus aureus antigens in the general population. Front. Immunol. *12*, 651619. https://doi.org/10.3389/fimmu.2021.651619.

83. Radke, E.E., Brown, S.M., Pelzek, A.J., Fulmer, Y., Hernandez, D.N., Torres, V.J., Thomsen, I.P., Chiang, W.K., Miller, A.O., Shopsin, B., et al. (2018). Hierarchy of human IgG recognition within the Staphylococcus aureus immunome. Sci. Rep. *8*, 13296. https://doi.org/10.1038/s41598-018-31424-3.

84. Nho, Y., Lawson, K., Banovic, F., and Han, L. (2022). Staphylococcus aureus phenol-soluble modulins induce itch sensation. J. Dermatol. Sci. *107*, 48–51. https://doi.org/10.1016/j.jdermsci.2022.07.002.

85. Bao, C., Chen, O., Sheng, H., Zhang, J., Luo, Y., Hayes, B.W., Liang, H., Liedtke, W., Ji, R.R., and Abraham, S.N. (2023). A mast cell-thermoregulatory neuron circuit axis regulates hypothermia in anaphylaxis. Sci. Immunol. *8*, eadc9417. https://doi.org/10.1126/sciimmunol.adc9417.

86. Stefansson, K., Brattsand, M., Roosterman, D., Kempkes, C., Bocheva, G., Steinhoff, M., and Egelrud, T. (2008). Activation of proteinase-activated receptor-2 by human kallikrein-related peptidases. J. Invest. Dermatol. *128*, 18–25. https://doi.org/10.1038/sj.jid.5700965.

87. Frateschi, S., Camerer, E., Crisante, G., Rieser, S., Membrez, M., Charles, R.P., Beermann, F., Stehle, J.C., Breiden, B., Sandhoff, K., et al. (2011). PAR2 absence completely rescues inflammation and ichthyosis caused by altered CAP1/Prss8 expression in mouse skin. Nat. Commun. *2*, 161. https://doi.org/10.1038/ncomms1162.

88. Steinhoff, M., Neisius, U., Ikoma, A., Fartasch, M., Heyer, G., Skov, P.S., Luger, T.A., and Schmelz, M. (2003). Proteinase-activated receptor-2 mediates itch: a novel pathway for pruritus in human skin. J. Neurosci. *23*, 6176–6180. https://doi.org/10.1523/JNEUROSCI.23-15-06176.2003.

89. Williams, M.R., Nakatsuji, T., Sanford, J.A., Vrbanac, A.F., and Gallo, R.L. (2017). Staphylococcus aureus induces increased serine protease activity in keratinocytes. J. Invest. Dermatol. *137*, 377–384. https://doi.org/10.1016/j.jid.2016.10.008.

90. Chua, W., Poh, S.E., and Li, H. (2022). Secretory proteases of the human skin microbiome. Infect. Immun. *90*, e0039721. https://doi.org/10.1128/IAI.00397-21.

91. Cau, L., Williams, M.R., Butcher, A.M., Nakatsuji, T., Kavanaugh, J.S., Cheng, J.Y., Shafiq, F., Higbee, K., Hata, T.R., Horswill, A.R., et al. (2021). Staphylococcus epidermidis protease EcpA can be a deleterious component of the skin microbiome in atopic dermatitis. J. Allergy Clin. Immunol. *147*, 955–966.e16. https://doi.org/10.1016/j.jaci.2020.06.024.

92. Lukomski, S., Montgomery, C.A., Rurangirwa, J., Geske, R.S., Barrish, J.P., Adams, G.J., and Musser, J.M. (1999). Extracellular cysteine protease produced by Streptococcus pyogenes participates in the pathogenesis of invasive skin infection and dissemination in mice. Infect. Immun. *67*, 1779–1788. https://doi.org/10.1128/IAI.67.4.1779-1788.1999.

93. Baral, P., Udit, S., and Chiu, I.M. (2019). Pain and immunity: implications for host defence. Nat. Rev. Immunol. *19*, 433–447. https://doi.org/10.1038/s41577-019-0147-2.

94. Sorkin, L.S., Eddinger, K.A., Woller, S.A., and Yaksh, T.L. (2018). Origins of antidromic activity in sensory afferent fibers and neurogenic inflammation. Semin. Immunopathol. *40*, 237–247. https://doi.org/10.1007/s00281-017-0669-2.

95. Chiu, I.M., von Hehn, C.A., and Woolf, C.J. (2012). Neurogenic inflammation and the peripheral nervous system in host defense and immunopathology. Nat. Neurosci. *15*, 1063–1067. https://doi.org/10.1038/nn.3144.

96. Souza-Moreira, L., Campos-Salinas, J., Caro, M., and Gonzalez-Rey, E. (2011). Neuropeptides as pleiotropic modulators of the immune response. Neuroendocrinology *94*, 89–100. https://doi.org/10.1159/000328636.

97. de Garavilla, L., Vergnolle, N., Young, S.H., Ennes, H., Steinhoff, M., Ossovskaya, V.S., D'Andrea, M.R., Mayer, E.A., Wallace, J.L., Hollenberg, M.D., et al. (2001). Agonists of proteinase-activated receptor 1 induce plasma extravasation by a neurogenic mechanism. Br. J. Pharmacol. *133*, 975–987. https://doi.org/10.1038/sj.bjp.0704152.

98. Ruhl, C.R., Pasko, B.L., Khan, H.S., Kindt, L.M., Stamm, C.E., Franco, L.H., Hsia, C.C., Zhou, M., Davis, C.R., Qin, T., et al. (2020). Mycobacterium tuberculosis Sulfolipid-1 activates nociceptive neurons and induces cough. Cell *181*, 293–305.e11. e211. https://doi.org/10.1016/j.cell.2020.02.026.

99. Bennett, C.F., Kordasiewicz, H.B., and Cleveland, D.W. (2021). Antisense drugs make sense for neurological diseases. Annu. Rev. Pharmacol. Toxicol. *61*, 831–852. https://doi.org/10.1146/annurev-pharmtox-010919-023738.

100. Halvorsen, J.A., Dalgard, F., Thoresen, M., Bjertness, E., and Lien, L. (2012). Itch and pain in adolescents are associated with suicidal ideation: a population-based cross-sectional study. Acta Derm. Venereol. *92*, 543–546. https://doi.org/10.2340/00015555-1251.

101. Schneider, G., Driesch, G., Heuft, G., Evers, S., Luger, T.A., and Ständer, S. (2006). Psychosomatic cofactors and psychiatric comorbidity in patients with chronic itch. Clin. Exp. Dermatol. *31*, 762–767. https://doi.org/10.1111/j.1365-2230.2006.02211.x.

102. Frey, A.M., Chaput, D., and Shaw, L.N. (2021). Insight into the human pathodegradome of the V8 protease from Staphylococcus aureus. Cell Rep. *35*, 108930. https://doi.org/10.1016/j.celrep.2021.108930.

103. Motta, J.P., Denadai-Souza, A., Sagnat, D., Guiraud, L., Edir, A., Bonnart, C., Sebbag, M., Rousset, P., Lapeyre, A., Seguy, C., et al. (2019). Active thrombin produced by the intestinal epithelium controls mucosal biofilms. Nat. Commun. *10*, 3224. https://doi.org/10.1038/s41467-019-11140-w.

104. Maurer, K., Reyes-Robles, T., Alonzo, F., 3rd, Durbin, J., Torres, V.J., and Cadwell, K. (2015). Autophagy mediates tolerance to Staphylococcus aureus alpha-toxin. Cell Host Microbe *17*, 429–440. https://doi.org/10.1016/j.chom.2015.03.001.

105. Joo, H.S., Cheung, G.Y., and Otto, M. (2011). Antimicrobial activity of community-associated methicillin-resistant Staphylococcus aureus is caused by phenol-soluble modulin derivatives. J. Biol. Chem. *286*, 8933–8940. https://doi.org/10.1074/jbc.M111.221382.

106. Austin, C.M., Garabaglu, S., Krute, C.N., Ridder, M.J., Seawell, N.A., Markiewicz, M.A., Boyd, J.M., and Bose, J.L. (2019). Contribution of YjbIH to virulence factor expression and host colonization in Staphylococcus aureus. Infect. Immun. *87*. https://doi.org/10.1128/IAI.00155-19.

107. Boucher, A.A., Rosenfeldt, L., Mureb, D., Shafer, J., Sharma, B.K., Lane, A., Crowther, R.R., McKell, M.C., Whitt, J., Alenghat, T., et al. (2020). Cell type-specific mechanisms coupling protease-activated receptor-1 to infectious colitis pathogenesis. J. Thromb. Haemost. *18*, 91–103. https://doi.org/10.1111/jth.14641.

108. Liu, Q., Tang, Z., Surdenikova, L., Kim, S., Patel, K.N., Kim, A., Ru, F., Guan, Y., Weng, H.J., Geng, Y., et al. (2009). Sensory neuron-specific GPCR Mrgprs are itch receptors mediating chloroquine-induced pruritus. Cell *139*, 1353–1365. https://doi.org/10.1016/j.cell.2009.11.034.

109. Nassar, M.A., Stirling, L.C., Forlani, G., Baker, M.D., Matthews, E.A., Dickenson, A.H., and Wood, J.N. (2004). Nociceptor-specific gene deletion reveals a major role for Nav1.7 (PN1) in acute and inflammatory pain. Proc. Natl. Acad. Sci. USA *101*, 12706–12711. https://doi.org/10.1073/pnas.0404915101.

110. Luong, T.T., and Lee, C.Y. (2007). Improved single-copy integration vectors for Staphylococcus aureus. J. Microbiol. Methods *70*, 186–190. https://doi.org/10.1016/j.mimet.2007.04.007.

111. Crosby, H.A., Schlievert, P.M., Merriman, J.A., King, J.M., Salgado-Pabón, W., and Horswill, A.R. (2016). The Staphylococcus aureus global regulator MgrA modulates clumping and virulence by controlling surface protein expression. PLoS Pathog. *12*, e1005604. https://doi.org/10.1371/journal.ppat.1005604.

112. Madisen, L., Zwingman, T.A., Sunkin, S.M., Oh, S.W., Zariwala, H.A., Gu, H., Ng, L.L., Palmiter, R.D., Hawrylycz, M.J., Jones, A.R., et al. (2010). A robust and high-throughput Cre reporting and characterization system for the whole mouse brain. Nat. Neurosci. *13*, 133–140. https://doi.org/10.1038/nn.2467.

113. Hou, B., Reizis, B., and DeFranco, A.L. (2008). Toll-like receptors activate innate and adaptive immunity by using dendritic cell-intrinsic and -extrinsic mechanisms. Immunity *29*, 272–282. https://doi.org/10.1016/j.immuni.2008.05.016.

114. Schmidlin, F., Amadesi, S., Dabbagh, K., Lewis, D.E., Knott, P., Bunnett, N.W., Gater, P.R., Geppetti, P., Bertrand, C., and Stevens, M.E. (2002). Protease-activated receptor 2 mediates eosinophil infiltration and hyperreactivity in allergic inflammation of the airway. J. Immunol. *169*, 5315–5321. https://doi.org/10.4049/jimmunol.169.9.5315.

115. Valtcheva, M.V., Copits, B.A., Davidson, S., Sheahan, T.D., Pullen, M.Y., McCall, J.G., Dikranian, K., and Gereau, R.W.t. (2016). Surgical extraction of human dorsal root ganglia from organ donors and preparation of primary sensory neuron cultures. Nat. Protoc. *11*, 1877–1888. https://doi.org/10.1038/nprot.2016.111.

116. Monk, I.R., Shah, I.M., Xu, M., Tan, M.W., and Foster, T.J. (2012). Transforming the untransformable: application of direct transformation to manipulate genetically Staphylococcus aureus and Staphylococcus epidermidis. mBio *3*. https://doi.org/10.1128/mBio.00277-11.

117. Mootz, J.M., Malone, C.L., Shaw, L.N., and Horswill, A.R. (2013). Staphopains modulate Staphylococcus aureus biofilm integrity. Infect. Immun. *81*, 3227–3238. https://doi.org/10.1128/IAI.00377-13.

118. Deng, L., Schilcher, K., Burcham, L.R., Kwiecinski, J.M., Johnson, P.M., Head, S.R., Heinrichs, D.E., Horswill, A.R., and Doran, K.S. (2019). Identification of key determinants of Staphylococcus aureus vaginal colonization. mBio *10*. https://doi.org/10.1128/mBio.02321-19.

119. VanDrisse, C.M., and Escalante-Semerena, J.C. (2016). New high-cloning-efficiency vectors for complementation studies and recombinant protein overproduction in Escherichia coli and Salmonella enterica. Plasmid *86*, 1–6. https://doi.org/10.1016/j.plasmid.2016.05.001.

120. Nesvizhskii, A.I., Keller, A., Kolker, E., and Aebersold, R. (2003). A statistical model for identifying proteins by tandem mass spectrometry. Anal Chem. *75*, 4646–4658. https://doi.org/10.1021/ac0341261.

121. DuBreuil, D.M., Chiang, B.M., Zhu, K., Lai, X., Flynn, P., Sapir, Y., and Wainger, B.J. (2021). A high-content platform for physiological profiling and unbiased classification of individual neurons. Cell Rep. Methods *1*. https://doi.org/10.1016/j.crmeth.2021.100004.

122. Yousuf, M.S., Samtleben, S., Lamothe, S.M., Friedman, T.N., Catuneanu, A., Thorburn, K., Desai, M., Tenorio, G., Schenk, G.J., Ballanyi, K., et al. (2020). Endoplasmic reticulum stress in the dorsal root ganglia regulates large-conductance potassium channels and contributes to pain in a model of multiple sclerosis. FASEB J. *34*, 12577–12598. https://doi.org/10.1096/fj.202001163R.

123. Voisin, T., Perner, C., Messou, M.A., Shiers, S., Ualiyeva, S., Kanaoka, Y., Price, T.J., Sokol, C.L., Bankova, L.G., Austen, K.F., et al. (2021). The CysLT(2)R receptor mediates leukotriene C4-driven acute and chronic itch. Proc. Natl. Acad. Sci. USA *118*. https://doi.org/10.1073/pnas.2022087118.

124. Mihara, K., Ramachandran, R., Renaux, B., Saifeddine, M., and Hollenberg, M.D. (2013). Neutrophil elastase and proteinase-3 trigger G protein-biased signaling through proteinase-activated receptor-1 (PAR1). J. Biol. Chem. *288*, 32979–32990. https://doi.org/10.1074/jbc.M113.483123.

STAR★METHODS

KEY RESOURCES TABLE

REAGENT or RESOURCE	SOURCE	IDENTIFIER
Antibodies		
eBioscience™ Fixable Viability Dye eFluor™506	Thermo Fisher	Cat. # 65-0866-18
Alexa Fluor® 700 anti-mouse CD45 Antibody	Biolegend	Cat. # 103128; RRID:AB_493715
APC anti-mouse CD45 Antibody	Thermo Fisher	Cat. # 17-0451-82; RRID:AB_469392
CD11c Monoclonal Antibody, Biotin	Thermo Fisher	Cat. # 13-0114-85; RRID:AB_466364
F4/80 Monoclonal Antibody, FITC	Thermo Fisher	Cat. # 11-4801-82; RRID:AB_2637191
Ly-6G/Ly-6C Monoclonal Antibody, FITC	Biolegend	Cat. # 108406; RRID:AB_313370
CD3 Monoclonal Antibody, PerCP-eFluor 710	Thermo Fisher	Cat. # 46-0032-82; RRID:AB_1834427
CD117 (c-Kit) Monoclonal Antibody, APC	Thermo Fisher	Cat. # 17-1172-83; RRID:AB_469434
BV421 Rat Anti-Mouse IgE	BD Biosciences	Cat. # 564207; RRID:AB_2738668
Brilliant Violet 605™ anti-mouse CD4 Antibody	Biolegend	Cat. # 100548; RRID:AB_11125962
APC/Cyanine7 anti-mouse CD8a Antibody	Biolegend	Cat. # 100714; RRID:AB_312753
PE-CF594 Rat Anti-Mouse Siglec-F	BD Biosciences	Cat. # 562757; RRID:AB_2687994
TCR gamma/delta Monoclonal Antibody, PE	Thermo Fisher	Cat. # 12-5711-82; RRID:AB_465934
PE/Cyanine7 anti-mouse/human CD11b	Biolegend	Cat. # 101216; RRID:AB_312799
SAV-BV605	Biolegend	Cat. # 405229
Bacterial and virus strains		
Staphylococcus aureus CA-MRSA LAC/USA300	Chiu et. al.[12]	N/A
GFP-MRSA	Chiu et. al.[12]	N/A
MRSA Δ*agr*	Maurer et al.[104]	N/A
MRSA Δ*hla*	Maurer et al.[104]	N/A
MRSA ΔPsms (Δ*psmα* Δ*psmβ* Δ*hld*)	Joo et al.[105]	N/A
MRSA ΔProteases (Δ*aur* Δ*scpA* Δ*sspAB spl*::*Erm*)	Austin et al.[106]	N/A
MRSA Δ*aur*	Austin et al.[106]	N/A
MRSA Δ*scpA* Δ*sspB*	Austin et al.[106]	N/A
MRSA *spl*::*Erm*	Austin et al.[106]	N/A
MRSA Δ*sspA*	This study	N/A
MRSA Δ*sspA* + *sspA*	This study	N/A
E. coli BL21 (Novagen)	EMD Millipore	Cat. # 70235-3
Biological samples		
Human dorsal root ganglia	Southwest Transplant Alliance	N/A
Human skin swabs	University of California San Diego	Cau et al.[91]
Chemicals, peptides, and recombinant proteins		
Tryptic Soy Agar	BD Difco	Cat. #236920
Tryptic Soy Broth	Sigma	Cat. #T8907
CHROMagar Staph aureus	Hardy Diagnostics	Cat. #G311
Cefoxotin	Cayman Chemical Company	Cat. #15990
Terrific Broth	BD Difco	Cat. # BD 243820
Ampicillin	Sigma	Cat. #A9518
Chloramphenicol	Sigma	Cat. #C0857
Isopropyl β-D-1-thiogalactopyranoside	Sigma	Cat. #I6758
RNA Protect Bacteria Reagent	Qiagen	Cat. #76506
Beta-mercaptoethanol	Sigma	Cat. #63689
V8 protease	Worthington	Cat. #LS003605

(*Continued on next page*)

Continued

REAGENT or RESOURCE	SOURCE	IDENTIFIER
Histamine	Sigma	Cat. #H7125
Capsaicin	Tocris	Cat. #0462
Sphingosine-1-phosphate	Tocris	Cat. #1370
Vorapaxar	Axon Med Chem	Cat. #17555
SCH79797 dihydrochloride	Tocris	Cat. #1592
BMS 986120	Cayman Chemicals	Cat. #23497
Keratinocyte serum-free medium	Gibco	Cat. #17005-042
Keratinocytes supplements	Gibco	Cat. #37000-015
Human recombinant epidermal growth factor	BD	Cat. #354052
Pierce Ni-NTA Magnetic Agarose Beads	Thermo Fisher	Cat. #78605
Collagenase A	Sigma	Cat. #10103586001
Dispase II	Sigma	Cat. #D4693
Neuralbasal^{Tm} Medium	Thermo Fisher	Cat. #21103049
B27 serum-free supplement	Invitrogen	Cat. #17504-044
L-Glutamine	Invitrogen	Cat. #25-030-081
Pen/Strep	Thermo Fisher	Cat. #15140122
Nerve growth factor	Invitrogen	Cat. #50385-MNAC-250
Fura-2-AM	Life Technologies	Cat. #F-1221
STEMxyme I	Worthington	Cat. #LS004106
DNAse I	Worthington	Cat. #LS002139
BrainPhys media	STEMCell	Cat. #0752
SM1	STEMCell	Cat. #05711
GlutaMax	Thermo Fisher	Cat. #35050061
Fluo-4-AM	Thermo Fisher	Cat. #F14201
Pluronic F-127	Thermo Fisher	Cat. #P3000MP
Ham's F-12	Gibco	Cat. #11765054
Fetal bovine Serum	R&D Systems	Cat. #S11150H
Geneticin™ selective antibiotic	Thermo Fisher	Cat. #10131035
DMEM	Gibco	Cat. #10313039
In Vivo JetPEI	Polyplus Transfection	Cat. #101000040
Critical commercial assays		
Pierce BCA Protein Assay	ThermoFisher	Cat. #23227
Direct-zol RNA MiniPrep Plus kit	Zymo Research	Cat. #R2071
iScript cDNA synthesis kit	Bio-Rad	Cat. #1708891
RNAscope Probe-Mm-F2r	Advanced Cell Diagnostics	Cat. #438511
RNAscope Probe-Mm-Tubb3-C2	Advanced Cell Diagnostics	Cat. #423391-C2
RNAscope Multiplex V2 kit	Advanced Cell Diagnostics	Cat. #323110
RNAscope Probe-Hs-F2R-C2	Advanced Cell Diagnostics	Cat. #471081-C2
RNAscope Probe-HS-TRPV1-C3	Advanced Cell Diagnostics	Cat. #415381-C3
RNAscope Probe-Hs-NPPB-C1	Advanced Cell Diagnostics	Cat. #448511
NucleoSpin RNA isolation kit	Macherey-Nagel	Cat. #740955.50
Deposited data		
Mouse nervous system transcriptomic data http://mousebrain.org/	Zeisel et al.[61]	NCBI SRA repository (SRP135960)
Human dorsal root ganglia transcriptomic data http://sensoryomics.com/	Tavares-Ferreira et al.[65]	dbGaP repository (phs001158)
Experimental models: Cell lines		
KERTr immortalized human keratinocytes	ATCC	CRL-2309

(*Continued on next page*)

Continued		
REAGENT or RESOURCE	SOURCE	IDENTIFIER
CHO-K1	ATCC	CCL-61
HEK-293	ATCC	CFL-1573
Experimental models: Organisms/strains		
C57/BL6NTac (Opportunist Free)	Taconic Biosciences	Strain #B6
C57/BL6J	JAX	Strain #000664
B6.Rosa26-stop(flox)- tdTomato	JAX	Strain #007914
B6.129P2(SJL)-*Myd88*$^{tm1.1Defr}$/J	JAX	Strain #009088
B6.Cg-*F2rl1*^{tm1Mslb}/J	JAX	Strain #004993
B6.Cg-*Kit*$^{W\text{-}sh}$	JAX	Strain #030764
B6.129-*Trpv1*$^{tm1(cre)Bbm}$/J strain	JAX	Strain #0017769
C57BL/6NTac.Cg-*Rag2*^{tm1Fwa} *Il2rg*^{tm1Wjl}	Taconic Biosciences	Strain #4111
F2r-flox	Boucher et al.[107]	N/A
Balbc/J	JAX	Strain #00651
BALB/c-*Il4ra*^{tm1Sz}/J	JAX	Strain #003514
Mrgpr knockout	Liu et al.[108]	N/A
Nav1.8-Cre	Nassar et al.[109]	N/A
B6.129S4-*F2r*^{tm1Ajc}/J	JAX	Strain #002862
Oligonucleotides		
sspA-F: ACCTGTAGCAACAATGTGGGA	Synthesized by Thermo Fisher	N/A
sspA-R: ATTTGGTACACCGCCCCAAT	Synthesized by Thermo Fisher	N/A
psmA1-F: GTATCATCGCTGGCATCA	Synthesized by Thermo Fisher	N/A
psmA1-R: AAGACCTCCTTTGTTTGTTATG	Synthesized by Thermo Fisher	N/A
hla-F: AGCAGCAGATAACTTCCT	Synthesized by Thermo Fisher	N/A
hla-R: TGGTAGTCATCACGAACT	Synthesized by Thermo Fisher	N/A
il31ra-F: CCCTGTGTTGTCCTGATGTTCCCA	Synthesized by Thermo Fisher	N/A
il31ra-R: ACCCTTTCCAGCTTCCTCTGTCAA	Synthesized by Thermo Fisher	N/A
f2r-F: CCTATGAGCGAGCCAGAATC	Synthesized by Thermo Fisher	N/A
f2r-R: TAGACTGCCCTACCCTCCAG	Synthesized by Thermo Fisher	N/A
Recombinant DNA		
Plasmid pLL29erm	Luong and Lee[110] Crosby et al.[111]	N/A
Software and algorithms		
FlowJo™ Software version 10.2	BD Life Sciences	www.flowjo.com
Graphpad Prism version 9.5.1	Graphpad	www.graphpad.com
LAS X Life Science Microscope Software	Leica	N/A
Other		
Stellaris 8 FALCON CFS confocal microscope	Leica	N/A
QuantStudio Real-Time PCR Instrument	Thermo Fisher	N/A
CFX96 Real-Time Detection System	Bio-Rad	N/A
LSR Fortessa flow cytometer	BD Biosciences	N/A
Eclipse Ti inverted microscope	Nikon	N/A
Zyla sCMOS camera	Andor	N/A

RESOURCE AVAILABILITY

Lead contact

Please direct requests for further information, resources, and reagents to the lead contact, Isaac Chiu (Isaac_chiu@hms.harvard.edu).

Materials availability

Bacterial strains generated in this study are available upon signing a materials transfer agreement (MTA).

Data and code availability

- Microscopy data, flow cytometry data, and mouse behavior recordings will be shared by the lead contact upon request. This paper analyzes existing, publicly available single cell RNA-seq data. These accession numbers for the datasets are listed in the key resources table.
- This study did not generate any sequencing data or original code.
- Any additional information required to reanalyze the data reported in this paper is available from the lead contact upon request.

EXPERIMENTAL MODEL AND STUDY PARTICIPANT DETAILS

Mice

All animal experiments were approved by the Institutional Animal Care and Use Committee (IACUC) at Harvard Medical School under protocol numbers IS000000543 and IS000000546 and were conducted in accordance with National Institutes of Health (NIH) animal research guidelines. Mice were bred and housed in individually ventilated micro-isolator cages within a full barrier, specific pathogen-free animal facility at Harvard Medical School under a 12h light/dark cycle with *ad libitum* access to food and water. Age-matched littermate male and female mice were used for experiments.

C57/BL6 mice that were free of rodent pathogens and *Staphylococcus aureus* were purchased from Taconic Biosciences. C57/BL6J mice, Ai14 strain B6.Rosa26-stop(flox)-tdTomato (#007914),[112] *Myd88* knockout strain B6.129P2(SJL)-*Myd88*$^{tm1.1Defr}$/J (#009088),[113] *F2rl1* knockout strain B6.Cg-*F2rl1*^{tm1Mslb}/J (#004993),[114] mast cell deficient B6.Cg-*Kit*$^{W\text{-}sh}$ mice (#030764), and Trpv1-Cre$^{+/+}$ B6.129-Trpv1$^{tm1(cre)Bbm}$/J strain (#017769) were obtained from the Jackson Laboratory (Bar Harbor, ME). Rag2$^{-/-}$/Il2rg$^{-/-}$ strain C57BL/6NTac.Cg-Rag2^{tm1Fwa} Il2rg^{tm1Wjl} was obtained from Taconic Biosciences. *F2r*-flox mice were generated previously.[107] Trpv1-Cre$^{+/+}$ mice were crossed with *F2r*-flox mice to generate *Trpv1*$^{\Delta F2r}$ mice. Balbc/J (#00651) and Il4ra$^{-/-}$ (#003514) strain BALB/c-Il4ra^{tm1Sz}/J were purchased from Jackson Laboratory (Bar Harbor, ME). *Mrgpr* knockout mice[108] were provided by Xinzhong Dong (Johns Hopkins University). *Nav1.8*-Cre mice[109] were provided by John Wood (University College London). *Nav1.8*-Cre$^{+/+}$ mice were crossed with Ai14 mice to generate Nav1.8^{tdTomato} mice. *F2r* knockout strain *B6.129S4-F2r*^{tm1Ajc}/J mice were obtained by recovery from cryopreservation from Jackson Laboratories (#002862).

Human subjects for skin swab collection

Experiments involving human subjects were done according to protocols approved by University of California, San Diego IRB (Project#140144). Written informed consent was obtained from all subjects. Swabs of surface microbiota from a 5 cm^2 area of the antecubital fossa skin of both left and right arms were collected from 14 healthy subjects and 13 patients with AD as previously described.[91] Demographic details including age, sex, and race are given in Table S3. For subjects with AD, swabs were collected from both lesional and non-lesional skin. Swabs were stored in tryptic soy broth (TSB) and 16.67% glycerol at -80°C with swab intact until follow-on analysis was performed.

Human DRG samples from organ donors

Human lumbar DRGs were obtained from organ donors in collaboration with Southwest Transplant Alliance, as previously described.[65] Demographic details including age, sex, and race are given in Table S3. Human DRGs were immediately frozen in pulverized dry-ice on-site for RNAscope analysis or immersed in N-methyl-D-glutamate-artificial cerebrospinal fluid (NMDG-aCSF) for subsequent calcium imaging experiments.[115] All tissue procurement procedures were approved by the institutional review board at University of Texas at Dallas.

METHOD DETAILS

Bacterial strains and culture

All procedures related to bacterial strains and infectious disease work were approved by the Committee on Microbiological Safety (COMS) at Harvard medical school and were conducted under Biosafety Level 2 protocols and guidelines. All *Staphylococcus aureus* strains used in this study are listed in the key resources table. Bacteria were grown in tryptic soy broth (TSB) at 37°C and growth was monitored by measuring the optical density at 600 nm (OD_{600}). *S. aureus* CA-MRSA strains LAC/USA300 (wildtype, WT) and GFP-MRSA are previously described.[12] Δ*agr* and Δ*hla* MRSA were obtained from Dr. Victor Torres.[104] The Δ*psmα* Δ*psmβ* Δ*hld* (ΔPsms) MRSA strain was a gift from Dr. Michael Otto.[105]

Deletions of aureolysin (Δ*aur*), staphopain A and staphopain B (Δ*scpA* Δ*sspB*) and SplA-F (Δ*spl::erm*) strains were generated as previously described.[106] The V8 protease deletion (Δ*sspA*) was generated using homologous recombination as previously described, resulting in an encoded small peptide MKGPR* in its place.[116] Complementation of Δ*sspA* was achieved by cloning *sspA* with 245 bp of the promoter sequence into a pLL29-derived vector where the tetracycline antibiotic resistance cassette was replaced with an

erythromycin resistance cassette (pLL29erm).[110,111] The resulting plasmid was integrated at the φ11 *attP* site in RN4220 using helper plasmid pLL2787 and moved into the Δ*sspA* strain by phage transduction. The resulting strains were PCR and sequence verified.

V8 protease activity assays

Activity assays for V8 protease were performed as previously described with some modifications.[117] Filtered supernatants were further concentrated with an Amicon Ultra-15 Centrifugal Filter (10 kDa cutoff), dialyzed in 20 mM Tris pH 7.4, and normalized to a protein concentration of 0.45 mg/mL by the Pierce BCA Protein Assay (ThermoFisher) before beginning the FRET assay.

Epicutaneous MRSA exposure and measurement of itch and inflammation

The murine model of epicutaneous *Staphylococcus aureus* exposure was adapted from Liu et al.[20] and Nakagawa et al.[23] Prior to MRSA application, mice were shaved and treated with chemical depilation to remove back fur. Two days after fur removal, a 1 cm^2 gauze piece of soaked with 100uL of bacterial suspension was placed onto the skin just below the shoulder blades and the animals were covered with Tegaderm occlusive tape. Control animals were treated with gauze soaked with 100uL sterile PBS. Mice were monitored daily and the Tegaderm tape and gauze were removed at the endpoint so that inflammation and itch could be measured.

S. aureus exposure site dermatitis

Inflammation caused directly by bacterial exposure was measured immediately after tape and gauze removal (before mice were able to scratch the back skin). Four parameters (edema, skin scale, erythema, and thickness) were assigned a score from 0 (none) to 3 (severe) and these measurements were summed for a total score of between 0 to 12 per mouse (Figure S1B).

Transepidermal water loss

Following skin score assessment, a Tewameter TM300 device (Courage and Khazaka Electronic GmbH) was used to record TEWL at the site of gauze placement on the skin.

Alloknesis

Mice were stimulated 9 times with a 0.07g von Frey filament on the back skin near the exposure site. Bouts of scratching that occurred immediately after stimulation were recorded as a response.

Spontaneous itch

Prior to MRSA exposure, mice were habituated to the infrared behavior observation box (iBOB). Following tape and gauze removal at the endpoint of exposure, mice were returned to their home cage for several hours and allowed to groom the skin/fur that was previously covered by tape. After grooming behaviors returned to baseline, mice were place in iBOB for 90 minutes of video recording. Bouts of scratching were counted by observers blinded to the treatment groups.

Scratch-induced skin damage

Immediately after tape and gauze removal, mice were photographed from above, returned to their home cage, and allowed to freely scratch the back skin for 7 hours. After scratching, mice were anesthetized and photographed. Blinded observers analyzed the images to measure the total shaved skin area and the skin area that appeared inflamed (including the infected lesion site and the surrounding scratched areas) using ImageJ. The area of damaged skin was calculated as the percentage of inflamed skin area out of the total shaved area.

Bacterial load

Mice were euthanized according to approved veterinary protocols and the back skin was dissected and placed in 1 mL sterile PBS and bead beaten for 10 min to homogenize the tissue. The resulting tissue homogenate was serially diluted and plated on CHROMagar (Hardy Diagnostics) supplemented with 5.2 μg/mL cefoxitin to enumerate MRSA CFU.

Histology

Mice were euthanized by CO_2 inhalation and the back skin was dissected and fixed for 24h at 4°C in 4% paraformaldehyde. Fixed skin samples were embedded with paraffin, sectioned, and stained with hematoxylin and eosin (H&E) dyes by the Harvard Medical School Rodent Histopathology Core. Stained sections were imaged by light microscopy on an Eclipse Ti-S/L100 inverted microscope (Nikon) and images collected by NIS-Elements AR software.

Subcutaneous MRSA infection

Mice were injected subcutaneously with 50μL of 10^7 CFU of MRSA in PBS. At 5-days post-infection, mice developed large dermonecrotic lesions at the infection site. Alloknesis was assessed by stimulating the skin close to the necrotic tissue. Spontaneous itch was measured by counting bouts of scratching to both the infected area and the healthy back skin surrounding the lesion.

Whole mount confocal microscopy

Nav1.8^{tdTomato} mice were treated epicutaneously with GFP-MRSA or sterile PBS. At 5 days post-treatment, mice were euthanized following approved veterinary protocols and the skin was dissected and fixed for 24h at 4°C in 4% paraformaldehyde. Following fixation, the skin was imaged using a Leica Stellaris 8 confocal microscope.

Mouse skin RNA isolation and quantitative real-time PCR

Mouse skin tissue was placed into TRIzol reagent (thermos Fisher) and homogenized by bead beating for 10 min. RNA was isolated using the Direct-zol RNA MiniPrep Plus kit according to manufacturer's instructions (Zymo Research). RNA was reverse-transcribed using the iScript cDNA synthesis kit (Bio-Rad). Primers (*sspA* primers sspA-F AND sspA-R, *psmA1* primers psmA1-F and psmA1-R, and *hla* primers hla-F and hla-R) and cDNA were mixed with Power SYBR green PCR master mix (Life Technologies) and qPCR was performed using a QuantStudio Real-Time PCR instrument (Thermo Fisher).

Human skin swab RNA isolation quantitative real-time PCR

RNA was isolated using the Purelink RNA isolation kit according to manufacturer's instructions (Thermo Fisher Scientific). For human swabs, 250μL of sample was removed from collection tubes and added to 500μL of RNA Protect Bacteria Reagent (Qiagen) for 10min at RT, then pelleted (13,000RPM, 10', RT). Pellet was resuspended with 700μl of RNA lysis buffer with 1% Beta-mercaptoethanol followed by column-based isolation of RNA. RNA was reverse-transcribed using the iScript cDNA synthesis kit (Bio-Rad). qPCR reactions were run on a CFX96 Real-Time Detection System (Bio-Rad) with cDNA, 2x SYBR Green qPCR Master Mix, and *sspA* specific primers sspA-F and sspA-R previously described.[78]

Cheek injections and measurement of itch and pain

Mouse cheeks were shaved 2 days before experiments and were habituated for 30 minutes in iBOB chambers. Male and female mice were injected intradermally in the cheek with 20μL of PBS, V8 protease (40U), histamine (100μg), or capsaicin (40μg). For injections with antagonists, V8 protease was mixed with vorapaxar, SCH79797, or BMS986120 30 minutes prior to injection. Immediately after injection, mice were place into iBOB chambers and recovered for 30 minutes. Itch and pain behaviors were scored by blinded observers.

Alloknesis

The napes of mouse necks were shaved 2 days before experiments and mice were habituated in alloknesis chambers for 1 hour. Mice were injected intradermally in the upper back with 50μL of PBS, V8 protease (40U), or histamine (100μg). The skin surrounding the injection site was mechanically stimulated for 1 second 3 times in a row with a 0.07g Von Frey filament, and this was repeated 3 times for a total of 9 stimulations.

KERTr cell culture and adherence assays

KERTr immortalized human keratinocytes were obtained from the American Type Culture Collection (#CRL-2309) and maintained in keratinocyte serum-free medium (Gibco #17005-042) with added Keratinocytes Supplements (Gibco #37000-015) including bovine pituitary extract (BPE; Gibco 13028-014) and human recombinant epidermal growth factor (EGF, Gibco #10450-013) and further supplemented with 35 ng/mL human recombinant epidermal growth factor (EGF; BD #354052).

Assays to quantify cell surface-adherent bacteria were performed as previously described.[118] Briefly, MRSA strains were grown to mid-log phase to infect confluent cell monolayers (multiplicity of infection [MOI], 1). Following a 30 min incubation, cells were treated with trypsin and lysed with 0.025% Triton X-100. The lysates were then serially diluted and plated on tryptic soy agar (TSA) to enumerate bacterial CFU. Experiments were performed four times with four replicates per MRSA strain, and results from a representative experiment are shown in Figure S5D.

Expression and purification of recombinant PAR1 N-terminus

A codon-optimized sequence of human PAR1A22-T102 with a starting methionine was cloned into vector pTEV20 at the BspQ1 site.[119] The construct was transformed into *E. coli* BL21-Rosetta cells (Novagen) and grown overnight in LB supplemented with ampicillin (100 μg/mL) and chloramphenicol (10 μg/mL) at 37 °C. Overnight was subcultured at a 1:8 dilution in Terrific Broth (TB, BD Difco) supplemented with ampicillin (100 μg/mL) and chloramphenicol (10 g/mL) and grown at 37 °C shaking at 220 RPM to a cell density of OD600 0.8-1.0 as measured in a cuvette with 1 cm pathlength. Isopropyl β-D-1-thiogalactopyranoside (IPTG) was added at a final concentration of 1 mM, and the culture was incubated at 25 °C for 2 hours. Cells were then centrifuged at 3,900 x *g* in an Eppendorf 5810R centrifuge set at 4 °C for 30 minutes. Centrifuged cell paste was stored at -80 °C. For purification, thawed cell paste was resuspended in Buffer A (0.1 M sodium phosphate buffer, pH 7.8, 0.2 M NaCl, 6 M urea) at a ratio of 5 mL buffer: 1 g cell mass, and cells were lysed by pushing lysate through a 28G needle attached to a syringe three times or until cells were lysed. Lysate was centrifuged at 3,900 x *g* in an Eppendorf 5810R centrifuge set at 4 °C for 30 minutes, and supernatant was filtered with a 0.45 μm filter. Filtered lysate was loaded onto a 5 mL HisTrap-FF column (Cytiva) equilibrated with Buffer A. A gradient of Buffer B (0.1 M sodium phosphate

buffer, pH 7.8, 0.2 M NaCl, 0.5 M imidazole, 6 M urea) was applied from 0-100% over 10 column volumes (CV). PAR1$^{A22\text{-}T102}$-His$_6$ eluted at 41-56% Buffer B. Fractions were collected, dialyzed thrice in 1 L storage buffer (0.01 M sodium phosphate buffer pH 7.8, 6 M urea), and flash frozen in liquid nitrogen for storage at -80 °C.

Limited proteolysis of PAR1 N-terminus

Unless otherwise specified, tubes were incubated at room temperature for 10 min on a tube revolver (Thermo Scientific) set to 15 speed, and beads were separated from supernatant with a magnetic separation rack for 2 min (New England Biolabs). Per tube, 400 μL of Pierce™ Ni-NTA Magnetic Agarose Beads were equilibrated with storage buffer, and 1.5 mg of thawed PAR1 recombinant N-terminus was applied to the beads. Beads were washed thrice with storage buffer and thrice with reaction buffer (0.01 M sodium phosphate buffer, pH 7.8) to wash off unbound protein and renature N-terminus. V8 protease (E.C. 3.4.21.19, Sigma) was added at a concentration of 10 μg/mL V8 protease in 500 μL total volume, and reaction was incubated rotating for 30 minutes. Supernatant was removed and added to formic acid for a final concentration of 0.5% formic acid and immediately flash frozen. Resin beads were washed thrice with reaction buffer and incubated for 10 minutes with 400 μL elution buffer (0.01 M sodium phosphate buffer, pH 7.8, 500 mM imidazole). Supernatant was removed and added to formic acid for a final concentration of 2% formic acid and immediately flash frozen. Samples were submitted to Dr. Greg Sabat at the University of Wisconsin-Madison Mass Spectrometry Core for solid phase purification and LC-MS/MS analysis.

Mass Spectrometry

Samples were desalted using Pierce C-18 Tips, 100μl bed (ThermoFisher Scientific) per manufacturer protocol and eluted in 10μl of 70/30/0.1% ACN/H2O/TFA. Dried to completion in the speed-vac and finally reconstituted in 20μl of 0.1% formic acid / 3% ACN. Peptides were analyzed by nanoLC-MS/MS using the Agilent 1100 nanoflow system (Agilent) connected to hybrid linear ion trap-orbitrap mass spectrometer (LTQ-Orbitrap Elite™, Thermo Fisher Scientific) equipped with an EASY-Spray™ electrospray source (held at constant 35°C). Chromatography of peptides prior to mass spectral analysis was accomplished using capillary emitter column (PepMap® C18, 3μM, 100Å, 150x0.075mm, Thermo Fisher Scientific) onto which 2 μl of extracted peptides was automatically loaded. NanoHPLC system delivered solvents A: 0.1% (v/v) formic acid, and B: 99.9% (v/v) acetonitrile, 0.1% (v/v) formic acid at 0.50 μL/min to load the peptides (over a 30 minute period) and 0.3μl/min to elute peptides directly into the nano-electrospray with gradual gradient from 0% (v/v) B to 30% (v/v) B over 80 minutes and concluded with 5 minute fast gradient from 30% (v/v) B to 50% (v/v) B at which time a 5 minute flash-out from 50-95% (v/v) B took place. As peptides eluted from the HPLC-column/electrospray source survey MS scans were acquired in the Orbitrap with a resolution of 120,000 followed by CID-type MS/MS fragmentation of 30 most intense peptides detected in the MS1 scan from 350 to 1800 m/z; redundancy was limited by dynamic exclusion. Elite acquired MS/MS data files were converted to mgf file format using MSConvert (ProteoWizard: Open Source Software for Rapid Proteomics Tools Development). Resulting mgf files were used to search against Uniprot Escherichia coli reference database (UP000000625, 4,520 total sequences) appended with PAR1 (1-102 aa) protein along with a cRAP common lab contaminant database (116 total entries) using in-house Mascot search engine 2.7.0 [Matrix Science], assuming the digestion enzyme GluC, with fixed Cysteine carbamidomethylation and variable Methionine oxidation plus Asparagine or Glutamine deamidation. Peptide mass tolerance was set at 10 ppm and fragment mass at 0.6 Da. Protein annotations, significance of identification and spectral based quantification was done with Scaffold software (version 4.11.0, Proteome Software Inc., Portland, OR). Peptide identifications were accepted if they could be established at greater than 60.0% probability to achieve an FDR less than 1.0% by the Scaffold Local FDR algorithm. Protein identifications were accepted if they could be established at greater than 98.0% probability to achieve an FDR less than 1.0% and contained at least 2 identified peptides. Protein probabilities were assigned by the Protein Prophet algorithm[120]. Proteins that contained similar peptides and could not be differentiated based on MS/MS analysis alone were grouped to satisfy the principles of parsimony. Proteins sharing significant peptide evidence were grouped into clusters.

Culturing and calcium imaging of mouse DRG neurons

One day prior to calcium imaging, DRGs from male and female mice were collected and digested using a mixture of 2.5mg/mL Collagenase A and 1mg/mL Dispase II for 40 min. A single cell suspension was obtained by triturating the samples through 18G, 21G, and 26G needles. Neurons were separated from other cells and debris using BSA gradient and plated onto laminin-coated 35mm dishes or 96-well plates in Neural Basal Medium (NBM) (Thermo Fisher) supplemented with B27 serum-free supplement (Invitrogen), L-Glutamine (Invitrogen), Pen/Strep (Cellgro), and 25ng/mL NGF (Invitrogen).

Neurons were cultured overnight at 37C with 5% CO_2, then loaded with 5μM Fura-2-AM in NBM for 30 min. For experiments with histamine, chloroquine, S1P, and capsaicin, neurons were washed with Krebs-Ringer buffer (KR) (Boston BioProducts) and 100μL of KR, V8 (69.2μM), histamine (100μM), chloroquine (1mM), S1P (1μM), capsaicin (1μM), and KCl (100μM) were sequentially pipetted into the 35mm dish. Images were acquired with alternating 340/380 nm excitation wavelengths using a Nikon Eclipse Ti inverted microscope and Zyla sCMOS camera (Andor). For experiments with Hla, fMLF, and V8 protease, neurons were washed with KR and 100μL of KR, V8, Hla, fMLF, and KCl were sequentially pipetted onto the cells. Ratiometric analysis of 340/380 signal intensities was performed as described in Pinho-Ribeiro et al.[14] For V8 dose-response experiments, calcium imaging of neurons in 96-well plates was performed as described in DuBreuil et al.[121]

Culturing and calcium imaging of human neurons

Human lumbar DRGs were cleaned of any fat and connective tissue surrounding the ganglion. The protocol for the dissociation of DRGs for calcium imaging was inspired by Yousuf et al.[122] The DRG was cut into roughly 1-2 mm chunks and immersed in pre-warmed 5 ml enzyme solution containing 2 mg/ml STEMxyme I (Worthington, LS004106) and 0.1 mg/ml DNAse I (Worthington, LS002139) in HBSS without calcium and magnesium (ThermoFisher, 14170161). The tissue-enzyme solution was gently and constantly mixed at 37°C in a shaking water bath. The tissue was triturated every 20 min using fire-polished glass pipette until a roughly homogenous solution was obtained (about 40 min). This mixture was passed through a 100 μm cell strainer (Corning, 352360) and the flow-through was layered onto 3ml of 10% bovine serum albumin density gradient. The resulting solution was centrifuged for 900 x g for 5 min at room temperature. The supernatant was removed and the pellet was resuspended in BrainPhys media (STEMCell, 05790) containing 1% penicillin-streptomycin (ThermoFisher, 15070063), 1% N2-A (STEMCell, 07152), 2% SM1 (STEMCell, 05711) and 1% GlutaMax (ThermoFIsher, 35050061). Cells were plated onto 35 mm dishes that were pre-coated with poly-D-lysine (>300,000, Sigma Aldrich, P7405) overnight and then coated with laminin from human placenta (Sigma Aldrich, L6274) for 2-3 hours at 37°C right before culturing. Cells were initially cultured for 2 hours in a 50μl droplet followed by immersion in 2 ml of pre-warmed BrainPhys media.

Calcium imaging with Fluo-4 AM was performed 24 hours after plating. Fluo-4 AM (ThermoFisher, F14201) was reconstituted in 2% of Pluronic F-127 (20% in DMSO, ThermoFisher, P3000MP) in BrainPhys Imaging media (STEMCell, 05796). Cells were loaded with Fluo-4 AM (1:100) for 30 min prior to imaging. The Fluo-4 AM solution was replaced with 2mL of pre-warmed BrainPhys Imaging media. Cells were imaged at 20X on an Olympus IX73 inverted microscope and data was acquired using the MetaFluor software (Olympus). A 120 second baseline was acquired prior to the addition of V8 protease (2 mg/ml, Worthington, LS003605), capsaicin (400nM) at 500 seconds, and KCl (50mM) at 700 seconds for a total imaging time of 840 seconds. Cells with an increase in the intracellular Fluo-4 signal over 10% of their baseline were deemed to be responsive to V8 administration. Only cells that responded to KCl (50 mM) were used in the analysis. Calcium imaging was performed on cells from DRGs from two donors (see Table S3).

RNAscope of mouse DRGs

Mouse samples for RNAScope were prepared as previously described.[123] Briefly, mouse DRGs were embedded in OCT and sectioned at 16μm on a cryostat. Sections were stored in -80C for 24 hrs, then brough to room temperature and fixed with 4% paraformaldehyde. In situ hybridization with *F2r* and *Tubb3* probes was performed using the RNAscope Multiplex V2 kit (ASD) according to manufacturer's instructions. All tissues were also tested with negative and positive control probe cocktails (ACD). Sections were imaged on a Leica Stellaris 8 confocal microscope.

RNAscope of human DRGs

Human samples for RNAScope were prepared as previously described.[65] Frozen human DRG samples were gradually embedded in OCT in a cryomold. Tissue was cryosectioned at 20μm, thawing momentarily in order to adhere to the slide. In situ hybridization using the RNAscope Multiplex V2 kit (ACD) was performed according to the manufacturer's recommendations and with Akoya fluorescein, Cy3, Cy5 dyes, as previously described.[65] All tissues were tested against a positive control probe cocktail (ACD) containing mRNAs with high, medium, and low expressions. Negative control probe against the bacterial DapB gene (ACD) was also used.

DRG sections were imaged on Olympus FV3000 confocal microscope at 20X or 40X magnification as per previously published parameters.[65] Background lipofuscin was identified as large globular intracellular structures that autofluoresced at 488, 550, and 647 wavelengths. Lipofuscin was not analyzed. Three 20X images were obtained from each human DRG section, and three sections were imaged per human donor. Images were analyzed using Olympus CellSens software (v1.18) as previously described.[65] Pie charts represent the average percentage of neurons that express each target from all donors (see Table S3). Probes used in this study: Hs-F2R-C2 (ACD, 471081-C2), Hs-TRPV1-C3 (ACD, 415381-C3), Hs-NPPB-C1 (ACD, 448511).

Luciferase-based PAR cleavage assays

CHO-K1 cells stably transfected with nLuc-PAR1-eYFP, nLuc-PAR2-eYFP, and nLuc-PAR4-eYFP pcDNA3.1(+) plasmids separately were seeded in a 96-well cell culture plate (flat-clear bottom, polystyrene, Nunc, ThermoFisher Scientific) at a density of 1×10^4 cells per well and cultured for 48 h in Ham's F-12 (1×) Nutrient Mix (Gibco ThermoFisher Scientific) supplemented with 1 mM L-Glutamine, 100 U/ml penicillin, 100 μg/mL streptomycin, 1 mM sodium pyruvate, 10% v/v heat inactivated Fetal Bovine Serum (FBS), and 600 μg/mL geneticin selective antibiotic (G418 Sulfate, Gibco® ThermoFisher Scientific). The cells were rinsed with HBSS (100 μL × 3) and incubated with 100 μL HBSS at 37°C for 15 minutes. Cell supernatant (50 μL) was aliquoted into a white 96-well plate (polystyrene, Nunc, ThermoFisher Scientific) to measure the basal luminescence. The cells were further incubated with 50 μL V8 protease or controls in a half-log scale concentrations at 37°C for 15 minutes, and 50 μL of cell supernatant from each well was aliquoted as before. Furimazine (2 μl/mL, Promega) was added and the nLuc cleavage of the receptor was measured on Mithras LB 940 (Berthold Technologies, measurement time: 1 s per well) plate reader. The luminescence measurements of the samples were normalized by subtracting the basal luminescence. The concentration-effect curves were plotted and analyzed using the dose-response stimulation three parameters model and the $\log_{10}$EC50 ± SEM values were obtained on GraphPad Prism 8.

PAR1 calcium signaling in HEK-293 cells

HEK-293 cells (0.01x106) were plated in poly-d-lysine coated black walled clear bottom 96 well plates (Nunc) and cultured for 48 h in DMEM containing 10% FBS (Gibco). Media was removed and cells were incubated with the calcium indicator Fluo-4 NW (Thermo Fisher Scientific) at 37°C for 30 minutes and for a further 15 minutes at room temperature in the dark. Agonists were added and Ca2+ mobilization induced change in fluorescence (λEx/Em 494/516 nm) was measured in real time using a FlexStation3 microplate reader (Molecular Devices). The total run time for each spectrum was 180 s with baseline recorded for 20 s prior to the addition of agonists. To measure disarming of PAR1, cells were incubated with V8 for 15 minutes before measuring thrombin and TFLLR-NH_2 stimulated responses. (A23187, 6 μM, Sigma-Aldrich) was used as a control to ensure equivalent levels of Fluo-4 NW loading in each well.

PAR1 cleavage at HEK cell membrane

Dually tagged PAR1 in HEK cells was used as previously described.[124] Cells were placed in growth media containing E64 (5uM) and heparin (5 units/ml). After 1h stimulation, cells were fixed with 10% buffered formalin, and images were recorded with confocal microscope (Infinity image facility, Toulouse, France).

Skin cell preparation and flow cytometry

Skin from mice injected intradermally with PBS or V8 protease were obtained 30 minutes after injection. Cells were isolated and stained for flow cytometry as previously described.[44] Cells were preincubated with the Fcγ receptor–specific blocking mAb (clone 2.4G2, BioLegend) and washed before staining mAbs and analysis on LSR Fortessa (BD Biosciences). Data were analyzed with FlowJo software.

Intrathecal siRNA injection

Intrathecal delivery of siRNA was performed as in Silva et al.[37] Briefly, siRNA purchased from Thermo Scientific were mixed with In Vivo JetPEI (Polyplus Transfection) according to the manufacturer's protocol. The N:P ratio used was 6. Mice were injected intrathecally between L5 and L6 spinal levels with 5μL volume for 3 days in a row prior to itch experiments.

Mouse DRG RT-qPCR

One day after the last intrathecal siRNA injection, thoracic DRGs were dissected out of mice and placed in RNAprotect reagent (Qiagen). Tissues were homogenized by beadbeating with 0.1mm silica beads, RNA was extracted with the NucleoSpin RNA isolation kit (Macherey Nagel) and converted to cDNA with the iScript cDNA synthesis kit (Bio-Rad) following manufacturer's instructions. Primers (*il31ra* primers il31ra-F and il31ra-R, or *f2r* primers f2r-F, f2r-R) and cDNA were mixed with Power SYBR green PCR master mix (Life Technologies) and qPCR was performed using a QuantStudio Real-Time PCR instrument (Thermo Fisher).

Oral Vorapaxar treatment

Mice were gavaged daily with 100μL volume of either vehicle or Vorapaxar solution starting 2-days prior to *S. aureus* topical application and until the endpoint of 5 days.

QUANTIFICATION AND STATISTICAL ANALYSIS

Analysis of data was performed using GraphPad Prism version 9.5.1 (GraphPad Software). Comparison of data between two groups was performed using Mann-Whitney tests. Comparison of data between more than two groups with one independent variable was performed using one-way ANOVA with Tukey's multiple comparisons tests. Comparison of two independent variables was performed using two-way ANOVA with Tukey's multiple comparisons tests. P-values of less than 0.05 were considered statistically significant. Statistical details including statistical tests used, number of samples (n), and P-values are reported in figure legends.

Supplemental figures

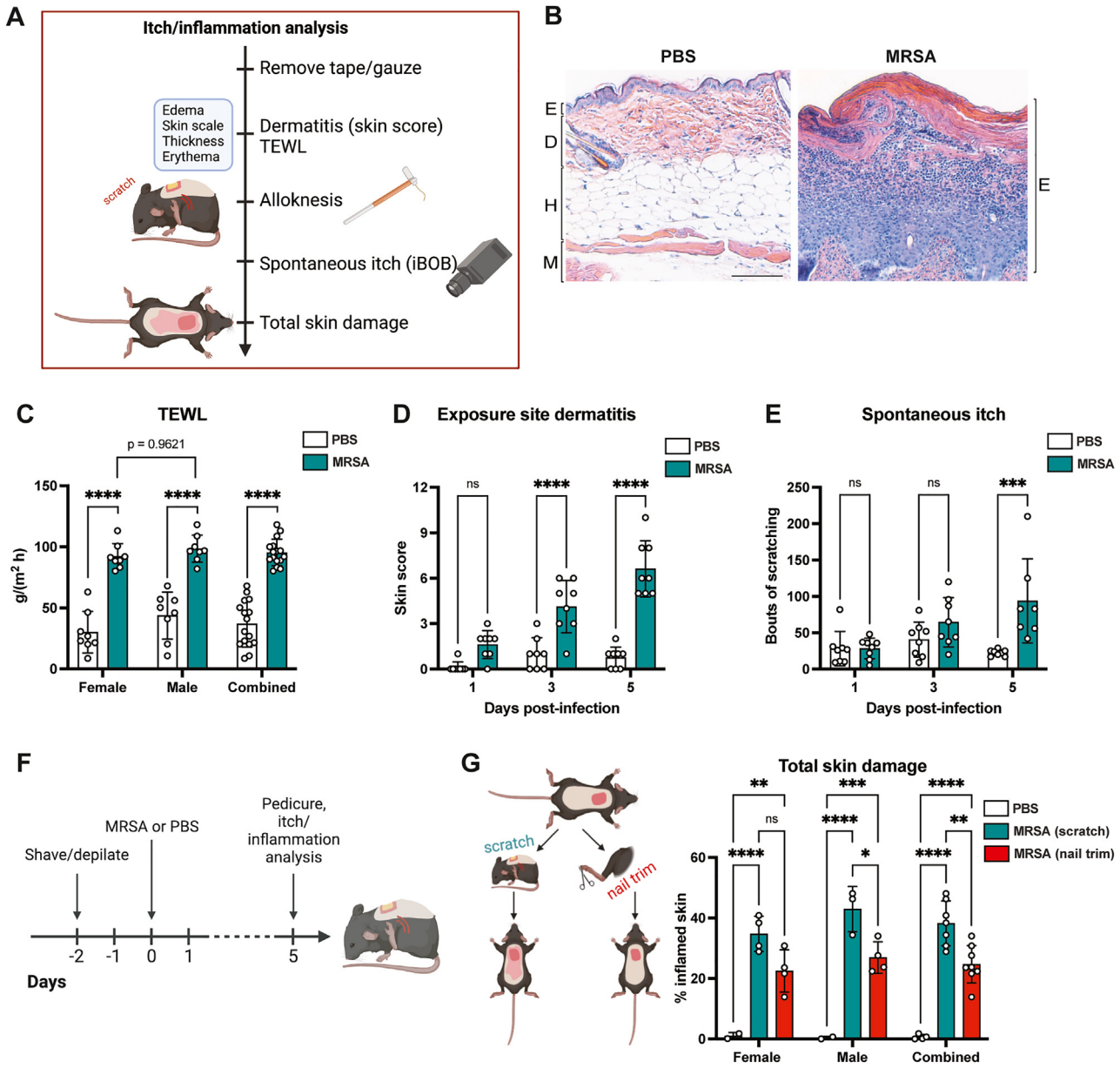

Figure S1. Epicutaneous *S. aureus* exposure induces inflammation, itch, and skin barrier damage, related to Figure 1

(A) Measurement of inflammation caused by bacterial exposure (skin score), skin barrier damage (TEWL), alloknesis, spontaneous itch, and total skin damage driven by scratching.

(B) Histopathology of skin samples from mice 5 days after treatment with PBS or application of 10^7 colony-forming unit (CFU) MRSA. Scale bars, 50 μm. E, epidermis; D, dermis; H, hypodermis; M, muscle.

(C) Female and male transepidermal water loss (TEWL) 5 days post-exposure (n = 8 males, 8 females per group).

(D) Dermatitis measured 1, 3, and 5 days post-exposure with 10^7 CFU MRSA (n = 8 per group).

(E) Spontaneous itch recorded 1, 3, and 5 days post-exposure with 10^7 CFU MRSA (n = 7–8 per group).

(F) Mice treated with PBS or MRSA, and day 5 post-inoculation, nails of one group were trimmed; mice were placed in home cages for 7 h, and total damaged skin area measured.

(G) Total skin damage in PBS, treated, MRSA (scratch), MRSA (nail trimmed mice) (n = 2–4 males, 2–4 females per group).

For each panel, data from 2 independent experiments are combined and shown. Data are represented as mean ± SD.

Statistical analysis: in (C)–(E) and (G), two-way ANOVA, Sidak's multiple comparisons tests. *p < 0.05; **p < 0.01; ***p < 0.001; ****p < 0.0001; ns, not significant.

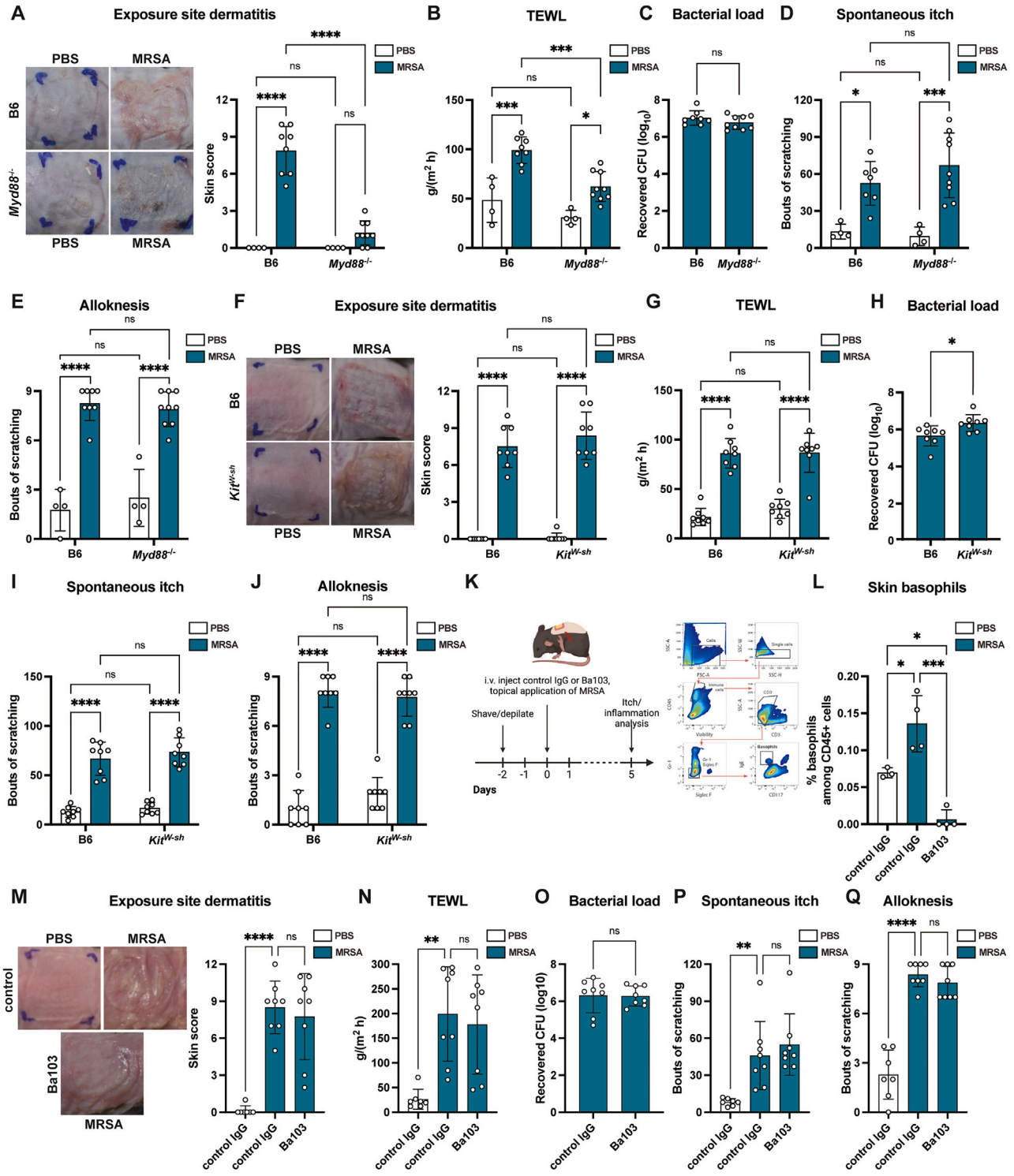

Figure S2. MYD88-mediated inflammation, mast cells, and basophils are not required for itch, related to Figure 1

(A) Representative images of skin from PBS-treated or MRSA-treated wild-type or *Myd88*$^{-/-}$ mice and dermatitis scores (n = 3–6 males, 1–3 females per group).

(B) TEWL for PBS-treated or MRSA-treated wild-type and *Myd88*$^{-/-}$ mice (n = 3–6 males, 1–3 females per group).

(C) Skin bacterial load for PBS-treated or MRSA-treated wild-type and *Myd88*$^{-/-}$ mice (n = 3–6 males, 1–3 females per group).

(D) Spontaneous itch for PBS-treated or MRSA-treated wild-type and *Myd88*$^{-/-}$ mice (n = 3–6 males, 1–3 females per group).

(E) Alloknesis for PBS-treated or MRSA-treated wild-type and *Myd88*$^{-/-}$ mice (n = 3–6 males, 1–3 females per group).

(legend continued on next page)

(F) Representative images of skin from PBS-treated or MRSA-treated wild-type or $Kit^{W\text{-}sh}$ mice and dermatitis scores (n = 8 per group).
(G) TEWL for PBS-treated or MRSA-treated wild-type and $Kit^{W\text{-}sh}$ mice (n = 8 per group).
(H) Skin bacterial load for PBS-treated or MRSA-treated wild-type and $Kit^{W\text{-}sh}$ mice (n = 8 per group).
(I) Spontaneous itch for PBS-treated or MRSA-treated wild-type and $Kit^{W\text{-}sh}$ mice (n = 8 per group).
(J) Alloknesis for PBS-treated or MRSA-treated wild-type and $Kit^{W\text{-}sh}$ mice (n = 8 per group).
(K) Control IgG or Ba103 antibody treatment and flow cytometry gating strategy.
(L) Quantification of skin basophils (n = 3–4 mice per group).
(M) Representative images of back skin and exposure site dermatitis for mice injected with control IgG and treated with PBS or MRSA, and mice injected with Ba103 antibody and exposed to MRSA (n = 3–4 males, 4 females per group).
(N) TEWL for mice injected with control IgG and treated with PBS or MRSA, and mice injected with Ba103 antibody and exposed to MRSA (n = 3–4 males, 4 females per group).
(O) Skin bacterial load for mice injected with control IgG and exposed to MRSA, and mice injected with Ba103 antibody and exposed to MRSA (n = 4 males, 4 females per group).
(P) Spontaneous itch for mice injected with control IgG and treated with PBS or MRSA, and mice injected with Ba103 antibody and exposed to MRSA (n = 3–4 males, 4 females per group).
(Q) Alloknesis for mice injected with control IgG and treated with PBS or MRSA, and mice injected with Ba103 antibody and exposed to MRSA (n = 3–4 males, 4 females per group).
For each panel, data from 2 independent experiments are combined and shown. Data are represented as mean ± SD.
Statistical analysis: in (A), (B), (D), and (F)–(J), two-way ANOVA, Sidak's multiple comparisons tests. In (C), (F), and (L)–(Q), Mann-Whitney test. *$p < 0.05$; **$p < 0.01$; ***$p < 0.001$; ****$p < 0.0001$; ns, not significant.

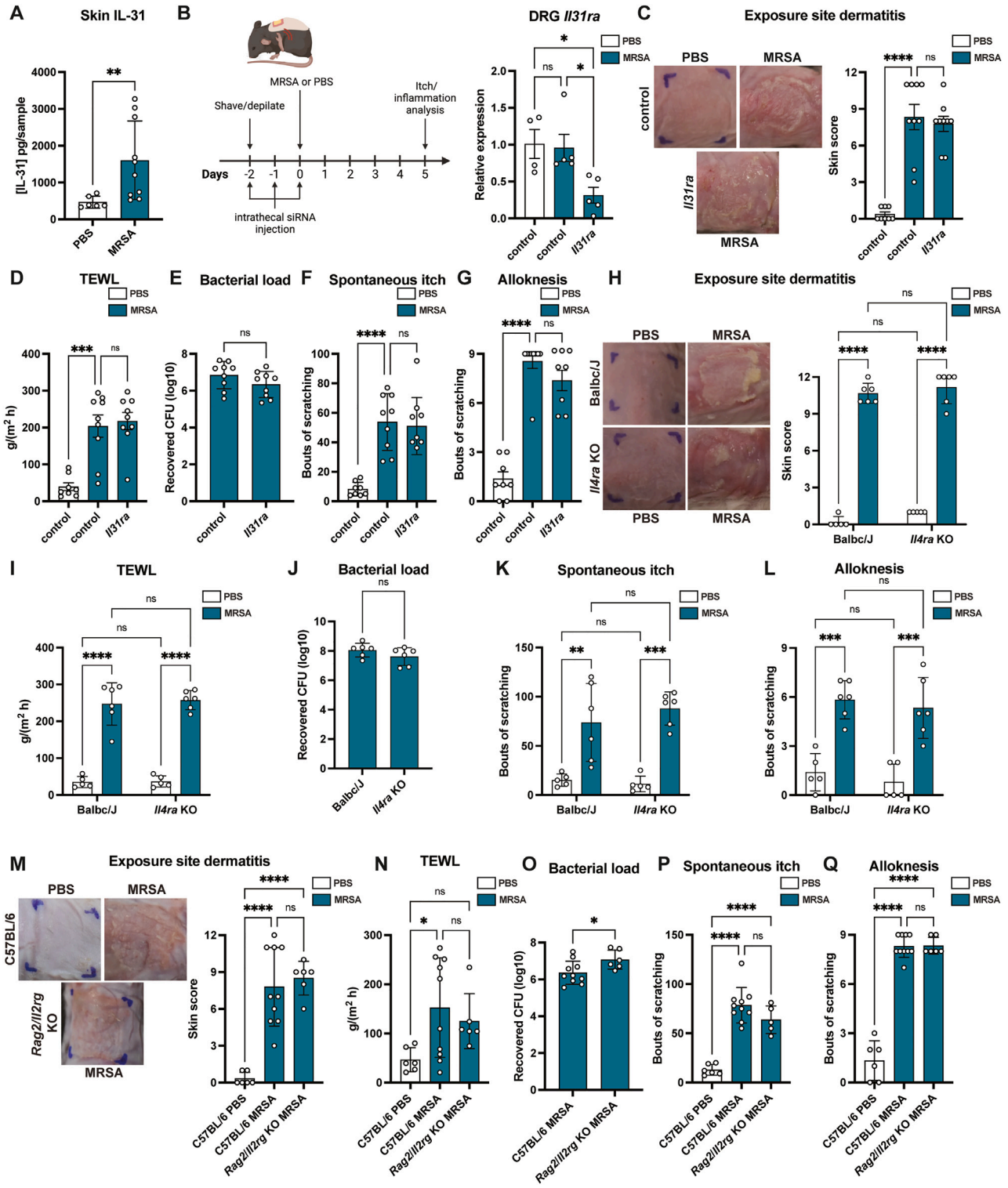

Figure S3. *Il31ra*, *Il4ra*, and lymphocytes are not required for itch and inflammation, related to Figure 1

(A) ELISA to quantify IL-31 levels in the skin 5 days after treatment with PBS or MRSA exposure. (n = 3–5 males, 3–5 females per group).

(B) Mice were injected intrathecally with *Il31ra* siRNA then treated with PBS or exposed to MRSA. *Il31ra* expression in DRG tissue was confirmed by RT-qPCR (n = 4–5 males per group).

(legend continued on next page)

(C) Representative images of back skin and exposure site dermatitis for mice injected with control or *Il31ra* siRNA and treated with PBS or exposed to MRSA (n = 3–4 males, 4 females per group).
(D) TEWL for mice injected with control or *Il31ra* siRNA and treated with PBS or exposed to MRSA (n = 3–4 males, 4 females per group).
(E) Skin bacterial load for mice injected with control or *Il31ra* siRNA and treated with PBS or exposed to MRSA (n = 4 males, 4 females per group).
(F) Spontaneous itch for mice injected with control or *Il31ra* siRNA and treated with PBS or exposed to MRSA (n = 4 males, 3–4 females per group).
(G) Alloknesis for mice injected with control or *Il31ra* siRNA and treated with PBS or exposed to MRSA (n = 4 males, 4 females per group).
(H) Representative images of skin from PBS-treated or MRSA-treated wild-type BALBc/J or *Il4ra*$^{-/-}$ mice and dermatitis scores (n = 2 males, 3–4 females per group).
(I) TEWL for PBS-treated or MRSA-treated wild-type BALBc/J or *Il4ra*$^{-/-}$ mice (n = 2 males, 3–4 females per group).
(J) Skin bacterial load for PBS-treated or MRSA-treated wild-type BALBc/J or *Il4ra*$^{-/-}$ mice (n = 2 males, 3–4 females per group).
(K) Spontaneous itch for PBS-treated or MRSA-treated wild-type BALBc/J or *Il4ra*$^{-/-}$ mice (n = 2 males, 3–4 females per group).
(L) Alloknesis for PBS-treated or MRSA-treated wild-type BALBc/J or *Il4ra*$^{-/-}$ mice (n = 2 males, 3–4 females per group).
(M) Representative images of skin from PBS-treated or MRSA-treated wild-type C57BL/6NTac or *Rag2*$^{-/-}$*Il2rg*$^{-/-}$ mice and dermatitis scores (n = 3–5 males, 3–5 females per group).
(N) TEWL for PBS-treated or MRSA-treated wild-type C57BL/6NTac or *Rag2*$^{-/-}$*Il2rg*$^{-/-}$ mice (n = 3–5 males, 3–5 females per group).
(O) Skin bacterial load for PBS-treated or MRSA-treated wild-type C57BL/6NTac or *Rag2*$^{-/-}$*Il2rg*$^{-/-}$ mice (n = 3–5 males, 3–5 females per group).
(P) Spontaneous itch for PBS-treated or MRSA-treated wild-type C57BL/6NTac or *Rag2*$^{-/-}$*Il2rg*$^{-/-}$ mice (n = 2–5 males, 3–5 females per group).
(Q) Alloknesis for PBS-treated or MRSA-treated wild-type C57BL/6NTac or *Rag2*$^{-/-}$*Il2rg*$^{-/-}$ mice (n = 3–5 males, 3–5 females per group).
For each panel, data from 2 independent experiments are combined and shown. Data are represented as mean ± SD.
Statistical analysis: in (A), (E), (J), and (O), Mann-Whitney test. In (B)–(D), (F), (G), (M), (N), and (P), one-way ANOVA. In (H), (I), (K), and (L), two-way ANOVA. *$p < 0.05$; ***$p < 0.001$; ****$p < 0.0001$; ns, not significant.

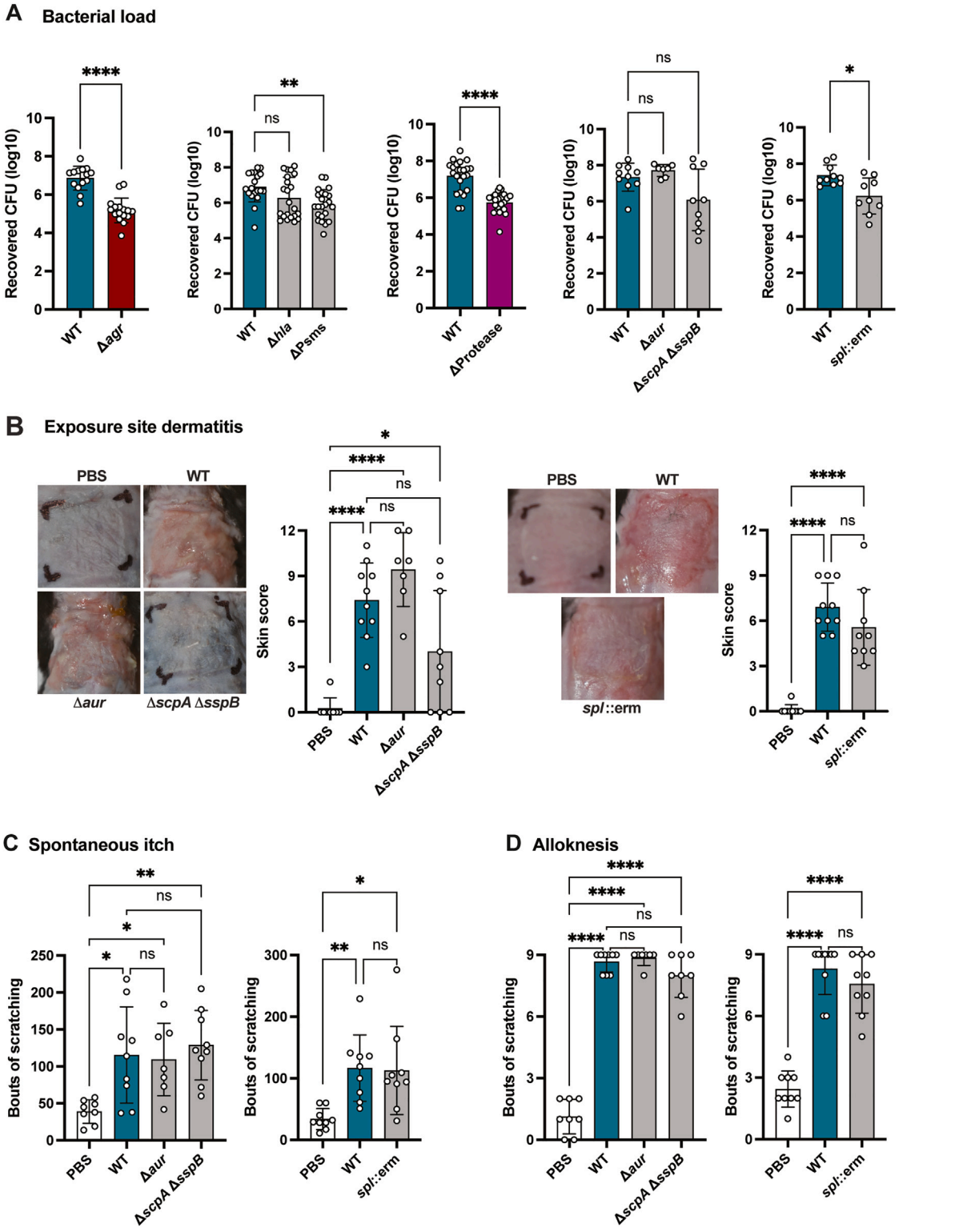

Figure S4. Roles of proteases, Hla, and PSMs in epicutaneous *S. aureus* exposure, related to Figure 2

(A) Skin bacterial load from mice inoculated with WT, Δ*agr*, Δ*hla* or ΔPSMs, ΔProtease, Δ*aur* or Δ*scpA*Δ*sspB*, and *spl*::erm MRSA strains (n = 7–12 males, 7–12 females per group).

(B) Spontaneous itch for mice exposed to protease knockout MRSA strains (n = 3–5 males, 4 females per group).

(legend continued on next page)

(C) Alloknesis for mice exposed to protease knockout MRSA strains (n = 3–5 males, 4 females per group).
(D) Representative images of back skin and dermatitis scores for mice infected with protease knockout MRSA strains (n = 3–5 males, 4 females per group).
For each panel, data from 2 to 6 independent experiments are combined and shown. Data are represented as mean ± SD.
Statistical analysis: in (A)–(D), one-way ANOVA. In (A), Mann-Whitney test. *p < 0.05; **p < 0.01; ****p < 0.0001; ns, not significant.

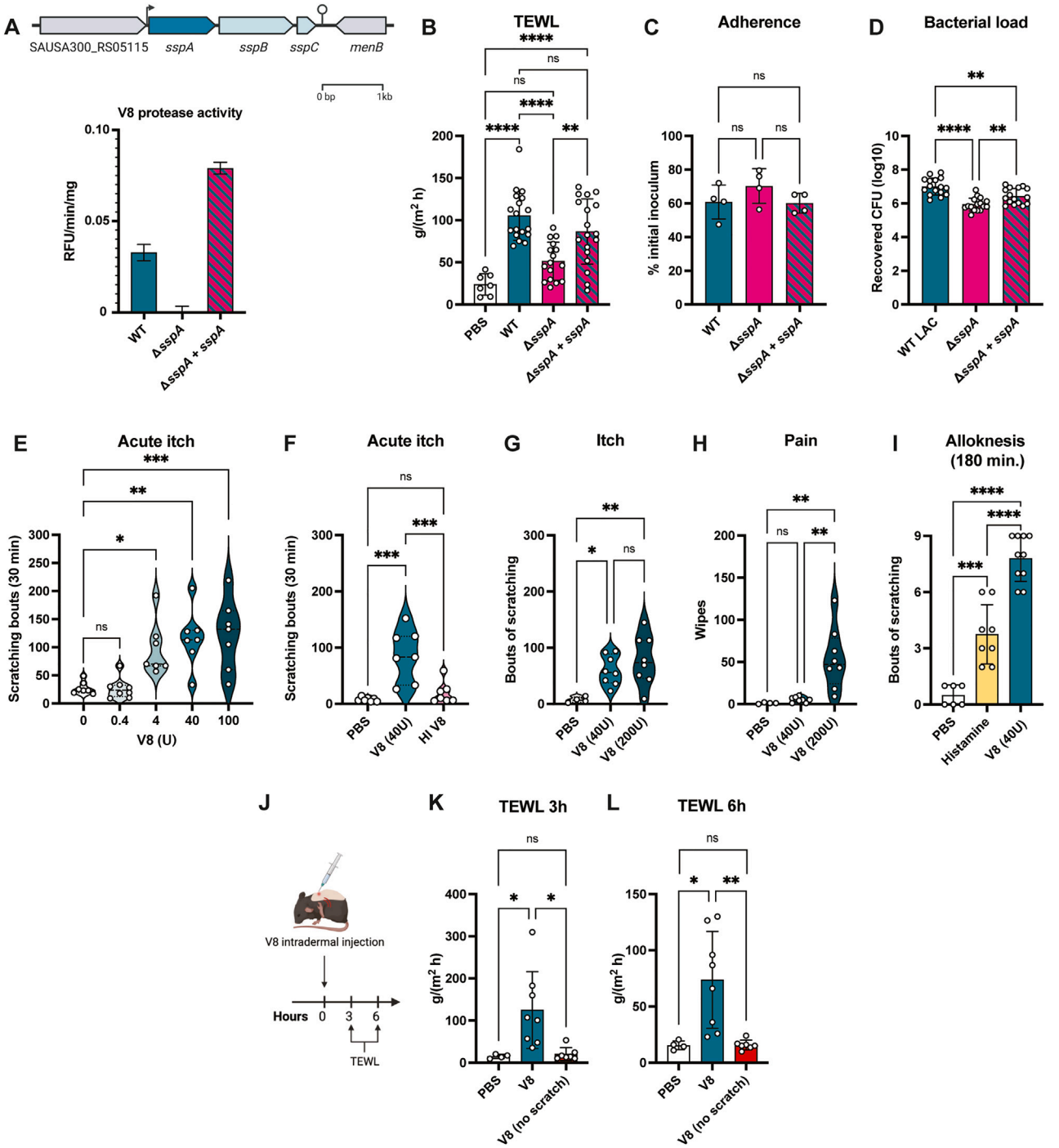

Figure S5. Role of V8 protease in inflammation and itch, related to Figure 3

(A) Diagram of *ssp* gene locus. *sspA* (V8), *sspB* (staphopain B), *sspC* (staphostatin B), and V8 protease activity assay with WT, Δ*sspA*, or Δ*sspA* + *sspA* MRSA strains.

(B) Transepidermal water loss for control mice (PBS) or mice inoculated with WT, Δ*sspA*, or Δ*sspA* + *sspA* MRSA strains (n = 4–9 males, 3–9 females per group).

(C) WT, Δ*sspA*, or Δ*sspA* + *sspA* MRSA adherence to KERTr cells *in vitro* (n = 4 per group).

(D) Skin bacterial load for or mice inoculated with WT, Δ*sspA*, or Δ*sspA* + *sspA* MRSA strains (n = 8 males, 8 females per group).

(E) Acute itch following intradermal cheek injection with PBS or increasing doses of V8 protease (0.4–100 U) (n = 3–4 males, 4 females per group).

(F) Acute itch following intradermal cheek injection with PBS, V8 (40 U), or heat-inactivated V8 (n = 3 males, 4 females per group).

(G and H) Acute itch (hindpaw scratching) and pain (forepaw wiping) behaviors following cheek intradermal injection with PBS or V8 (40 or 200 U) (n = 2–4 males, 2–4 females per group).

(legend continued on next page)

(I) Alloknesis 3 h after injection with PBS, V8 (40 U), or histamine (100 μg) (n = 3–5 males, 3–5 females per group).
(J) Mice were intradermally injected with PBS or V8 protease, followed by TEWL measurement. One group was wrapped with a bandage to prevent scratching.
(K and L) TEWL measured at 3 h post-injection and at 6 h post-injection in PBS, V8 (scratch), and V8-treated (no scratch) (n = 2–4 males, 2–4 females per group).
For each panel, data from 2 independent experiments are combined and shown. Data are represented as mean ± SD.
Statistical analysis: in (A)–(I), (K), and (L), one-way ANOVA. *p < 0.05; **p < 0.01; ***p < 0.001; ****p < 0.0001; ns, not significant.

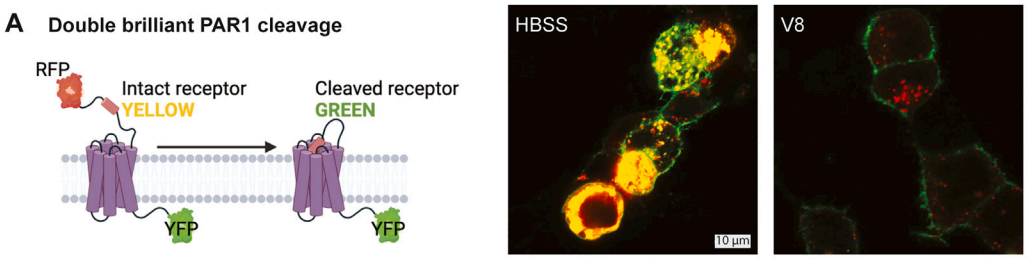

B V8 cleavage of PAR1 N-terminus

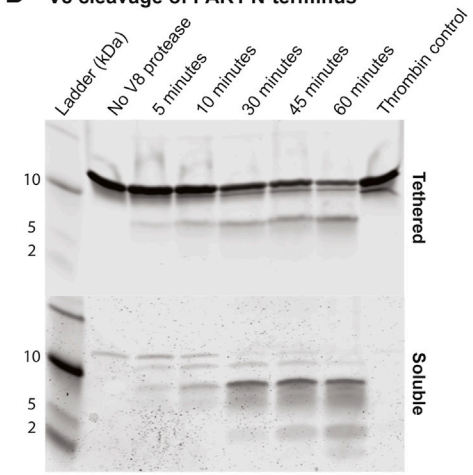

Peptide (30 minutes)	Total Spectral Count	
	Soluble Fraction	Tethered Fraction
ASGYLTSSWLTE	4	2
ASGYLTSSWLTENLYFQGHHHHHH		4
DASGYLTSSWLTE	60	50
DASGYLTSSWLTENLYFQGHHHHHH	1	25
DEEKNESGLTE	8	2
EEKNESGLTE	1	
EKNESGLTE	3	1
KNESGLTE	4	4
KNESGLTEYRLVSINKSSPLQKQLPAFISEDASGYLTSSWLTENLYFQGHHHHHH		1
KYEPFWE	1	
KYEPFWEDEEKNE	2	2
KYEPFWEDEEKNESGLTE	2	
NLYFQGHHHHHH	2	227
SGLTEYRLVSINKSSPLQKQLPAFISE		1
SGLTEYRLVSINKSSPLQKQLPAFISEDASGYLTSSWLTE	1	7
SGLTEYRLVSINKSSPLQKQLPAFISEDASGYLTSSWLTENLYFQGHHHHHH		10
SKATNATLDPRSFLLRNPND	1	
SKATNATLDPRSFLLRNPNDKYEPFWE	8	4
SKATNATLDPRSFLLRNPNDKYEPFWEDE	2	
SKATNATLDPRSFLLRNPNDKYEPFWEDEE	1	
SKATNATLDPRSFLLRNPNDKYEPFWEDEEKNE	11	2
YRLVSINKSSPLQKQLPAFISE	40	10
YRLVSINKSSPLQKQLPAFISED	2	1
YRLVSINKSSPLQKQLPAFISEDASGYLTSSWLTE	105	92
YRLVSINKSSPLQKQLPAFISEDASGYLTSSWLTENLYFQGHHHHHH	5	151

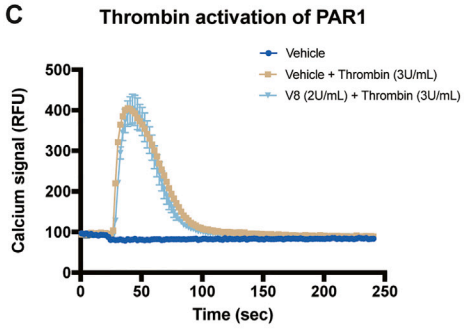

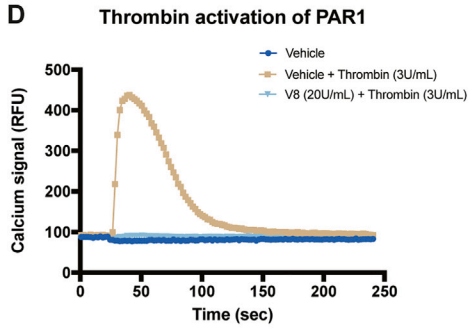

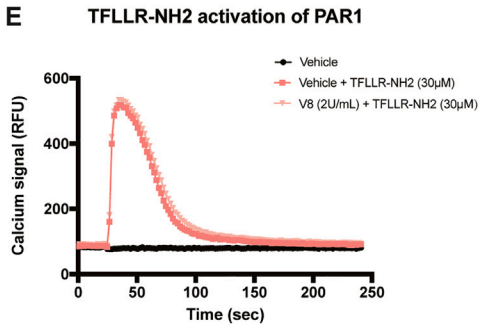

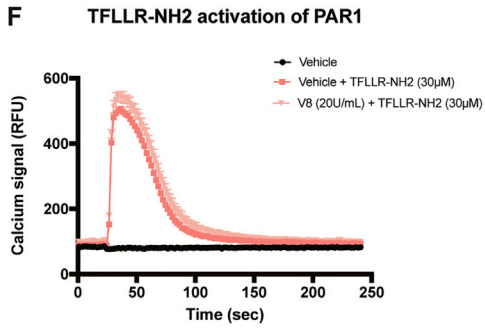

Figure S6. V8 protease cleaves PAR1, related to Figure 4

(A) HEK cells expressing double brilliant PAR1 were exposed to HBSS or V8 (2 U/mL) for 3 min. Scale bars, 10 µm.

(B) Left: time course of N-terminal PAR1 cleavage by V8 protease, the canonical PAR1 protease thrombin was included as a control. Right: peptides at 30 min identified by mass spec with their total spectral counts in the soluble and tethered fractions. Amino acids in red are a result of the His6-tagged construct and not native to PAR1 sequence.

(legend continued on next page)

(C) Calcium signaling measured in HEK cells expressing human PAR1 were incubated with thrombin (3 U/mL) and/or V8 (2 U/mL).
(D) Calcium signal measured in HEK cells expressing human PAR1 were incubated with thrombin (3 U/mL) and/or V8 (20 U/mL).
(E) Calcium signal measured in HEK cells expressing human PAR1 were incubated with TFLLR-NH_2 (20 μM) and/or V8 (2 U/mL).
(F) Calcium signal measured in HEK cells expressing human PAR1 were incubated with TFLLR-NH_2 (20 μM) and/or V8 (20 U/mL).

A Mouse DRG neurons

	Peptidergic								Neurofilament			Non Peptidergic					
	TrpM8	TrpM8	TrpM8	PEP1.2	PEP1.3	PEP1.1	PEP1.4	PEP2	NF2/3	NF4/5	NF1	TH	NP1.1	NP1.2	NP2.1	NP2.2	NP3
Scn10a	0.00	0.08	0.00	0.20	1.56	1.16	2.51	3.28	0.61	0.04	0.03	1.08	3.71	5.28	5.47	4.99	4.00
Trpv1	2.21	0.67	0.31	3.07	2.68	1.02	3.26	0.56	0.00	0.05	0.00	0.01	0.06	0.05	0.04	0.73	1.95
Trpa1	0.00	0.00	0.00	0.00	0.20	0.00	0.12	0.00	0.00	0.00	0.00	0.05	0.36	0.31	0.07	0.00	0.13
Mrgprd	0.00	0.00	0.00	0.00	0.00	0.00	0.04	0.00	0.00	0.05	0.00	0.01	10.60	9.00	1.20	1.43	0.48
Mrgpra3	0.00	0.00	0.00	0.00	0.00	0.00	0.01	0.00	0.00	0.10	0.00	0.00	0.00	0.01	8.40	3.30	0.06
Mrgprx1	0.00	0.00	0.00	0.00	0.00	0.00	0.00	0.00	0.00	0.00	0.00	0.00	0.00	0.00	0.00	0.01	0.00
Nppb	0.00	0.00	0.00	0.00	0.00	0.00	0.00	0.01	0.00	0.00	0.00	0.01	0.00	0.00	0.04	0.00	9.17
Hrh1	0.00	0.00	0.00	0.00	0.12	0.00	0.02	0.01	0.10	0.00	0.03	0.01	0.00	0.01	0.25	0.63	0.47
S1pr3	0.07	0.05	0.11	0.57	3.54	1.29	2.05	2.89	2.31	0.26	0.97	0.07	0.06	0.08	0.00	0.10	0.51
F2rl1	0.00	0.00	0.00	0.00	0.00	0.00	0.00	0.00	0.00	0.00	0.00	0.00	0.10	0.02	0.18	0.03	0.97
F2rl3	0.00	0.00	0.00	0.00	0.01	0.01	0.00	0.02	0.00	0.02	0.00	0.00	0.01	0.01	0.04	0.00	0.01
F2r	0.04	0.06	0.02	0.03	0.81	0.00	0.01	0.54	0.55	0.11	0.26	0.05	0.03	0.28	0.56	0.15	0.05

B Human DRG neurons

	C-LTMRs	Nociceptors							Mechanoreceptors			Prop.
		Pruri-ceptor	Silent	TRPA1+	PENK+	Aδ HTMRs	Cold	Aβ noc.	Aδ LTMRs	Aβ RA LTMRs	Aβ SA LTMRs	
SNAP25	3.09	3.98	4.68	6.02	8.35	9.96	8.51	9.22	10.19	9.02	10.52	15.11
TRPV1	2.18	3.29	3.07	2.06	0.76	1.36	0.54	0.70	0.37	0.35	0.29	0.28
SCN10A	0.74	1.20	0.95	0.84	0.52	1.18	0.95	0.74	0.09	0.12	0.09	0.07
SCN11A	3.11	6.69	2.64	0.92	0.58	0.92	2.08	0.82	0.16	0.24	0.16	0.20
GFRA2	1.58	2.71	0.12	0.11	0.11	0.11	0.10	0.22	0.25	0.27	0.10	0.08
IL31RA	1.23	2.13	4.92	0.36	0.10	0.09	0.14	0.13	0.14	0.10	0.09	0.10
NPPB	0.27	0.57	0.60	0.04	0.01	0.02	0.01	0.05	0.01	0.03	0.01	0.02
F2R	**0.02**	**0.09**	**0.02**	**0.03**	**0.02**	**0.02**	**0.03**	**0.02**	**0.02**	**0.02**	**0.01**	**0.02**

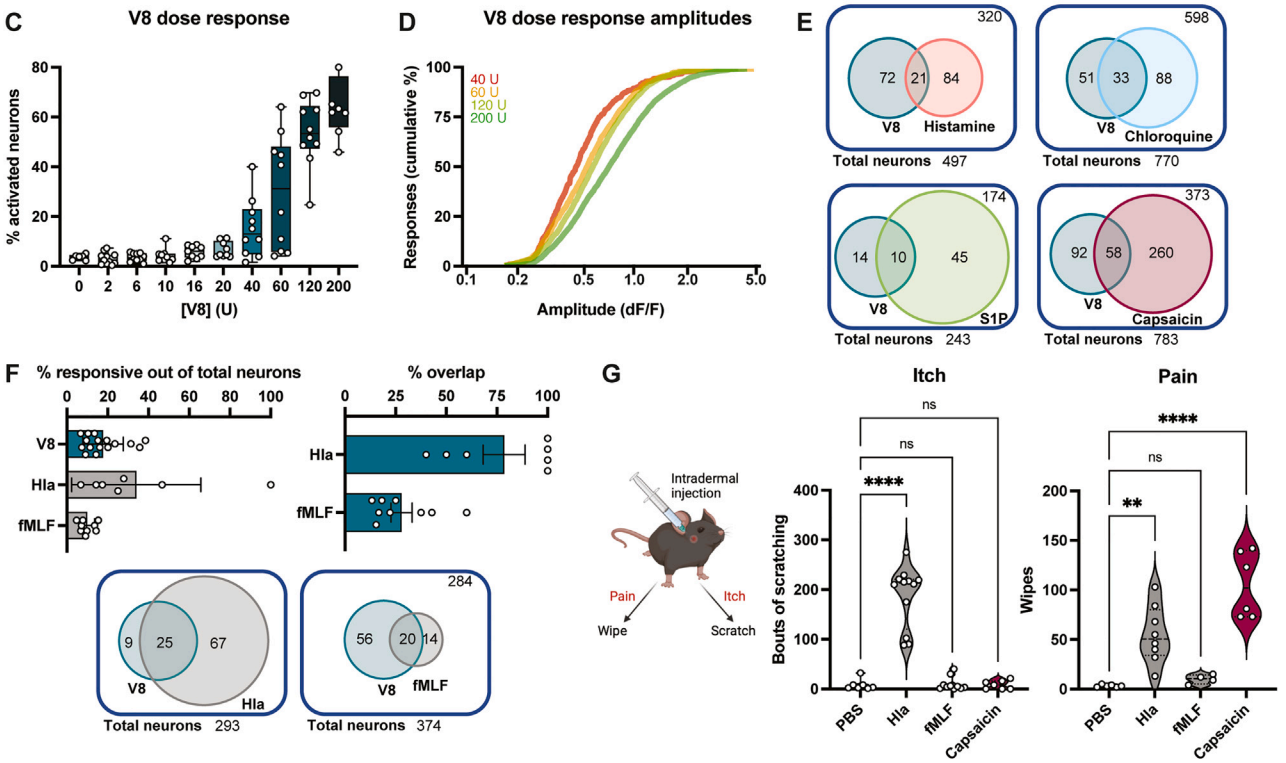

Figure S7. PAR1 expression in DRG neurons and calcium response to V8 protease, related to Figure 5

(A) Expression of *F2r* and select itch-related transcripts by mouse DRG neuron populations based on published single-cell RNA-seq datasets[61]
Scn10a, Nav1.8 voltage gated sodium channel; *Trpv1*, transient receptor potential cation channel subfamily V member 1; *Trpa1*, transient receptor potential cation channel subfamily A member 1; *Mrgprd*, MAS-related GPR member D; *Mrgpra3*, MAS-related GPR member A3; *Mrgprx1*, MAS-related GPR member X1; *Nppb*, natriuretic peptide B; *Hrh1*, histamine receptor H1; *S1pr3*, sphingosine-1-phosphate receptor 3; *F2rl1*, coagulation factor II receptor-like 1 (PAR2); *F2rl3*, coagulation factor II receptor-like 3 (PAR4); *F2r*, coagulation factor II receptor (PAR1).

(legend continued on next page)

(B) Spatial transcriptomic RNA sequencing data from Tavares-Ferreira et al.[65] demonstrates that *F2R* is predominantly expressed in pruriceptors which also highly express *GFRA2*, *IL31RA*, and *NPPB*. Data are presented as estimated counts from Seurat analysis. *GFRA2*, GDNF family receptor alpha 2; *IL31RA*, interleukin-31 receptor alpha; *NPPB*, natriuretic peptide B; *F2R*, coagulation factor II receptor (PAR1).
(C) Mouse DRG neurons were loaded with Fura-2AM and treated with increasing doses of V8 protease for calcium imaging analysis (n = 6–11 fields per group).
(D) Cumulative distributions of peak amplitudes after stimulation with increasing doses of V8.
(E) Venn diagrams showing numbers of mouse DRG neurons responding to V8 and to histamine, chloroquine, S1P, or capsaicin.
(F) Percentages of total mouse DRG neurons (responsive to KCl) that respond to V8 (69.2 μM), Hla (10 μg/mL), or fMLF (1 μM); overlap in V8-responsive neurons that also respond to Hla or fMLF; Venn diagrams showing neuron numbers responding to V8 and Hla or fMLF.
(G) Acute itch (bouts of scratching) and pain (wipes) behavior following intradermal injection with PBS, Hla (330 μg), fMLF (1.3 μg), or capsaicin (40 μg) (n = 2–6 males, 2–6 females per group).
For each panel, data from 2 to 8 independent experiments are combined and shown. Data are represented as mean ± SD.

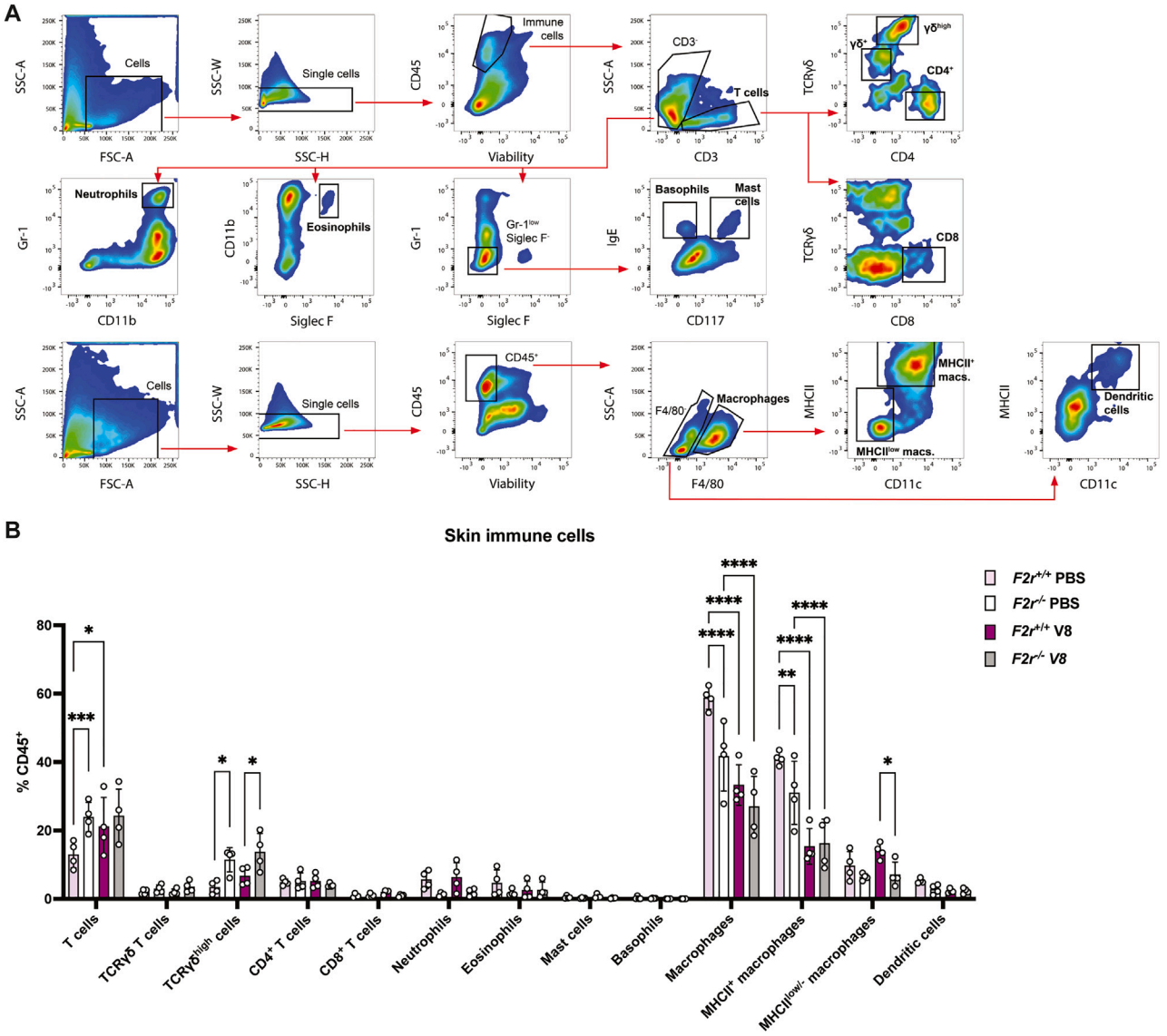

Figure S8. Characterization of skin immune cells after V8 injection, related to Figure 6

(A) Gating strategy for flow cytometric analysis of skin immune cells.

(B) Skin immune populations in WT B6 and *F2r*$^{-/-}$ mice treated with PBS or V8 protease (n = 4 males per group).

Data from 2 independent experiments are combined and shown. Data are represented as mean ± SD.

Statistical analysis: in (B), two-way ANOVA; in (G), Mann-Whitney test. *p < 0.05; **p < 0.01; ***p < 0.001; ****p < 0.0001.

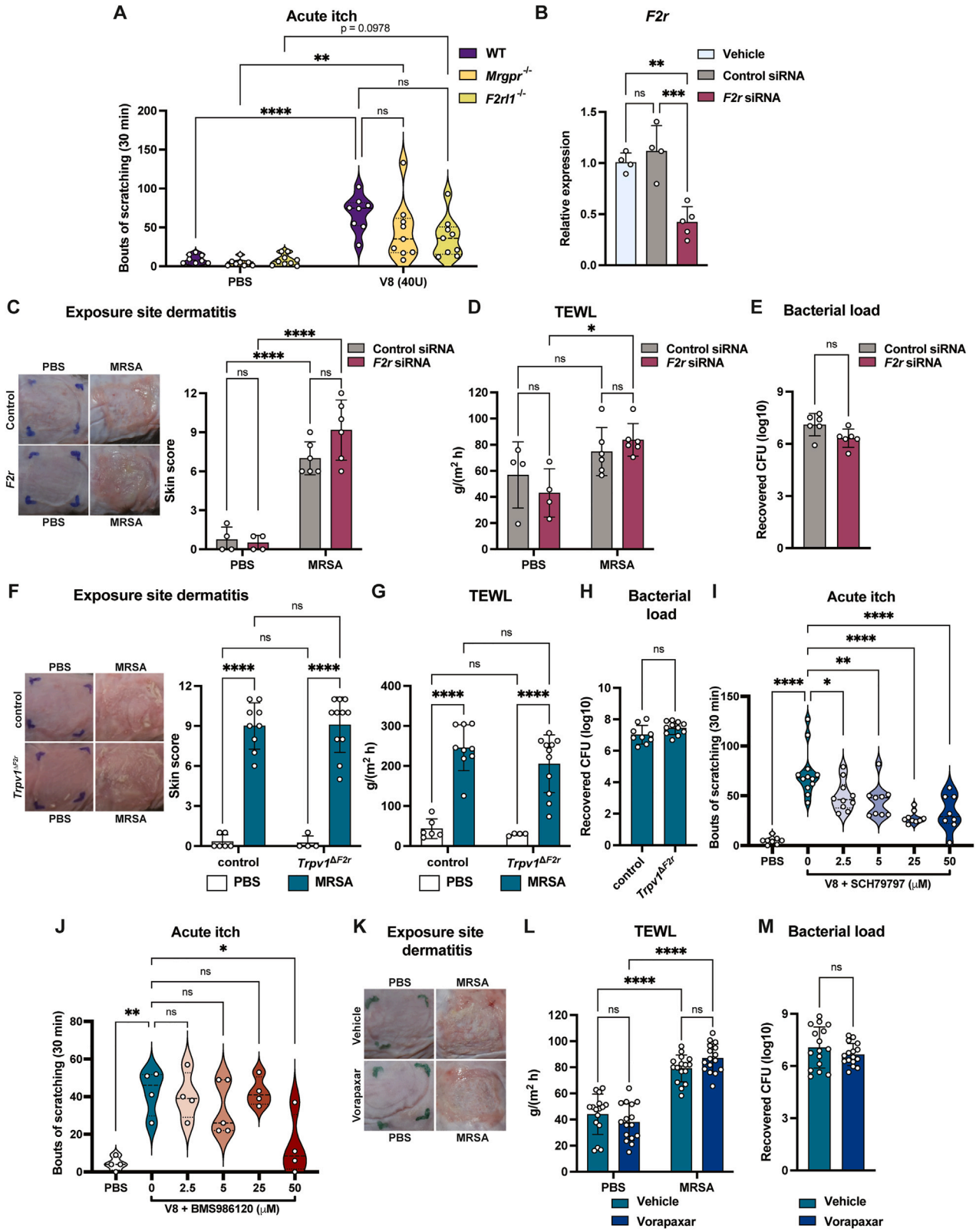

(legend on next page)

Figure S9. Targeting PAR1 reduces itch, related to Figure 7

(A) WT (n = 4–5 males, 4 females per group), *Mrgpr*$^{-/-}$ (n = 4 males, 4 females per group), and *F2rl1*$^{-/-}$ (n = 5 males, 4 females per group) mice were treated with PBS or V8 (40 U) intradermal cheek injections and monitored for acute itch behaviors.

(B) RT-qPCR quantification of *F2r* expression by mouse DRGs following injections with vehicle, control siRNA, or *F2r* siRNA (n = 2 males, 2–3 females per group).

(C) Representative images of back skin and dermatitis scores for control and MRSA-exposed mice injected with either control siRNA or *F2r* siRNA (n = 4–6 males per group).

(D) Transepidermal water loss measurements for control and MRSA-exposed mice injected with either control siRNA or *F2r* siRNA (n = 4–5 males per group).

(E) Skin bacterial load for MRSA-exposed mice injected with either control siRNA or *F2r* siRNA (n = 4–5 males per group).

(F) Representative images of skin from *Trpv1*$^{\Delta F2r}$ mice and WT controls treated with PBS or MRSA and exposure-site dermatitis scores (n = 3–8 males, 1–6 females per group).

(G) TEWL for *Trpv1*$^{\Delta rpv}$ mice and WT controls treated with PBS or MRSA (n = 3–8 males, 1–6 females per group).

(H) Skin bacterial load for *Trpv1*$^{\Delta F2r}$ mice and WT controls inoculated with MRSA (n = 5–6 males, 4–5 females per group).

(I) Bouts of hindpaw scratching following intradermal cheek injection with PBS or V8 (40 U) mixed with increasing doses of the PAR1 antagonist SCH79797 (0–50 μM). (n = 4–6 males, 4–6 females per group).

(J) Bouts of hindpaw scratching following intradermal cheek injection with PBS or V8 (40 U) mixed with increasing doses of the PAR4 antagonist BMS986120 (0–50 μM). (n = 2–3 males, 2–3 females per group).

(K) Representative images of back skin for control and MRSA-exposed mice gavaged with either vehicle or vorapaxar.

(L) Transepidermal water loss for control and MRSA-exposed mice treated with either vehicle or vorapaxar (n = 8 males, 8 females per group).

(M) Skin bacterial load for mice inoculated with MRSA and treated with either vehicle or vorapaxar (n = 8 males, 8 females per group).

For each panel, data from 2 independent experiments are combined and shown. Data are represented as mean ± SD.

Statistical analysis: in (A), (C), (D), (H), (I), and (L), two-way ANOVA with Sidak's multiple comparisons test. In (B), (E)–(G), (J), and (M), Mann-Whitney test. *$p < 0.05$; **$p < 0.01$; ***$p < 0.001$; ****$p < 0.0001$; ns, not significant.